THE USE OF INSTRUMENTED CAPILLARY RISE EXPERIMENTS WITH TIME-DOMAIN REFLECTOMETRY TO DETERMINE CAPILLARY RISE AND SOIL SALINITY IN REAL-TIME

Urooma Samoon

A THESIS SUBMITTED TO THE FACULTY OF GRADUATE STUDIES IN PARTIAL FULFILLMENT OF THE REQUIREMENTS FOR THE DEGREE OF MASTER OF APPLIED SCIENCE

GRADUATE PROGRAM IN CIVIL ENGINEERING

YORK UNIVERSITY

TORONTO, ONTARIO

AUGUST 2024

Abstract

The movement of saltwater in soils through capillary rise poses a concern, given its potential to affect both soil structure and hydraulic properties. This emphasizes the critical necessity of real-time monitoring to accurately measure and assess the salt concentration in the soil. Time-Domain Reflectometry (TDR) can be used to simultaneously measure the volumetric water content and bulk electrical conductivity of soil over time. Bulk electrical conductivity serves as a valuable metric for estimating pore water electrical conductivity, providing a basis for establishing a correlation with the salt concentration in the soil. Capillary rise experiments, instrumented with TDR probes, were conducted to measure the volumetric water content and bulk electrical conductivity of two distinct sand grades (30/40 and 40/50). These experiments encompassed a series of trials involving varying concentrations of salt solutions, juxtaposed with a control test utilizing deionized water. Further batch testing was conducted using the same sands to establish empirical relationships between bulk electrical conductivity and soil pore water concentration. The time series data, encompassing experimental volumetric water content and concentration from the capillary rise experiment, was used for inverse modelling to estimate soil hydraulic and solute transport properties. The findings from this study indicate that TDR provides accurate results for water content and electrical conductivity in column capillary rise experiments. The results also suggest that TDR observation data coupled with inverse modelling provides a soil water characteristic curve comparable to that measured using an evaporation method with the use of HYPROP. The outcomes of this study offer valuable insights into comprehending the intricate dynamics of water and salt within soil systems.

Acknowledgements

I am very grateful to Dr. Bashir for his utmost support and guidance throughout this research. Thank you for your constant words of encouragement and for giving me this opportunity.

Thank you to Kunjan Rupakheti for his constant support in the lab. Thank you for taking the time to teach me.

Thank you to Robert Reynolds for teaching me how to use Mathematica and always making himself available to help me out.

Lastly, thank you to all my friends from Lassonde and my family for offering encouragement and support throughout this journey.

Table of Contents

List of Figures

List of Tables

Chapter 1: Introduction

The rise of liquids in porous media against the forces of gravity is known as capillary rise. When studying capillary rise, it is crucial to consider certain factors, namely the height, liquid storage capacity, and rate of rise. The extent of capillary rise is influenced by the radius of the capillary, the surface tension and density of the liquid, as well as the contact angle formed at the interface between the liquid and solid materials.

The upward movement of water due to capillary rise can increase the water content in the soil, thereby leading to increased soil saturation. An increase in water content can result in a reduction in the soil's strength and bearing capacity which can lead to drastic consequences such as soil instability, soil erosion, landslides, and foundation failure. Furthermore, the rise of saltwater is problematic as it can lead to salt accumulation or soil salinization (Xing et al. 2019). Salt presence can occur due to irrigation, use of deicing salts, or weathering. Salt can reach the soil surface due to capillary rise which leads to salt accumulation. Increased concentrations of salt at the soil surface can negatively affect nearby infrastructure causing soil degradation, decrease in soil strength, erosion as well as corrosion of metal parts used in buildings such as steel reinforcement in concrete structures or metal pipes, which can compromise the integrity and longevity of the infrastructure.

There is a need to measure the salt concentration of soil in real time due to capillary rise. This will allow for better understanding of salt movement and concentration which can be beneficial for planning remediation strategies. Not many nondestructive testing methods exist that can measure the soil water content and salinity (Dalton et al. 1986). Field water content can be measured gravimetrically by using in-situ neutron scattering. However, this method has limitations as it requires large samples for testing, poses a radiation hazard, and requires individual soil calibration (Dalton et al. 1986). Methods that can be used to measure salinity include four-electrode cells (Rhoades et al. 1976), or a porous ceramic extraction cup. Furthermore, salinity

and water content testing methods conducted using different samples from the same field location can cause sampling errors (Dalton et al. 1986). Time-Domain Reflectometry (TDR) can be used to simultaneously measure the volumetric water content and bulk electrical conductivity of the soil. TDR measures the travel time of an electronic pulse in a waveguide surrounded by soil. The signal reaches the end of the probe and is then reflected. The travel time can be related to the dielectric permittivity which can then be related to the volumetric water content (Dalton et al. 1986). The bulk electrical conductivity is determined using the amplitude of the reflected voltage to the applied voltage as the reflected voltage of the pulse depends on the electrical conduction of the material (Dalton et al. 1986).

Capillary rise experiments can be enhanced by employing TDR, a technique that allows for precise measurement of volumetric water content and bulk electrical conductivity. Integrating TDR technology into these experiments enables a more accurate assessment of water movement dynamics within soil profiles. By tracking changes in volumetric water content over time, researchers can effectively correlate these fluctuations with capillary rise phenomena. Moreover, conducting these experiments for diverse soil types facilitates a comprehensive understanding of both water and saltwater capillary rise processes. Through systematic investigation and analysis, valuable insights can be gained into the intricate interactions between soil properties, water behavior, and the influence of salts, informing strategies for managing soil moisture and mitigating potential risks to infrastructure stability.

1.1 Problem Statement

Traditional methods using non-instrumented soil columns limit the accurate quantification of capillary rise in both field and laboratory settings due to a lack of precise data on water movement and salt concentration. Time-Domain Reflectometry (TDR) offers a promising solution as this technology enables continuous monitoring of capillary rise by measuring volumetric water content with time, thus facilitating accurate quantification of capillary rise and dynamics. Moreover, TDR

can also estimate soil salinity through bulk electrical conductivity measurements, offering valuable insights into saltwater behavior within the soil. This adaptability makes TDR suitable for deployment in both controlled laboratory settings and real-world field conditions.

By implementing TDR, researchers and practitioners can gain crucial insights into water movement dynamics and saltwater behavior within the soil, providing invaluable data for both research endeavors and practical applications aimed at mitigating environmental damage caused by saltwater intrusion. Additionally, utilizing instrumented columns equipped with TDR technology offers the added benefit of data that can be leveraged to estimate hydraulic and transport parameters through inverse modelling. These estimates can then be used in forward modelling efforts, to simulate various anticipated field conditions. Ultimately, this combined approach using TDR can significantly improve our ability to manage and mitigate environmental issues caused by saltwater intrusion.

1.2 Research Objectives

Prior studies on saltwater's impact on capillary rise have overlooked the inclusion of instrumentation in experimental setups (Jitrapinate, 2016; Truc et al., 2022), potentially compromising water rise estimations. Moreover, variations in bulk electrical conductivity due to salt presence have been disregarded in saltwater capillary rise experiments. Although Truc et al. (2022) conducted column experiments altering saltwater concentration, they failed to consider bulk and pore water electrical conductivity, critical for estimating salt quantity within the experimental column. Pore water electrical conductivity holds particular importance in salinity studies as it can be used to obtain salt concentration within the soil pores.

The primary objective of this research is to investigate water and saltwater capillary rise in different sand grades using an instrumented column. Given the underutilization of instrumentation in capillary rise studies, potential flaws in data collection need addressing. Time-Domain

Reflectometry (TDR) will measure bulk electrical conductivity, convertible to pore water electrical conductivity using empirical relationships, enabling salt concentration estimation. TDR results will be compared with alternative methods for assessing water content and electrical conductivity to evaluate TDR's accuracy in real-time salinity and volumetric water content assessment.

The research objectives are as follows:

1. Investigate capillary rise in two different sand grades.
2. Explore the effect of NaCl on capillary rise using an instrumented column.
3. Assess accuracy of TDR in measuring volumetric water content and salinity by comparing results with alternative methods.
4. Establish a correlation between measured pore water and bulk electrical conductivities.
5. Utilize the results of experimental studies in conjunction with the HYDRUS-1D software to conduct inverse modelling. This approach will aid in the prediction of soil hydraulic characteristics and parameters related to solute transport.

These objectives aim to rectify gaps in existing research by incorporating instrumentation for enhanced accuracy and leveraging empirical relationships to deepen understanding of saltwater behavior in capillary rise. Additionally, inverse modelling will provide insights into soil hydraulic properties and solute transport, aiding decision-making in environmental and agricultural contexts.

1.3 Thesis Outline

The section provides a brief description of the chapters within this thesis.

1.3.1 Chapter 1: Introduction

This chapter provides a brief introduction to the research topic, followed by the problem statement and research objectives.

1.3.2 Chapter 2: Background Information

This chapter provides crucial background information on the research. It delves into the fundamental principles of capillary rise in soils, exploring the various factors that can influence the rate and height at which water moves upward. It also discusses the specific effects of saltwater on capillary rise dynamics within the soil. Furthermore, it provides information on the use of Time-Domain Reflectometry (TDR) as a measurement technique. Additionally, the chapter explores the existing empirical relationships used to interpret TDR measurements in the context of water content and soil electrical conductivity. This chapter provides key background information that can be used to understand where there are knowledge gaps and unmet needs that justify and motivate the current research effort.

1.3.3 Chapter 3: Capillary Rise Experiments in an Instrumented Column

Chapter 3 includes details regarding the capillary rise experimental methodology, results, and inverse modelling. The chapter discusses the experimental methodologies and findings made by previous studies to acknowledge where there may be gaps in research. The experimental methods and materials used for conducting the capillary rise experiments are presented along with the experimental results. The experimental results from Time-Domain Reflectometry (TDR) are verified using gravimetric method and laboratory electrical conductivity meter. Furthermore, the capillary rise is obtained experimentally and compared with analytical solutions for estimating capillary rise established in literature. The experimental results are used to conduct inverse modelling using HYDRUS-1D and estimate soil hydraulic properties. This chapter verifies the use of TDR in column capillary rise experiments and achieves the objectives of this research.

1.3.4 Chapter 4: Use of TDR to Determine Soil Water Concentration and Solute Transport Parameters

This chapter discusses the experimental methods used to determine the pore water electrical conductivity. A relationship between the bulk and pore water electrical conductivity is established

by conducting a series of batch experiments. The methodology used to obtain this relationship is explained including a background context on various methods used to determine the pore water electrical conductivity. The pore water electrical conductivity is then used to obtain the salt concentration which can be used to obtain breakthrough curves. The salt concentration data is then used in HYDRUS-1D to inversely estimate the solute transport parameters. This chapter confirms that TDR instrumented column experiments can be used to understand soil salinity and salt movement due to capillary rise.

1.3.5 Chapter 5: Summary, Conclusions, Recommendations for Future Research

This chapter provides a summary of the major findings of the research as well as recommendations for future research. The outcomes and contributions of this research are also discussed.

Chapter 2: Background Information

This chapter includes findings established from literature with regards to the capillary rise phenomenon, the use of TDR, inverse numerical modelling, and any limitations found in research. The need for research is also presented within this chapter. This chapter serves as background information that can be used to further understand the context of this research.

2.1 Capillary Rise

Capillary rise is defined as the rise of liquids due to surface tension and adhesive forces (Truc et al. 2022). In terms of capillary rise, the height of capillary rise, liquid storage capacity of capillary rise, and the rate of capillary rise should be considered (Lu et al. 2004). For this research, the height of capillary rise is taken as the rise of liquid above the water table. The liquid storage capacity of water is the ability of the soil to hold the water, and the rate of capillary rise is how fast or slow the water rises with time.

Figure 2.1 below shows a schematic of the rise of capillary water and its relationship with the soil water characteristic curve. The 'h_c' represents the ultimate height of capillary water above the water table whereas 'h_a' is the air-entry head. The soil water characteristic curve is a relationship between the soil suction and volumetric water content as shown in Figure 2.1. At saturated water content, the soil suction is zero. The air entry point is the point in which air enters the largest pores of the soil. The water content decreases as air enters the pores of the soil. The soil profile on the left in Figure 2.1 depicts three zones: a fully saturated zone below groundwater table, a nearly saturated zone above the groundwater table and below the air-entry head or 'h_a', and finally an unsaturated zone located beyond the air-entry head or 'h_a' which essentially shows capillary fingers that reach the ultimate capillary height or 'h_c' (Lu et al. 2004). The hydraulic conductivity decreases quickly as air enters the soil pores and the zone becomes unsaturated. This also reduces the rate of capillary rise (Lu et al. 2004).

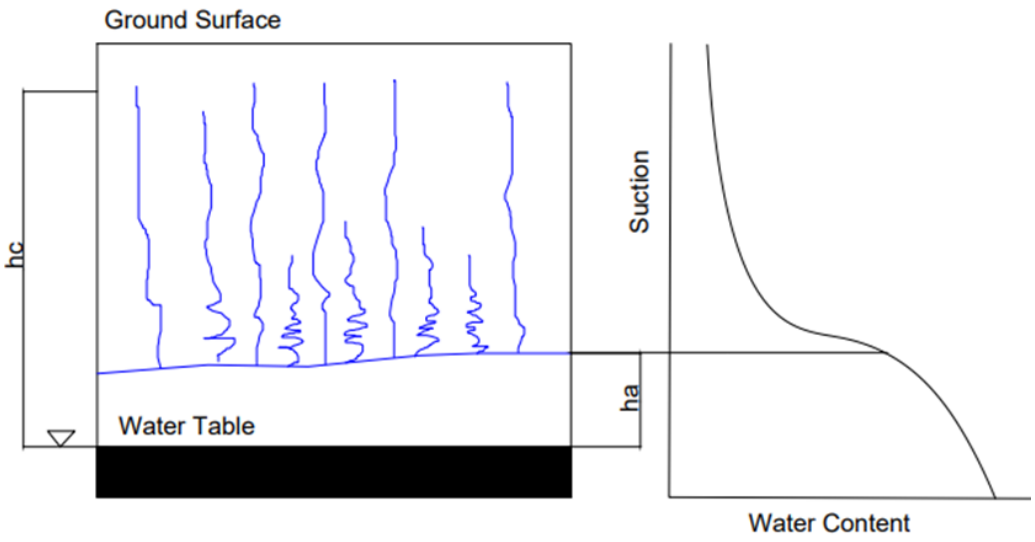

Figure 2.1: Schematic model for capillary rise and soil water characteristic curve, modified from Lu et al. (2004)

2.1.1 Factors Affecting Capillary Rise

The height of capillary rise is influenced by several key properties: surface tension and density of the liquid, contact angle at the solid-liquid interface, and capillary radius.

The equation for quantifying capillary rise in a tube as defined in Fetter (1994) is:

$$h_c = \frac{2\sigma cos\gamma}{\rho g r} \quad [2.1]$$

where, h_c is the height of the liquid rise, σ is the surface tension, γ is the contact angle, ρ is the density of the liquid, *g* is the gravitational acceleration, and *r* is the radius of the capillary (tube). This equation is also known as Jurin's Law.

Capillary rise is influenced by the surface tension force which acts along the surface of the liquid, and it causes particles that are at the liquid surface to be pulled inward which decreases the surface area, therefore creating a meniscus at the liquid-surface interface. A higher surface tension would lead to a higher capillary rise and vice versa. The contact angle is the angle

between the liquid-gas interface or the solid-liquid interface. A higher contact angle would translate to low wetting and thus a lower capillary rise. A contact angle less than 90 degrees correlates to hydrophilic surfaces whereas a contact angle higher than 90 degrees correlates to hydrophobic surfaces. A solid is wettable by the liquid when the liquid molecules are more strongly attracted to the solid molecules (Or et al. 2005). Lower wetting would indicate weak adhesive forces between the liquid and the capillary tube. The capillary rise is greater in tubes with smaller diameters. The density of the liquid also affects capillary rise as denser liquids will decrease the rise.

Capillary action can cause liquid to rise within the soil profile. Soil has interconnected pores or capillary fingers which create a path for water to move through (Lu et al. 2004). The water particles rise as they are drawn to the surface of soil particles. The liquid storage capacity of the soil determines the amount of water that can be retained in the soil (Lu et al. 2004). Finer soil tends to have a higher capillary rise due to the smaller pore spaces between particles. Capillary rise in soils is influenced by the same factors that capillary rise in tubes is affected by. It is crucial to be able to understand how water moves through soils and accurately estimate the capillary rise so that engineers can make informed decisions.

2.1.2 Height of Capillary Rise

Accurately estimating the height of capillary rise allows researchers and engineers to predict water movement within soil and make knowledgeable decisions. This section explores established empirical relationships that provide valuable tools for such estimations.

These relationships build upon the fundamental physics governing capillary action, expressed in the classical capillary equation defined in Equation 2.1. For soils, the analogy of capillary rise in a tube can apply (Jurin’s Law) however, the radius of the capillary would be taken as the effective pore radius of the soil rather than the radius of the tube. Researchers have also defined the radius

of the capillary (in Equation 2.1) for soil to be 0.2 times the effective grain diameter as reported in Salim (2016):

$$r = 0.2d_{10} \quad [2.2]$$

where, *r* is as defined previously and d_{10} is the effective grain diameter corresponding to 10% of finer particles of a given sample mass.

Researchers have developed various empirical relationships incorporating soil properties like porosity and grain size to aid in estimating the capillary rise. For example, the Polubarinova-Kochina (1962) relationship as reported by Salim (2016) considers porosity (ϕ) and d_{10} as defined earlier:

$$h_c = \frac{0.45\left(\frac{1-\phi}{\phi}\right)}{d_{10}} \quad [2.3]$$

Similarly, Peck et al. (1974) relate maximum capillary rise to void ratio (*e*) and d_{10}:

$$h_c = \frac{C}{e d_{10}} \quad [2.4]$$

here, *C* is an empirical constant depending on factors like particle shape and surface impurities. Kumar & Malik (1990) prioritize ease of use, estimating capillary rise based on air entry head (h_a) and effective pore radius (r_e) in micrometers:

$$h_c = h_a + 134.84 - 5.16\sqrt{r_e} \quad [2.5]$$

Lu & Likos (2004) offer a simpler approach, directly linking capillary rise to d_{10}:

$$h_c = -990\, ln(d_{10}) - 1540 \quad [2.6]$$

Liu et al. (2014) considered a comprehensive equation that factors in several parameters including porosity, surface tension, contact angle, gravity, and air-entry head as defined earlier, as well as dynamic viscosity (η), water density (ρ_w), and saturated hydraulic conductivity (k_s):

$$h_c = \frac{\sigma\phi}{\sqrt{2\eta\rho_w g k_s}} cos\gamma + (1-\phi)h_a \quad [2.7]$$

It's important to remember that these relationships are estimations and may not perfectly capture real-world complexities like soil heterogeneity, temperature variations, and dissolved salts. Choosing the most suitable relationship depends on the specific soil properties of interest and the desired level of accuracy. Combining estimations with actual measurements can provide a more reliable picture of capillary rise in a particular soil (Salim 2016).

In conclusion, these empirical relationships offer valuable tools for estimating capillary rise in soils. By considering various factors, these equations provide insights into water movement within soil and contribute to a better understanding of soil moisture movement. However, acknowledging the limitations of these estimations and using them alongside real-world measurements is crucial for optimal results.

2.1.3 Rate of Capillary Rise

Experimental results can be used to obtain the rate of capillary rise and then compared to empirical relationships proposed by Terzaghi (1943) or Lu & Likos (2004). The Terzaghi (1943) equation for the rate of capillary rise assumes that Darcy's Law is valid for unsaturated flow and that hydraulic gradient can be calculated using the difference between the capillary rise and wetting front divided by the wetting front.

The Terzaghi (1943) equation is as follows:

$$t = \frac{\phi h_c}{k_s}\left(ln\frac{h_c}{h_c - z} - \frac{z}{h_c}\right) \quad [2.8]$$

where t is the arrival time of the wetting front, ϕ is porosity, h_c is the height of capillary rise, k_s is the saturated hydraulic conductivity, and z is the distance from the water table (wetting front).

As mentioned previously, the soil profile consists of three zones (fully saturated zone below water table, nearly saturated zone above water table but below air-entry head, and unsaturated zone

above air-entry head). The hydraulic conductivity of the soil in the unsaturated zone above the air-entry head is important to consider in quantifying the rate of capillary rise because it decreases as the soil pores drain with increasing capillary rise (Lu & Likos, 2004). Therefore, as the wetting front is nearing the ultimate height of capillary rise, the hydraulic conductivity decreases by 5-7 orders of magnitude (Lu & Likos, 2004). This is not considered in Terzaghi (1943) equation as hydraulic conductivity is assumed to be constant and equivalent to saturated hydraulic conductivity (Lu & Liko, 2004). Lu & Likos (2004) provided a modified version of Terzaghi's original equation by accounting for the reduction in hydraulic conductivity using Gardner's (1958) exponential model in which the inverse of the air-entry head is used to represent the rate of decrease in hydraulic conductivity with suction head.

Gardner's (1958) model as mentioned in Lu & Likos (2004) is as follows:

$$k = k_s exp\ (-\alpha z) \qquad [2.9]$$

where, k is the hydraulic conductivity and α is the inverse of the air-entry head; k_s and z are as defined previously.

Lu & Likos (2004) consider Equation 2.9 along with the hydraulic gradient responsible for capillary rise to write the governing equation for the rate of capillary rise as follows:

$$\frac{dz}{dt} = \frac{k_s}{\phi} exp\ (-\alpha z) \left(\frac{h_c - z}{z}\right) \qquad [2.10]$$

The above equation can then be written in series form as follows:

$$t = \frac{\phi}{k_s} \sum_{j=0}^{m=\infty} \frac{a^j}{j!} \left(h_c^{j+1} \ln \frac{h_c}{h_c - z} - \sum_{s=0}^{j} \frac{h_c^s z^{j+1-s}}{j+1-s} \right) \qquad [2.11]$$

where t, ϕ, h_c, k_s,, z, and α are defined previously.

2.1.4 Saltwater Rise & Impact

Groundwater containing salt can rise in soil due to the capillary phenomenon. The height of capillary rise can decrease at very high salt concentrations due to the increased cohesion forces between saltwater molecules as well as increased density of the saltwater mixture (Or et al. 2005; Lubelli 2006).

The rise of saltwater is problematic as it can cause the salt to stay in the soil even after the water has evaporated which can lead to soil salinization (Xing et al. 2019). Saltwater can impact nearby infrastructure as well as building materials. Foundations can be impacted by salt if it reaches the soil surface and seeps into materials, reducing soil strength and infrastructure longevity (Lubelli 2006; Truc et al. 2022). Salt can impact concrete due to its corrosion effects. Concrete reinforced with metal components like steel can corrode which affects the structural integrity of the concrete. Corroded steel can expand creating further cracks and deterioration.

Research conducted by Tang et al. (2021) investigated the effects of salinity on soil structure and soil hydraulic characteristics which showed that increased soil salinity resulted in increasing the hydraulic conductivity. This can be due to flocculation or aggregation of soil particles. Saltwater contains dissolved ions like sodium (Na^{1+}) that can displace other cations (positively charged ions) like calcium (Ca^{2+}) and magnesium (Mg^{2+}) adsorbed on clay particles. These displaced cations are crucial for maintaining the structure and aggregation of clay particles. When replaced by sodium, the clay particles become more negatively charged, repelling each other, and leading to dispersion. Dispersed clay particles clog soil pores, reducing water infiltration and aeration.

Soil aggregates are clumps of soil particles bound together by organic matter, clay particles, and root hairs. These aggregates create space between them, allowing for air and water movement within the soil. When salinity increases, the dispersion of clay particles disrupts these aggregates, leading to a breakdown in soil structure. Furthermore, salt affects the soil water retention curve which is crucial in engineering as well as agriculture. The retention capacity of saline soils is

higher than that of non-saline soils due to the presence of sodium ions, thus impacting plant growth and production (Tang et al. 2021). Saltwater can pose a risk on civil infrastructure as well as the environment, thus creating a need for further research on the effects of saltwater on soil properties.

2.1.5 Importance of Capillary Rise and Need for Research

Capillary rise phenomenon is relevant in various areas of engineering and environment. Capillary rise problems exacerbate in areas prone to salt intrusion as salt that reaches the soil surface can compromise infrastructure integrity and longevity. Furthermore, the increase in water content due to capillary rise effects can impact the soil's elastic modulus which changes the soil's stress-strain response under applied loads (Baldovino et al. 2022). This stresses a need to understand and accurately estimate the height and rate of capillary rise so that engineers make informed decisions and design effective soil remediation strategies for areas prone to salt intrusion (Lubelli 2006; Jitrapinate 2015).

Moreover, understanding saltwater capillary rise in soils is crucial for efficient irrigation practices and salinity management in agricultural systems. Capillary rise can cause salt to fill the soil pores which can affect the crop water uptake and retention properties of plants (Salim 2016). It is important to understand how the solutes and water move within the soil so that one can better understand salt intrusion affects. By studying the capillary rise of saltwater in porous media, researchers can identify strategies to mitigate the adverse effects of soil salinization, such as developing appropriate irrigation schedules or selecting suitable crops for salt-affected areas.

Further research on saltwater rise facilitates the development and refinement of mathematical models and simulation tools that can predict and simulate saltwater movement in porous media. These models aid in decision-making processes, such as designing infrastructure, optimizing resource management strategies, and assessing the potential impacts of saltwater intrusion.

2.2 Introduction to Time-Domain Reflectometry (TDR)

Time-Domain Reflectometry (TDR) is a device used to measure the volumetric water content as well as the bulk electrical conductivity of the soil. It is easy to use in the field as well as in a laboratory setting. This method of measuring volumetric water content is known as an indirect method as it correlates dielectric measurements to water content. Dielectric measurement methods are efficient and easy to use (Hu et al. 2006). Other dielectric methods include water content reflectometry and amplitude-domain reflectometry (Hu et al. 2010). This section highlights findings from research with regards to the use of TDR along with some background information to understand TDR measurement principles.

2.2.1 TDR Measurement Principle for Volumetric Water Content

The TDR measurement system by Campbell Scientific consists of TDR probes (CS640 used in this research), a multiplexer device (SDM8X50), a datalogger (CR800), and a TDR system (TDR100) as shown in Figure 2.2. The multiplexer device allows the user to attach more than one probe to the TDR system whereas the datalogger is used to log the data from the TDR system to a datalogging software. The TDR system is responsible for sending an electromagnetic signal through the waveguide or probe surrounded by soil. It also produces a waveform of the signal for analysis, where the travel time of the electronic signal that is sent through the probe can be assessed. The signal reaches the end of the probe and is reflected back. The travel time of the signal is related to dielectric permittivity which can then be related to volumetric water content through calibration relationships. The waveform produced by TDR shows reflection points which can be used to analyze the impedance along the waveguide (Campbell Scientific Inc. 2015)

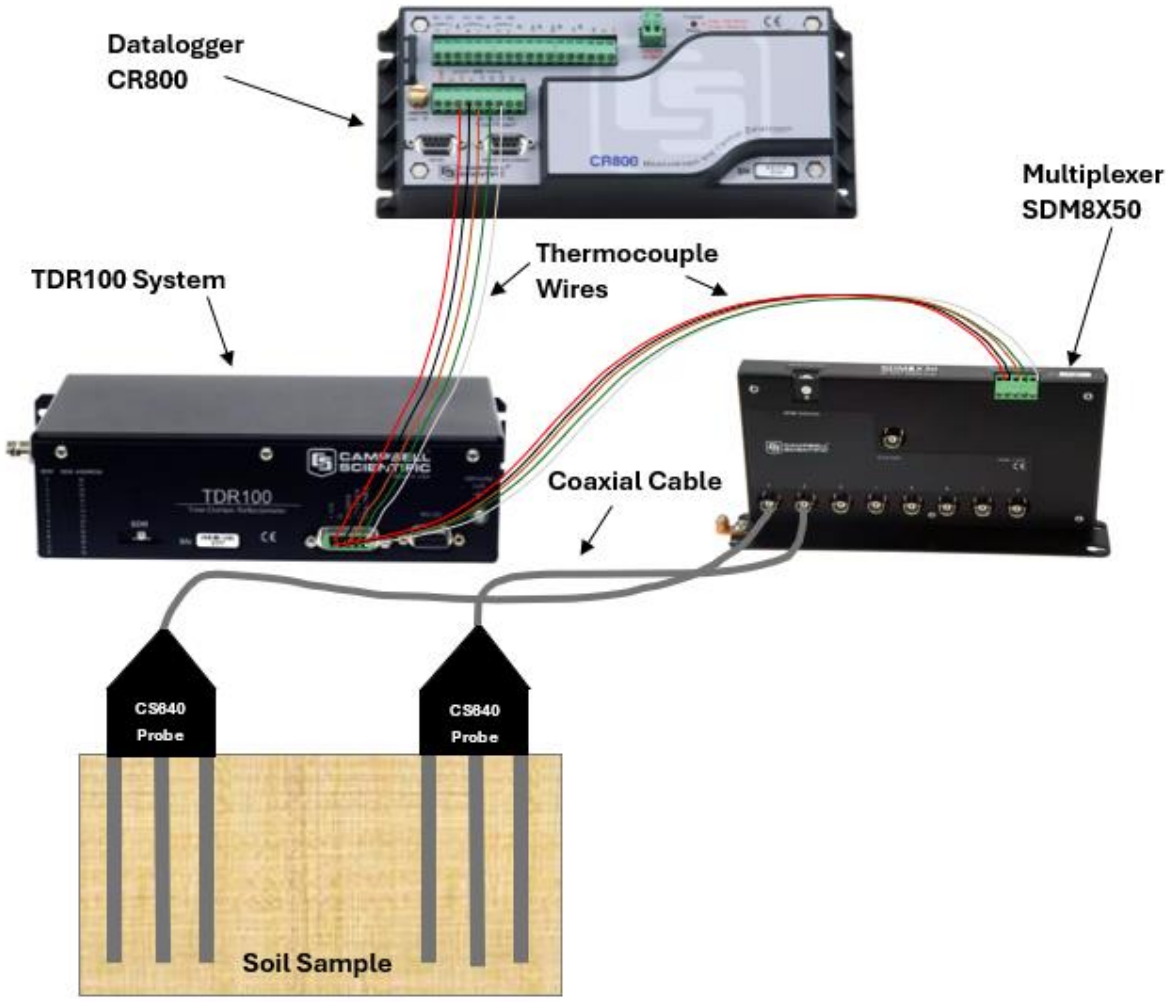

Figure 2.2: Schematic diagram of TDR system

Figure 2.3 depicts a typical TDR waveform at different water contents showing the relationship between reflection coefficient and apparent distance. The travel time of the pulse along the apparent length of the probe and back is recorded and is inversely related to the propagation velocity of the pulse (Jones et al. 2002; Campbell Scientific Inc. 2015). In Figure 2.3 below, x_1 is the point at which the signal enters the probe and x_2 is denoted as the reflection of the signal at the end of the probe (Jones et al. 2002). The difference between these two points is the apparent length of the probe.

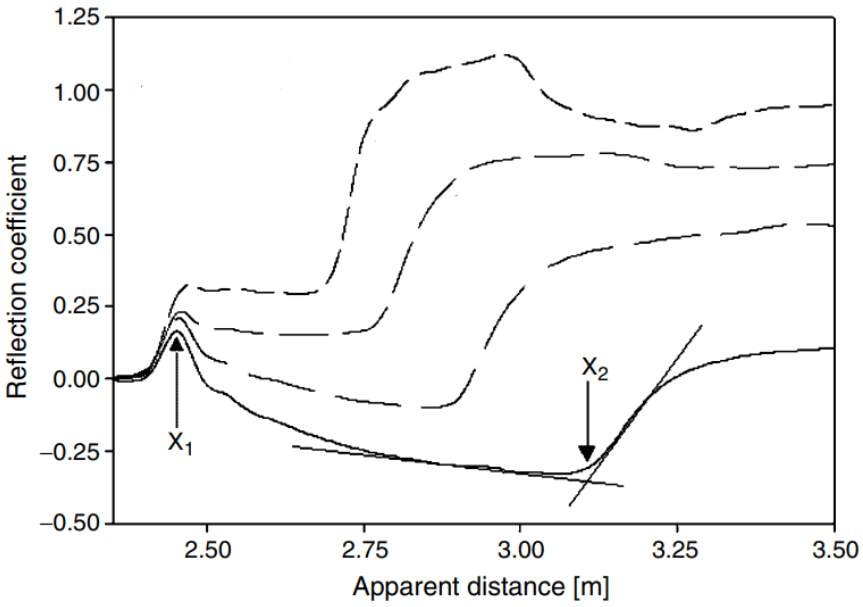

Figure 2.3: Sample TDR waveform, modified from Jones et al. (2002)

The apparent dielectric constant is related to the propagation velocity and travel time of the pulse as follows:

$$K_a = \left(\frac{ct}{2L}\right)^2 \qquad [2.12]$$

where, K_a is the apparent dielectric constant, *c* is the speed of light in a vacuum, *t* is the travel time of the pulse, and *L* is the apparent probe length.

The bulk dielectric permittivity is made up of 3 components: soil, air, and water. The permittivity (farad per meter units) is the ability of the soil to hold an electric charge, and the dielectric constant is the ratio of the permittivity to free space or a vacuum. Water generally has a dielectric constant ranging from 79 to 82 whereas air has a constant of 1 (Chen et al. 2010, Hu et al. 2010). Soil minerals dielectric constant ranges from 2 to 5 (Hu et al. 2010). Since water has the highest dielectric constant, it is the dominant factor in the bulk dielectric permittivity thus making it an indirect indicator of the volumetric water content (Chen et al. 2010, Hu et al. 2010). As the water content in soil increases, the dielectric permittivity and travel time also increases.

Topp et al. (1980) established a relationship between the apparent dielectric constant (K_a) and the volumetric water content (θ_w) as follows:

$$\theta_w = -5.3 \times 10^{-2} + 2.92 \times 10^{-2} K_a - 5.5 \times 10^{-4} K_a^2 + 4.3 \times 10^{-6} K_a^3 \quad [2.13]$$

Ledieu et al. (1986) developed a simpler relationship using apparent dielectric constant and volumetric water content:

$$\theta_w = 0.1138\sqrt{K_a} - 0.1758 \quad [2.14]$$

Topp et al. (1980) relationship can be applied for many types of soils. However, this equation may yield significant measurement errors in cases where the soil is highly conductive or highly plastic such as clayey soils, thus requiring a need for calibrated equations tailored to specific soil types (Hu et al. 2010). TDR probes must be calibrated before use. Calibration using the Ledieu et al. (1986) model yielded the most accurate estimations for permittivity with the use of the built-in calibration mode in PC-TDR (Campbell Scientific software) and thus was used for the TDR instrumented experiments.

2.2.2 TDR Measurement Principle for Bulk Electrical Conductivity

TDR uses electromagnetic principles to determine the bulk electrical conductivity. The electromagnetic pulse sent through the waveguide and the reflected signal of that pulse can be used to capture a trace plot or waveform in which the voltage can be found and used for assessing the electrical conductivity. The velocity of the pulse sent through the waveguide depends on the dielectric constant of the soil surrounding the probe whereas the reflected voltage depends on the electrical conductance of the pulse between the probe rods and soil medium (Campbell Scientific Inc. 2015). The reflected signals and travel time of the pulse can be used to find the electrical properties of the soil (Dalton et al. 1986).

Figure 2.4 depicts a waveform in which 3 points are identified. The first point identifies the section between the cable impedance and the probe head. The transition zone between point 1 and 2

shows a change in reflection coefficient due to impedance differences between the cable and the probe (Campbell Scientific Inc. 2015). At point 2, the pulse signal exits the probe head and point 3 is where it exits the probe rods. The waveform data points can be used to obtain the apparent length of the probe (difference between point 2 and 3). The reflections are caused by impedance changes which can be due to transitions between different materials and changes in moisture content. A longer cable length can impact impedance as it would cause changes to the travel time and the amplitude of the reflection (Campbell Scientific Inc. 2015). The soil's electrical conductivity may also impact the waveform reflection. At higher electrical conductivities, the reflected pulse is attenuated due to conduction losses which can impact TDR results (Dalton et al. 1986; Campbell Scientific Inc. 2015). The impedance can be used to obtain information about the electrical properties of the soil as it is inversely related to the dielectric constant of the soil and therefore can be used to obtain bulk electrical conductivity (Campbell Scientific Inc. 2015).

TDR system by Campbell Scientific uses the research established by Giese and Tiemann (1975) to obtain the electrical conductivity (Campbell Scientific Inc. 2015):

$$EC_b = \frac{K_p}{Z_c}\frac{1-\rho}{1+\rho} \quad [2.15]$$

here, EC_b is the bulk electrical conductivity, K_p is the constant specific to the probe in question, Z_c is the impedance, and ρ is the reflection coefficient.

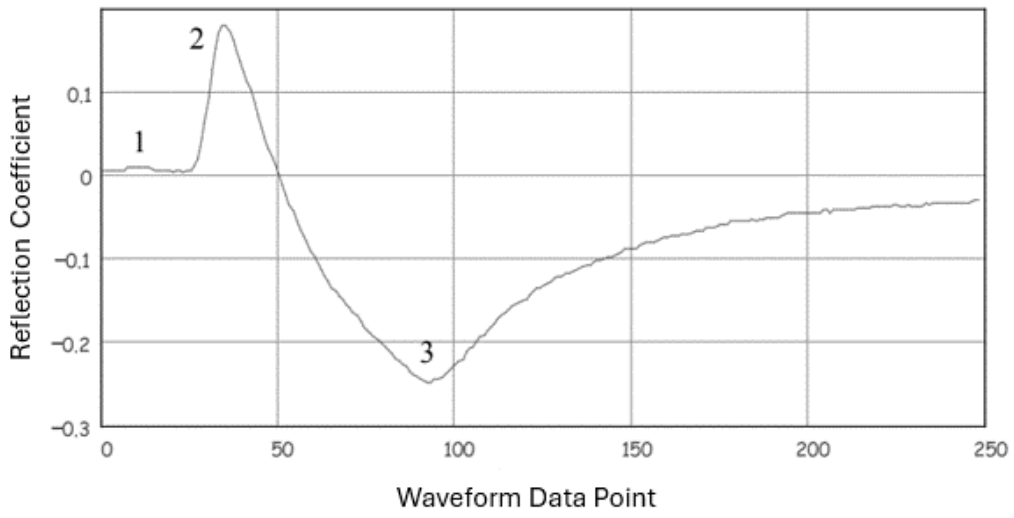

Figure 2.4: Typical TDR waveform, showing key points: 1, 2, and 3. Modified from Campbell Scientific Inc. 2015

2.3 Inverse Modelling

Characterizing unsaturated flow and transport processes within complex soil systems is paramount for various environmental and agricultural applications. Traditional methods often rely on predetermined soil hydraulic properties (SHPs) or established relationships. However, these approaches may not fully capture the inherent heterogeneity of field soils or require additional time consuming and expensive measurements for hydraulic and transport parameters. Inverse modelling emerges as a powerful alternative, enabling the direct estimation of SHPs and/or transport parameters from observed lab or field data.

Inverse modelling can be used to learn more about the movement of water and solute within soil mediums. HYDRUS-1D can be used to simulate water flow, solute transport, and heat transport in one-dimensional variably saturated domains. HYDRUS-1D uses a modified form of the Richards' equation for uniform water flow and advection-dispersion type equations for solute transport (Šimůnek et al. 2008). It assumes that thermal gradients and air phase effects on the water flow can be ignored (Šimůnek et al. 2018).

The modified Richards' equation for simulating water flow is as follows (Šimůnek et al. 2008):

$$\frac{\partial \theta(h)}{\partial t} = \frac{\partial}{\partial z}\left[K(h)\left(\frac{\partial h}{\partial z} + 1\right)\right] \quad [2.16]$$

here, θ is water content, h is the pressure head, t is time, z is the vertical coordinate, and $K(h)$ is the unsaturated hydraulic conductivity function.

Solute transport is typically described using the advection-dispersion equation in the following form:

$$\frac{\partial \theta c}{\partial t} + \rho \frac{\partial s}{\partial t} = \frac{\partial}{\partial z}\left[\theta D_H \frac{\partial c}{\partial z}\right] - \frac{\partial qc}{\partial z} \quad [2.17]$$

where, c is the solution concentration, s is the sorbed concentration, θ is water content, D_H is the hydrodynamic dispersion coefficient, ρ is the soil bulk density, q is the flux, t is time, and z is as defined previously (Šimůnek et al. 2008).

The hydrodynamic dispersion coefficient is described using the molecular diffusion coefficient (D_d), tortuosity factor (τ), longitudinal dispersivity (λ), and average pore water velocity (v) (Šimůnek et al. 2018):

$$D_H = D_d\tau + \lambda v \quad [2.18]$$

The above equations can be used in inverse mathematical models to obtain soil properties. The initial step in the process of inverse modelling involves clearly defining the research objective. This entails specifying the specific unsaturated flow and transport parameters targeted for estimation. Examples include soil hydraulic conductivity, soil water retention curve parameters, or dispersivity coefficients. The next stage focuses on constructing the model. This necessitates defining the soil profile geometry, boundary conditions, initial conditions, and the chosen simulation type. The hydraulic and transport parameters to be estimated are designated as variables within the model. The model relies on observed data relevant to the study's objective.

This data may encompass measurements of soil moisture content, pressure head, solute concentrations, breakthrough curves, or other relevant data collected from field or laboratory experiments (Šimůnek et al. 2008).

An objective function is then established to quantify the discrepancy between simulated and observed data for both flow and transport processes (Šimůnek et al. 2008). It should account for the differences in simulated and observed states or fluxes of water and contaminants over time and space. To minimize the objective function and estimate the unknown parameters, an appropriate optimization algorithm is chosen. The selection depends on the complexity of the problem and the characteristics of the data. Gradient-based methods or stochastic methods can be employed for parameter estimation. Utilizing the chosen optimization algorithm, the values of the unknown parameters in the model are iteratively adjusted to minimize the objective function, signifying a close match between simulated and observed data for both flow and transport processes.

Following the optimization process, the estimated parameter values and the overall goodness-of-fit between simulated and observed data are assessed. Visual inspection of model outputs also provides valuable insights into the performance of the optimized model. Sensitivity analysis is conducted to assess how individual parameters influence model predictions for both flow and transport processes. This helps identify which parameters contribute most to the uncertainty in parameter estimates. The robustness of the optimized model is further evaluated through validation by comparing simulated results with independent observed data not used in the parameter estimation process.

Finally, the estimated parameter values are interpreted in the context of soil properties, fluid flow mechanisms, and contaminant transport behavior. The optimized model can then be utilized for various purposes, such as predictive simulations, remediation strategy assessment, or informing

decision-making related to soil and groundwater management (Kirkham et al. 2019; Salahou et al. 2022)

Throughout the process, it's crucial to acknowledge the uncertainties associated with the observed data, the model structure, and the parameter estimation techniques. Iterative refinement and validation of the model can improve confidence in the estimated parameters and enhance the reliability of model predictions for both unsaturated flow and transport processes.

Several researchers have employed the use of HYDRUS-1D inverse modelling in determining solute transport properties and soil hydraulic properties using observation data from experiments (Inoue et al. 2000; Kirkham et al. 2019; Dragonetti et al. 2022). Inverse modelling aids in providing calibrated parameters with the added benefit of having optimized parameters that can be used to provide recommendations in the case that observation data is not readily available.

2.4 Limitations

While research on capillary rise and the use of Time-Domain Reflectometry (TDR) for indirectly measuring volumetric water content and bulk electrical conductivity has yielded valuable insights, limitations and constraints associated with both methods have been identified in literature. This section delves into these constraints, focusing on experimental methodologies and TDR applications.

2.4.1 Experimental Method Limitations

In experimental setups focusing on capillary rise, commonly, transparent columns made of clear glass or plexiglass are utilized, often with a geotextile or filter affixed to the base. This construction permits water passage while retaining the integrity of the material. Traditionally, the predominant method for gauging capillary rise during experiments involves visually estimating the ascent within the column using a ruler or scale (Salim 2016; Xing et al. 2019; Truc et al. 2022). However, owing to its reliance on visual assessment, this method is susceptible to errors. Yet, validation through

gravimetric water content measurements post-experiment offers a degree of assurance (Salim 2016). While this method may suffice in providing estimations of maximum capillary rise height, it primarily yields qualitative insights into the rate of rise.

To augment these conventional approaches, instrumentation for measuring volumetric water content at discrete locations within the columns can offer superior spatial and temporal resolution during capillary rise experiments. This enhancement, complemented by visual observations and post-experiment destructive sampling for gravimetric water content measurement, offers a more comprehensive understanding of the capillary rise phenomenon.

Furthermore, integrating the column onto a weighing balance capable of real-time weight recording enhances measurements by precisely tracking total water imbibition into the column. Continuous monitoring of water content at various locations throughout the capillary rise process not only enhances measurement accuracy but also presents an opportunity to utilize this data in inverse modelling to estimate soil hydraulic properties.

In summary, by combining traditional visual methods with advanced instrumentation and real-time monitoring, researchers can attain a deeper understanding of capillary rise dynamics and leverage this knowledge for improved estimation of soil hydraulic properties.

Capillary rise experiments coupled with investigations on the effects of saltwater discuss the qualitative trends observed for saltwater rise in soil columns, but they fail to provide quantitative data on the changing bulk and pore water electrical conductivity (Xing et al. 2019; Truc et al. 2022). Bulk electrical conductivity is an important factor to consider in studying the effects of soil salinity, however this is often disregarded in column capillary rise experiments.

The bulk electrical conductivity can be quantified with time using TDR. TDR results for conductivity can be further verified using laboratory electrical conductivity (*EC*) meters. This allows researchers to verify the accuracy of TDR in capillary rise experiments as well as gain an

understanding of how the conductivity varies spatially and temporally within the column. Furthermore, the quantified results for conductivity can be used to obtain breakthrough curves and solute transport properties through inverse modelling. The combination of traditional non-instrumented column experiments with advanced instrumentation can be useful in developing models and enhance the understanding of capillary rise and soil salinity.

2.4.2 Time-Domain Reflectometry Limitations

TDR has certain constraints that can impact the output data. TDR does not perform well in highly conductive soils or soils with a high clay content. The maximum bulk electrical conductivity limit for TDR is 5 dS/m, however the results for volumetric water content tend to be higher than the actual value when the bulk electrical conductivity is more than 2 to 3 dS/m. At less than 2 dS/m, the output results by TDR are justifiable (Wyseure et al. 1997).

This limitation can be overcome by using insulated materials along the probe length of TDR. However, this would require additional calibration for the insulated probe (Mojid et al. 1998). For this research, insulated probes are not required as the salt concentrations used remain under the maximum limit of TDR for bulk electrical conductivity.

2.5 Summary

The rise of saltwater due to capillary rise in soils can have detrimental effects on soil structure and hydraulic properties. This phenomenon, known as soil salinization, can significantly alter soil characteristics, impacting agricultural productivity, infrastructure stability, and groundwater quality. Understanding the interplay between soil salinity and capillary rise is crucial for developing effective mitigation strategies.

Traditional capillary rise experiments often rely on visual observations, which can be prone to errors. However, advancements in technology allow for a more robust approach. Time-Domain Reflectometry (TDR) probes can be integrated into capillary rise experiments to provide

continuous and accurate measurements of volumetric water content and electrical conductivity (*EC*) within the soil column.

These TDR equipped experiments offer a significant advantage over traditional methods. By measuring pore water *EC*, researchers can establish a relationship between the bulk *EC* obtained from the TDR and the actual conductivity of the pore water. This improved data acquisition allows for a more comprehensive understanding of the salinity distribution within the soil profile.

While numerous studies have investigated capillary rise and its effects using column experiments, many lack the benefits of instrumented columns. TDR equipped columns offer real-time, high-resolution data on capillary rise, water content, and *EC*. This data can be invaluable for researchers and can be further leveraged through numerical modelling.

By coupling instrumented columns with numerical modelling techniques, researchers can not only improve their understanding of capillary rise dynamics but also estimate crucial soil properties like water retention characteristics and solute transport behavior. These insights can be broadly applied to various environmental concerns related to contaminant transport and groundwater management.

Chapter 3: Capillary Rise Experiments in an Instrumented Column

3.1 Introduction

Capillary rise is described as the rise of liquid in porous media due to cohesion and surface tension forces. Capillary rise of saltwater can have negative consequences as it impacts soil structure and hydraulic properties emphasizing a need to determine the capillary rise and salt concentration in the soil due to capillary rise.

Time-Domain Reflectometry (TDR) measures the travel time of an electronic pulse in a waveguide surrounded by soil. Travel time is used to determine the volumetric water content in real time. TDR can provide simultaneous measurements for the volumetric water content and bulk electrical conductivity of soil with time.

Capillary rise experiments were conducted in a column instrumented with TDR probes to measure the volumetric water content and bulk electrical conductivity of two different sand grades (30/40 and 40/50). The results for water content were verified by comparing the TDR results to the gravimetric results obtained for water content (oven-drying the samples). The bulk electrical conductivity results obtained from TDR were verified by comparing the TDR results to results obtained from a lab *EC* meter. Other laboratory tests conducted included soil characterization tests for specific gravity, hydraulic conductivity, and soil water characteristic curve (SWCC).

The height of capillary rise was estimated using the TDR measured soil water content and analytical solutions from the literature. The results obtained from the capillary rise experiments for water content and time were used to determine the soil hydraulic properties by using inverse modelling employing HYDRUS-1D, a water flow, solute transport, and heat transport software. The estimates of hydraulic properties from inverse modelling were compared with independently measured soil hydraulic properties.

This chapter provides detailed insights into the experimental methodology, alongside a comprehensive explanation of the modelling procedure utilizing HYDRUS-1D. Experimental and modelling results are presented and discussed. The conclusions drawn from the experiments and

modelling indicate that capillary rise experiments instrumented with TDR can be used to estimate soil hydraulic properties.

3.2 Previous Experimental Studies on Capillary Rise

Several researchers have investigated the capillary rise of both freshwater and saltwater, finding generally consistent results across various experimental methods. This section will delve into the methodologies used in previous studies, analyze their findings, and identify any existing knowledge gaps.

Column experiments typically utilize a transparent plexiglass column to house the soil sample. A porous material, such as a stone or geotextile, is placed at the bottom to facilitate water entry. The water solution resides in a separate container, usually a glass tray or tank, positioned below the column (Cwiakala et al. 2012; Salim 2016; Xing et al. 2019; Ramli et al. 2020; Huo et al. 2021; Baldovino et al. 2022; Truc et al. 2022). This is the simplest and most widely used setup to conduct column capillary rise experiments.

In addition, most of the studies on capillary rise rely on visual observations to measure the height of capillary rise by using a scale attached to the column (Cwiakala et al. 2012; Salim 2016; Xing et al. 2019; Huo et al. 2021; Baldovino et al. 2022; Truc et al. 2022). There is a notable deficiency in studies that utilize alternative methods to validate height estimations derived solely from visual observations. While some studies employ destructive sampling after the experiment to determine water content gravimetrically, this approach lacks the ability to capture temporal changes in water content. This temporal data is crucial for quantifying the rate of capillary rise (Salim 2016; Baldovino et al. 2022). Furthermore, destructive sampling is prone to errors as water may drain during the sampling process thus emphasizing a need for a different method to accurately quantify water content changes during a capillary rise experiment.

Ramli et al. (2020) used a simplified image analysis method to estimate the height of capillary rise. This non-intrusive technique analyzes images captured by a camera within a laboratory setup to assess the distribution of water saturation throughout the soil sample. While this method effectively tracked changes in water content over time, the discussion lacked insights into the accuracy of the image analysis system and its applicability in different settings, such as field conditions. Additionally, the limitation of capturing images at 15-minute intervals raises concerns with regards to accurately capturing temporal changes in a column experiment.

Water content sensors can be used to temporally capture the changing water content during a capillary rise column experiment (Hird et al. 2017; Liu et al. 2022). Hird et al. (2017) used TDR probes to quantify the water content in capillary rise experiments and verified those results with gravimetric measurements. TDR probes can capture the waterfront as the water rises through the soil profile which can be used to better understand the movement of water. Liu et al. (2022) incorporated the use of SM3001B temperature and humidity sensors to monitor the water content of capillary water rising in tailing soil samples in a controlled laboratory setting. They used a data acquisition system to record and analyze the experimental results from the sensors. While these sensors can capture the changes in water content in a soil column, the accuracy of SM3001B sensors in a capillary rise experiment was not verified through alternative methods.

Several studies have been carried out to study the rise of salt water in column experiments (Xing et al. 2019; Truc et al. 2022). However, they do not quantify the electrical conductivity or concentration which is crucial in understanding solute transport. Xing et al. (2019) conducted capillary rise experiments using loam soil with four types of chemicals including KCl, NaCl, $CaCl_2$, and $MgCl_2$. They provided insights on how different saltwater mixtures affect the rate of rise, suggesting that increasing concentrations of $CaCl_2$ and $MgCl_2$ did not have a consistent relationship with the rate of rise however increasing concentrations of KCl and NaCl were shown to decrease the rate of rise. They suggested the reason for this could be due to ion interactions

between soil and Ca^{2+} or Mg^{2+}, however further research between soil colloid and chemical ions is needed to confirm this. They did not consider the salt concentration changes within the soil profile.

Truc et al. (2022) investigated the capillary rise of saltwater with varying NaCl concentrations in loose materials like gravel, sand (coarse, medium, and fine), granulated blast furnace slag, and coal bottom ash. Their study emphasizes the importance of understanding salt transport through capillary rise in coastal areas, where it can impact the longevity and load capacity of buildings. They found that increasing salt concentration leads to a decrease in capillary rise, likely due to salt particles blocking soil pores. However, while Truc et al. (2022) provide valuable qualitative insights, their work lacks quantitative data on salt concentration within the soil profile and its impact on bulk and pore water conductivity. Additionally, they don't address how engineers or researchers can utilize these findings to mitigate saltwater effects. Quantifying salt concentration within the soil profile is crucial for informed decision-making regarding strategies to lessen saltwater damage.

There is a lack in research on the effects of saltwater on capillary rise and means to quantify the bulk and pore water electrical conductivities during capillary rise. TDR can be used to not only quantify changes in water content but also bulk electrical conductivity. It can be used in a laboratory or field setting to capture the effects of saltwater in the soil profile due to capillary rise. TDR can also provide insight on the rate of capillary rise as it provides temporal data for water content.

3.3 Experimental Methodology

This section details the materials and experimental setup for the capillary rise experiments, including the methods employed. It covers the determination of initial soil properties and the execution of HYPROP tests. The HYPROP system was utilized to obtain the soil water characteristic curve for the two types of sands used in the experiments.

3.3.1 Materials

The materials used for the capillary rise and HYPROP experiments include silica sand of two different grades including 30/40 sand (passes 0.600 mm and is retained on 0.425 mm sieve) and 40/50 sand (passes 0.425 mm and is retained on 0.300 mm sieve). The sand was supplied by Bell & Mackenzie. It was sieved to achieve the designated grades. The sand is white in appearance and predominantly consists of silicon dioxide, as reported by the supplier. The chemical composition of the sand is shown in Table 3.1 below.

Table 3.1: Chemical composition of silica sand, retrieved from Vieira Concrete Supplies (n.d)

Chemical	**Percentage (%)**
Silicon Dioxide	94.85
Iron Oxide	0.21
Aluminum Oxide	2.81
Calcium Oxide	0.21
Magnesium Oxide	0.09
Clay Content	<0.10
Loss on Ignition	<0.50
Sodium Oxide	0.29
Potassium Oxide	<0.01

Laboratory NaCl salt in fine crystal form with a purity of 99% was supplied by Avantor VWR and used for the saltwater capillary rise experiments. Below in Table 3.2 are the salt properties retrieved from the safety data sheet provided by Ward's Science (supplier for Avantor VWR).

Table 3.2: NaCl physical and chemical properties, retrieved from Ward's Science (2013)

Property	**Percentage (%)**
Molecular Formula	NaCl
Description	White solid fine crystals
Melting/Freezing Point	801℃
Boiling Point	1465℃
Relative Density	2.16 g/ml at 25℃
Solubility	1 g per 2.8 ml water at 25℃
Molecular Weight	58.45 g/mol

3.3.2 Specific Gravity Determination

Specific gravity is a comparison between the density of a substance to a reference substance such as water. Specific gravity is needed to calculate various soil properties such as porosity or

dry density. The specific gravity was determined using the pycnometer method outlined in ASTM D854. The specific gravity for both sands (30/40 and 40/50 grades) was found to be 2.65.

3.3.3 Hydraulic Conductivity Determination

The hydraulic conductivity was determined using the falling head method as per ASTM D5084. The sample density was 1.68 g/cm^3 and 1.60 g/cm^3 for the 30/40 and 40/50 sands, respectively. The test was repeated 10 times for each sand to achieve an average conductivity using 10 replicates for each sand. The 30/40 sand had a conductivity of 8.28×10^{-3} cm/s with a standard deviation of 0.001 and coefficient of variance of 0.15 whereas the 40/50 sand had a conductivity of 1.36×10^{-3} cm/s with a standard deviation of 0.0003 and coefficient of variance of 0.23. The 40/50 sand was found to have a lower hydraulic conductivity due to its finer particle size as well as increased tortuosity of flow. Finer soils typically have smaller pore spaces in comparison to coarse grained soils, meaning that water will encounter narrow and tortuous pathways, owing to a lower hydraulic conductivity.

3.3.4 Measurement of Soil Water Characteristic Curve using HYPROP

HYPROP by the Meter Group was used to measure the soil water characteristic curve (SWCC) for the two sands used. The procedure for setting up the HYPROP experiments is outlined in the user manual provided by Meter Group (Meter Group, 2018). HYPROP uses a simplified evaporation method to measure the SWCC as it records the changes in water content and suction with time as the water evaporates from the soil sample.

Figure 3.1 depicts a schematic diagram of the HYPROP set up. The components included within the HYPROP set up include a sensor unit, balance, and a control unit. The soil sample and two tensiometers are held in the sensor unit. The tensiometers are responsible for measuring the suction within the soil sample. The sensor unit is placed over a balance which records the changes in mass of the sample. The balance is connected to a control unit (LABROS Soil View Program) which records the data from the tensiometers as well as the balance.

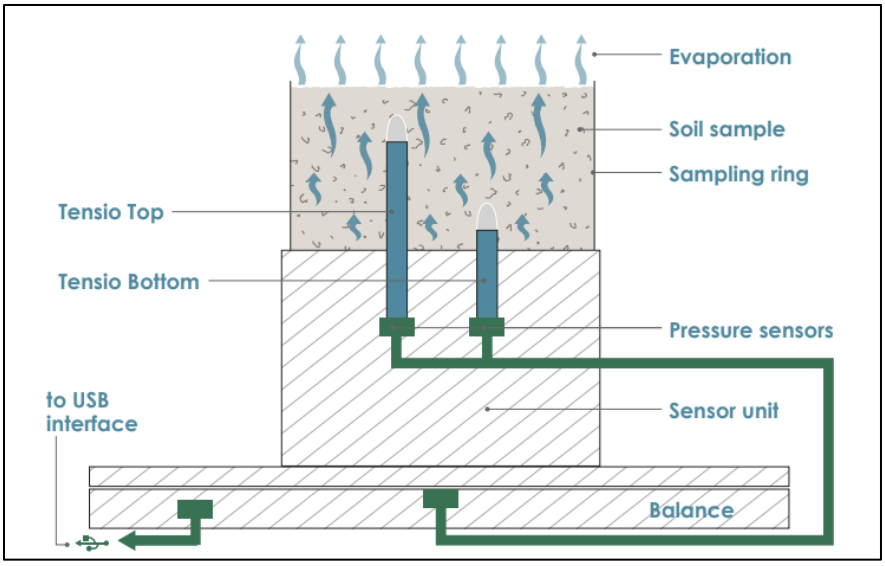

Figure 3.1: Schematic diagram of the HYPROP set up, modified from Meter Group (2018)

Figure 3.2 shows the experimental set up for the HYPROP experiment. The general methodology consists of preparing the soil sample in the sampling ring and saturating it with degassed water. The tensiometers along with the sampling ring are then placed on the sensor unit as pictured in Figure 3.2. The measurement system allows the water in the soil to evaporate with time. The LABROS Soil View program records the change in weight and tension in the bottom and top tensiometers with time. This data can then be used to obtain retention and conductivity data which can be fitted to retention models such as Brooks and Corey, van Genuchten, and Fredlund-Xing.

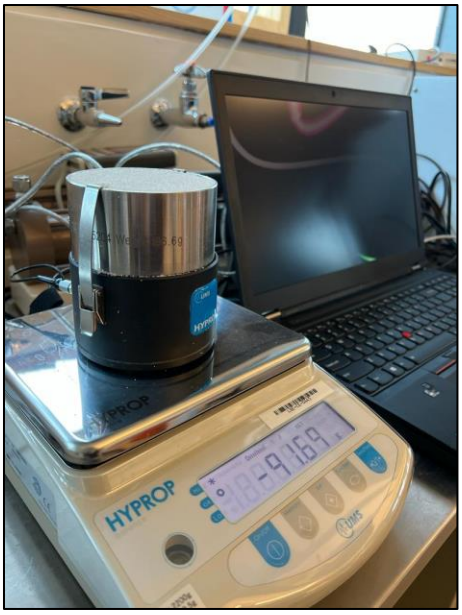

Figure 3.2: Experimental set up used for the HYPROP experiments

Soil Water Retention Curve (SWRC) Fit online program was used to fit the suction and water content experimental data to SWCC models (Seki 2007). The following model by van Genuchten (1980) was used:

$$S_e = \frac{\theta - \theta_r}{\theta_s - \theta_r} = [1 + (\alpha|\psi|)^n]^{-m} \quad [3.1]$$

where, S_e is the effective saturation, θ is the volumetric water content, θ_r and θ_s are the residual and saturated water contents respectively, α is a parameter that is the inverse of the air-entry value, ψ is the suction potential, *n* is a fitting parameter related to the pore size distribution, and *m* is a fitting parameter and can be found by using *n* as follows:

$$m = 1 - \frac{1}{n} \quad [3.2]$$

The experimental results and the fitted van Genuchten models are shown in Figure 3.3 below for both sands. The 40/50 sand is observed to have a higher air entry value in comparison to the 30/40 sand grade. This can be attributed to the smaller pores in the 40/50 sand, owing to smaller

particle size. The air entry value can be estimated to occur at a volumetric water content of 37.7% and 38.4% and suction head of 14 cm and 18 cm for the 30/40 and 40/50 sands, respectively. The R^2 value for both fits is 0.99, indicating that the experimental data fits the models accurately.

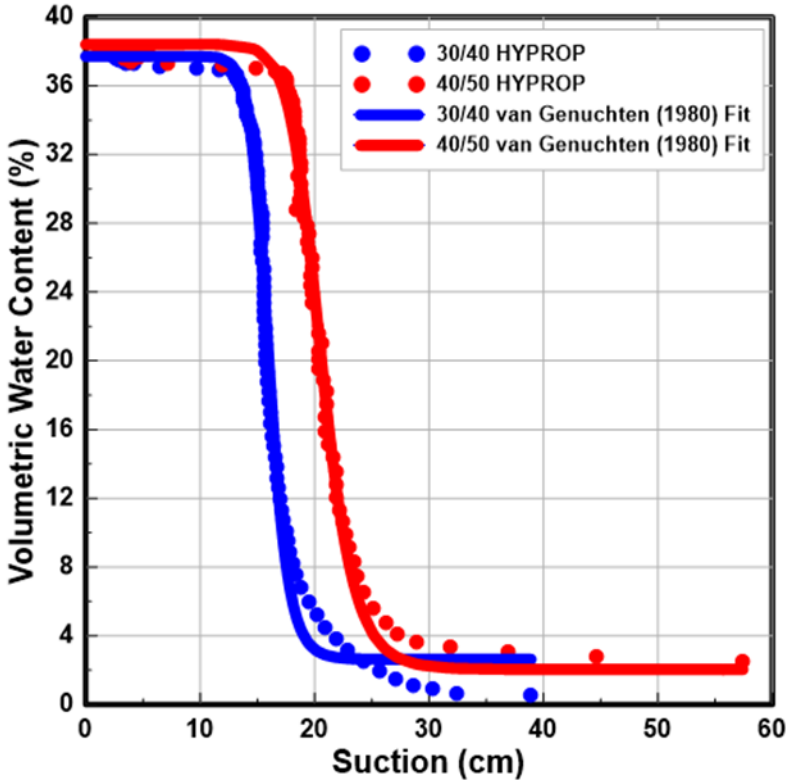

Figure 3.3: SWCC obtained from HYPROP and fitted to van Genuchten (1980) for the 30/40 and 40/50 sands

3.3.5 Experimental Set Up for Capillary Rise Experiments

The experimental set up for the capillary rise experiments includes several components such as plexiglass column, glass tray for holding water, TDR measurement system manufactured by Campbell Scientific, Mettler Toledo MS16000L scale, and a lab *EC* meter TetraCon® 925 with an accuracy of $\pm$ 0.5%. Other materials include silica sand, laboratory NaCl salt, and deionized water.

Figure 3.4 shows a schematic diagram of the experimental set up. The column used to house the soil sample is 40.5 cm in height with an inner diameter of 9.5 cm. A stand is used to hold the soil column with chain clamps that attach to the column. The stand sits on top of the Mettler Toledo scale so that the mass of water entering the column is recorded. The water solution is held in a glass tray that sits overtop a jack stand. Two TDR CS640 probes are inserted into the column which are connected to a multiplexer (SDM8X50). The multiplexer is connected to the TDR100 and datalogger, CR800. TDR100 is responsible for generating and sending an electromagnetic pulse through the cable. Multiplexers allow for more than one probe to be attached to the system. The data from the scale and TDR system is logged into a laptop.

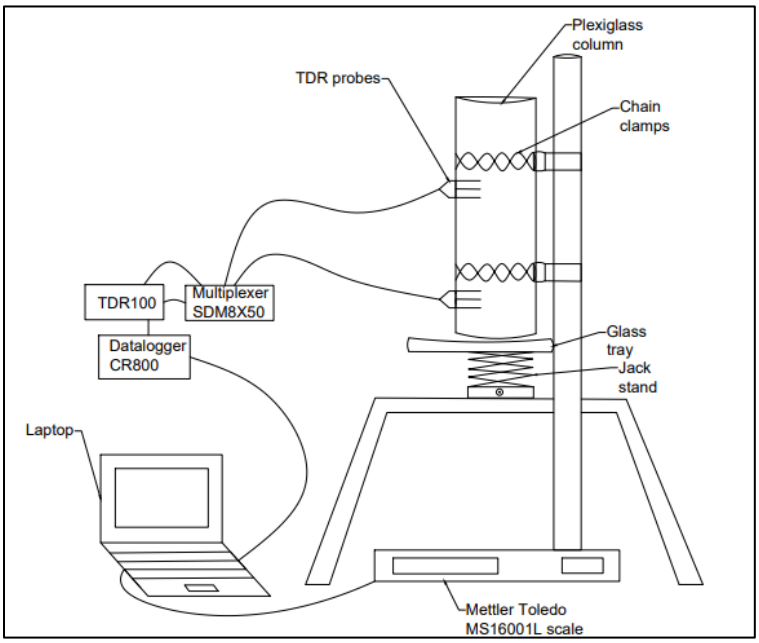

Figure 3.4: Schematic diagram of capillary rise experimental setup

The probes used in this research are the CS640 probes which have an accuracy of $\pm$ 2.5% for volumetric water content. The probe length and diameter are 7.5 cm and 0.16 cm, respectively. The probes are placed in the column at 5 cm and 12 cm from the bottom, respectively. This placement was chosen to leave an adequate amount of distance between the probes to avoid interference of signals and to accommodate for the anticipated capillary rise for each grade of

sand. It should be noted that the column used in this experimental set-up was chosen specifically to accommodate the probe dimensions and sensing region. Each probe has a sensing region equivalent to the volume of a cylinder around the center rod with diameter equivalent to the rod spacing (1.5 cm in this case) (Limsuwat et al. 2009). This means that the TDR at 5 cm can sense from 2 cm to 8 cm of the column height and the probe at 12 cm can sense from 9 cm to 15 cm of the column height. An adequate amount of space (at least 2 cm) needs to be left at the rod ends to ensure there is no interference from the other end of the plexiglass column. Columns with larger diameters may not be able to get representative readings from the TDR due to the limitations of the sensing region. Furthermore, the addition of extra probes was not possible (for this specific column height) as the probes would interfere with each other (given the large sensing range of each probe), leading to inaccuracies in results.

The experimental protocol consists of various steps. Firstly, the sand was prewetted to 1.5% gravimetric water content and sealed in a plastic bag for 24 hours to ensure the water content can become homogenous and to avoid particle segregation when packing the sand. One cup of sand which translates to 120 g of sand is packed at a time into the column and compacted for one minute. After which the top of the sand layer is scarified, and another cup of sand is added to the column. This process is repeated until the entire batch of sand is compacted into the column. Then the TDR probes can be inserted into the column at 5 cm and 12 cm, respectively.

After the probes are placed, the column can be attached to the stand using chain clamps. The column should be leveled using a level. The solution needs to be prepared and placed into the glass tray which sits on top of the jack stand. The solution can be prepared by taking deionized water and then adding the desired salt amount to the solution. A glass stirring rod can be used to stir this mixture to ensure the solution is mixed well. The solution's electrical conductivity can be checked using the TDR probes and the lab *EC* meter. A minimum of 36 mm of the tip of the *EC* meter needs to be immersed in the solution to get a reading.

After this, the jack stand can be moved upwards so that the water in the tray can form a connection with the bottom of the column. The scale and probes need to be directly connected to their respective data logging software programs on the laptop before starting the test and mounting the jack stand to ensure that the data is being recorded.

EasyDirect software is used to record the mass data from the Mettler Toledo scale. The mass of water going into the column is recorded through this software and is later processed. LoggerNet is used to retrieve the data that is sent to the CR800 datalogger. The capillary rise experiments were run for 6 days. The experiment was terminated when the change in water mass entering the system was less than 5 g per day. Post experiment, the column is split into 3 cm thick slices which are later oven dried to gravimetrically determine the amount of water that went into the column. The slices are cut using a knife and then taken out into pans. The weight of the wet soil is taken after which the pans are placed in the oven at 105℃ and left to dry for 24 hours. Before placing the samples in the oven to dry, the electrical conductivity of each slice was measured using a lab *EC* meter. These values were recorded and compared to bulk electrical conductivity values reported by the TDR system.

Soil properties measured for each experiment include dry density and porosity. The average dry density for the 30/40 sand was 1.69 g/cm^3 with a standard deviation of 0.02 between various experiments whereas the average porosity was 0.365 with a standard deviation of 0.01. For the 40/50 sand, the average dry density was also 1.69 g/cm^3 with a standard deviation of 0.01 and average porosity of 0.363 with a standard deviation of 0.003. This suggests variation in packing density and porosity between experiments were minimal for both sand grades.

3.4 Experimental Results and Discussion

The results obtained from the capillary rise experiments along with analysis and modelling results are presented in this section. The capillary rise experimental results include the water content results from TDR and gravimetric method, and the electrical conductivity results from the *EC*

meter and TDR. The height of capillary rise was obtained using the mass balance results as well as the TDR results which were then compared to analytical relationships. Furthermore, the rate of capillary rise was calculated and compared to relationships proposed by Terzaghi (1943) and Lu & Likos (2004).

3.4.1 Results for Volumetric Water Content

The volumetric water content obtained from TDR experiments is plotted against the time in Figure 3.5 and Figure 3.6 for the 30/40 and 40/50 sands, respectively. In Figure 3.5, the arrival time of the wetting front at a location of 5 cm from the bottom of the column for the 30/40 sand is on average at 80 seconds after which a peak in water content is observed. The water content then reaches equilibrium around 2 days, attaining a water content of 30% at location 5 cm and 17% at location 12 cm from the bottom of the column.

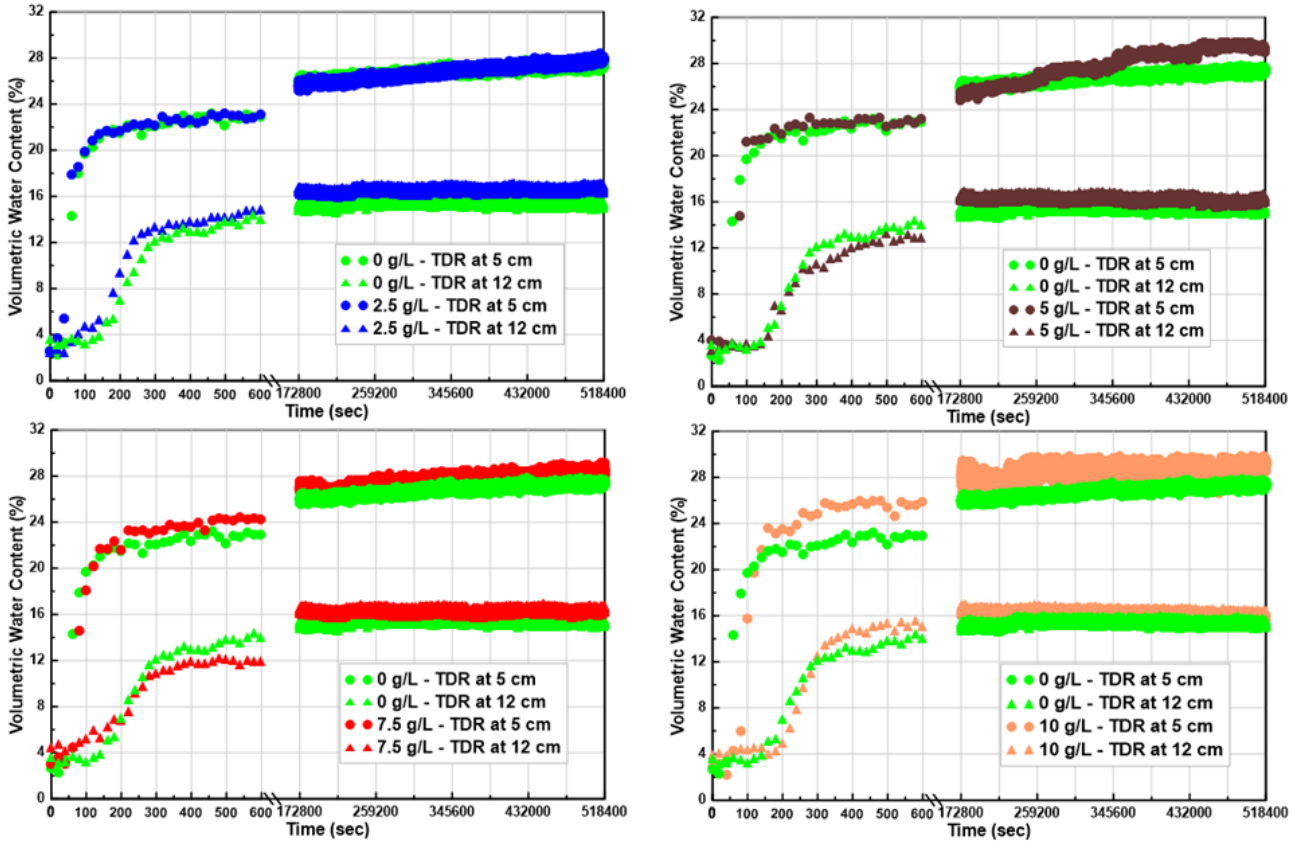

Figure 3.5: TDR volumetric water content (%) vs. Time (sec) for 30/40 sand

In Figure 3.6, the arrival time of the wetting front in the 40/50 sand is at around 80 seconds for the 0 g/L to 7.5 g/L experiments, whereas the 10 g/L experiment shows the arrival time of the wetting front to be approximately 100 seconds. The equilibrium water content is observed to be 32% at location 5 cm and 20% to 24% at location 12 cm from the bottom of the column. The 10 g/L experimental results at the 5 cm location was shown to have some fluctuations in data possibly due to the TDR limitations for electrical conductivity; therefore the running average was plotted in Figure 3.7 using a sample window of 5, which helped to reduce the dispersion of data.

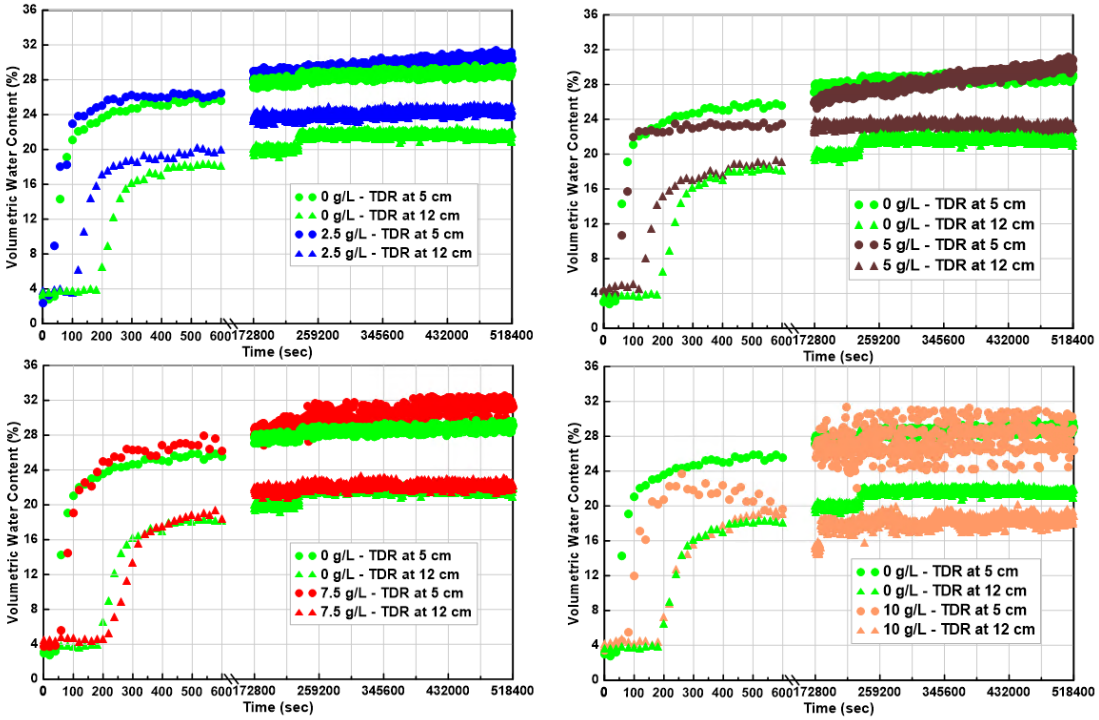

Figure 3.6: TDR volumetric water content (%) vs. Time (sec) for 40/50 sand

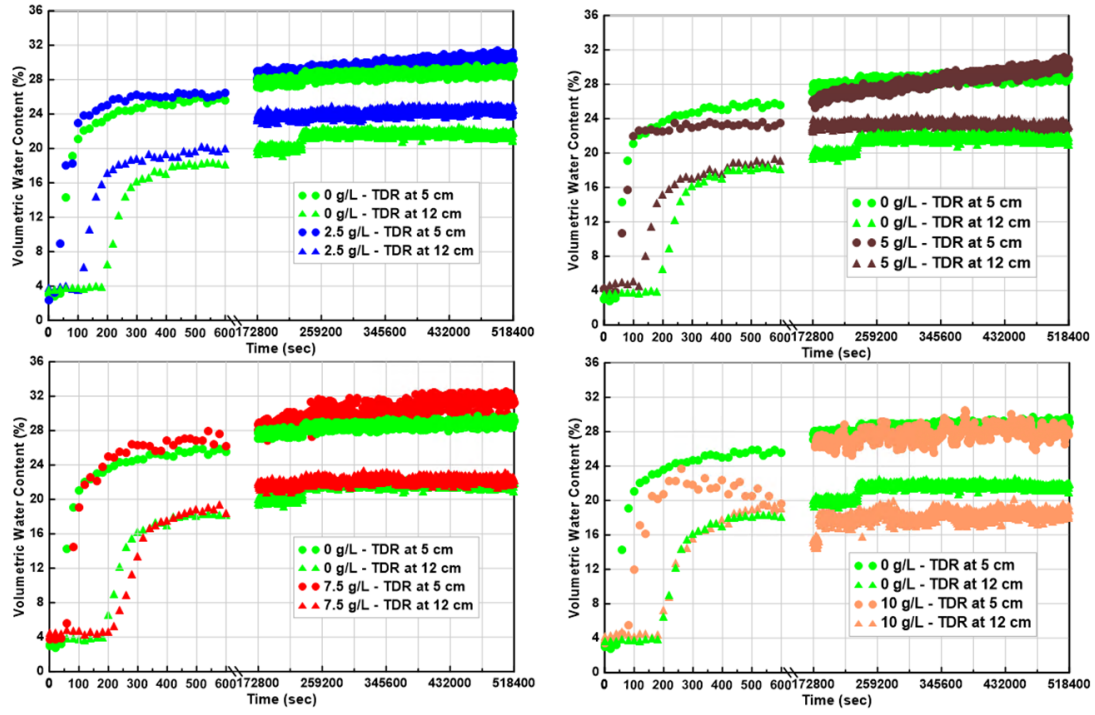

Figure 3.7: TDR volumetric water content (%) vs. Time (sec) for 40/50 sand, using running average for 10 g/L experiment

The location of the two TDRs can give an indication of the height of capillary rise reached. As mentioned previously, the TDR located at 5 cm has a sensing range that covers 2 cm to 8 cm of the column height from the bottom of the column and up whereas the TDR at 12 cm has a sensing range of 9 cm to 15 cm. Since the second TDR at 12 cm, records a water content of at least 17% for both sands, it suggests that water had reached the column at a height of at least 15 cm above the base of the column, thereby confirming capillary rise to be at least 15 cm for the two sands (using the upper limit of the sensing range).

The gravimetric water content was determined at different heights of the column so that the water distribution within the entire soil profile may be determined. The gravimetric results for water content along with dry density were used to obtain the volumetric water content. The results indicated that the water reached a height of at least 16 cm for the 30/40 sand and 20 cm for the 40/50 sand in the column as shown below in Figure 3.8 and Figure 3.9 where the water content is plotted with the depth for both 30/40 and 40/50 sands, respectively. Figure 3.8 and Figure 3.9 also include the SWCC measured with the HYPROP system and the SWCC obtained using the volumetric water content (from gravimetric results) and depth for each respective sand grade. Hydrostatic conditions are assumed, and that the matric suction is equivalent to the height above the groundwater table.

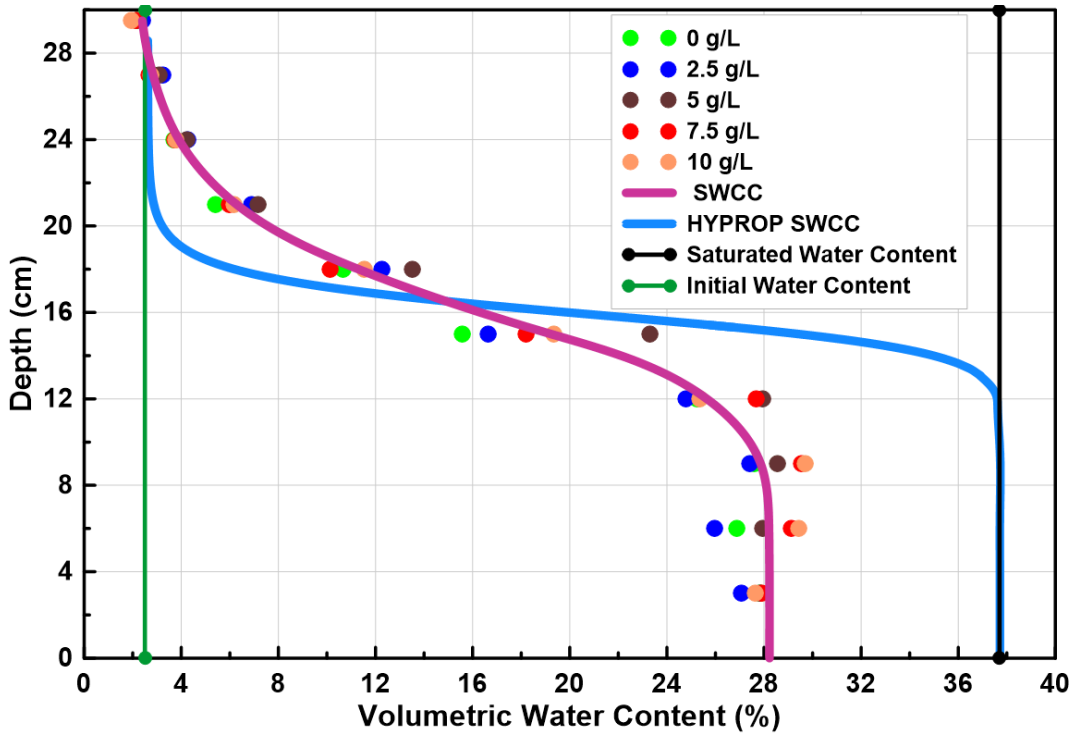

Figure 3.8: Volumetric water content (%) vs. Depth (cm) for 30/40 sand

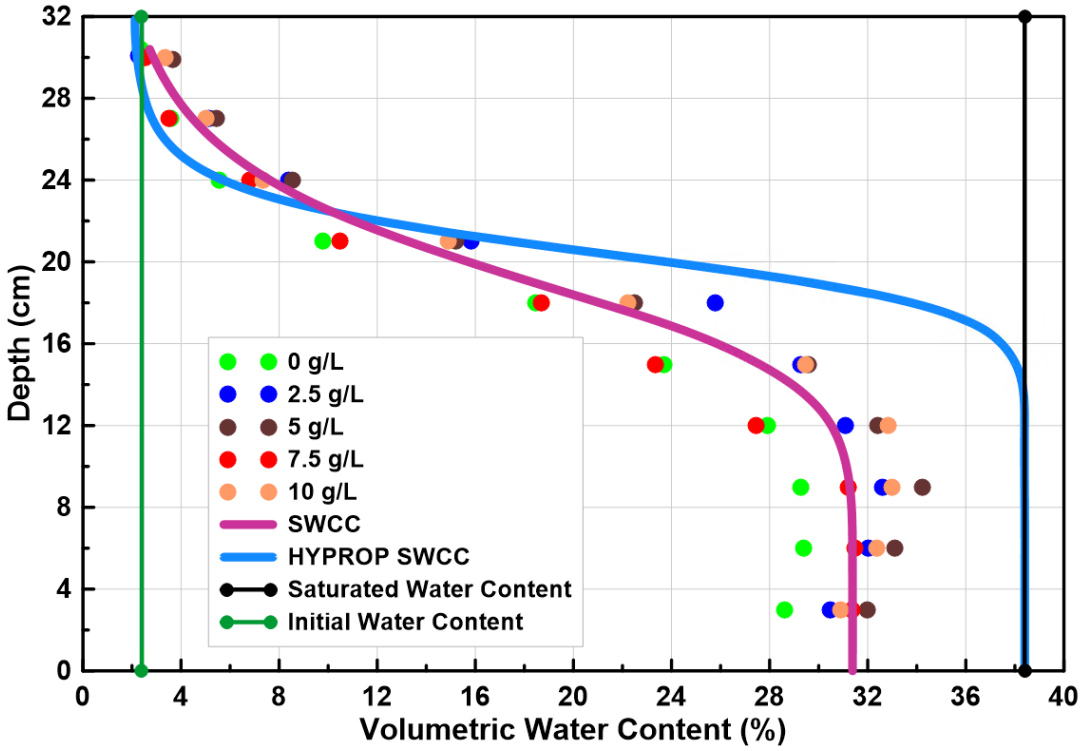

Figure 3.9: Volumetric water content (%) vs. Depth (cm) for 40/50 sand

In Figure 3.8, the 30/40 sand shows a maximum of 28% to 30% water content is reached around a depth ranging from the bottom of the column at 0 cm to 12 cm. The water content is 12% to 20% around a height of 16 cm to 18 cm which confirms that the water reached a height of at least 16 cm. The water content is shown to decrease as the depth increases. Increasing salt concentration is not observed to have a significant impact on the height of the capillary rise which can be due to the fact that the range of concentrations tested were relatively small (2.5 to 10 g/L) in comparison to the solubility limit of NaCl (360 g/L).

In comparison with the HYPROP measured SWCC, the SWCC obtained using the average experimental water content and depth (assuming suction is equivalent to the height above groundwater table) shows correlation with all 5 experiments as well as the measured SWCC, with the only major difference being in the saturated water content. It is observed that the experimental results exhibit lower saturated water contents with a maximum of 30% versus the 37.7% saturated water content measured by HYPROP, which can be due to the presence of air entrapment that hinders the movement of water through the soil pores. This shows that gravimetrically obtained SWCC can be used to obtain soil hydraulic properties in the case that one cannot measure SWCC.

Figure 3.9 shows the 40/50 sand reached a maximum of 28% to 32% water content at a depth ranging from 0 cm from the bottom of the column to 14 cm. The water content is 12% to 16% around a height of 20 cm to 22 cm which shows that the water reached a height of at least 20 cm. The SWCC measured using HYPROP shows that the saturated water content is higher (38.4%) than the saturation achieved in the capillary rise experiments (32%). This difference can be attributed towards air entrapment effects as well as the fact that HYPROP uses a simplified evaporation method and dries a carefully saturated sample to measure the soil retention properties, thus resulting in a higher saturated water content.

Gravimetric water content measurements along the soil profile can be used to obtain the SWCC and correlated with the capillary rise model in soils. It can help to identify the retention properties of soils. The TDR results for water content coupled with gravimetric results and visual observations show that the height of capillary rise reached at least 16 cm and 20 cm in the 30/40 and 40/50 sands, respectively.

Furthermore, gravimetric water content results can be used to verify the TDR results. Figure 3.10 shows the maximum water content obtained from TDR plotted against those obtained through the oven dry method for each experiment conducted along a direct variation line. The volumetric water contents measured at 5 cm for each sand grade plot closely to the direct variation line verifying the accuracy of the TDR in measuring water content. The water content measured at 12 cm for the 40/50 experiment shows some variation which may be because the oven dry results were averaged at the location where the TDR at 12 cm was located to account for the sensing range of the TDR. The Pearson correlation coefficient was obtained to compare the two water content methods which showed that at the 5 cm location, the correlation coefficient was 0.9 for the 30/40 sand and 0.8 for the 40/50 sand, suggesting good correlation between the two measurement methods. At the 12 cm location, the correlation coefficient was 0.4 for the 30/40 sand and 0.3 for the 40/50 sand. Differences at the 12 cm location are attributed towards the fact that average water contents along the column height were used to account for the sensing range of the TDR which may not be representative of the reading from TDR. Generally, the results plot closely to the direct variation line suggesting the accuracy of TDR in estimating water content.

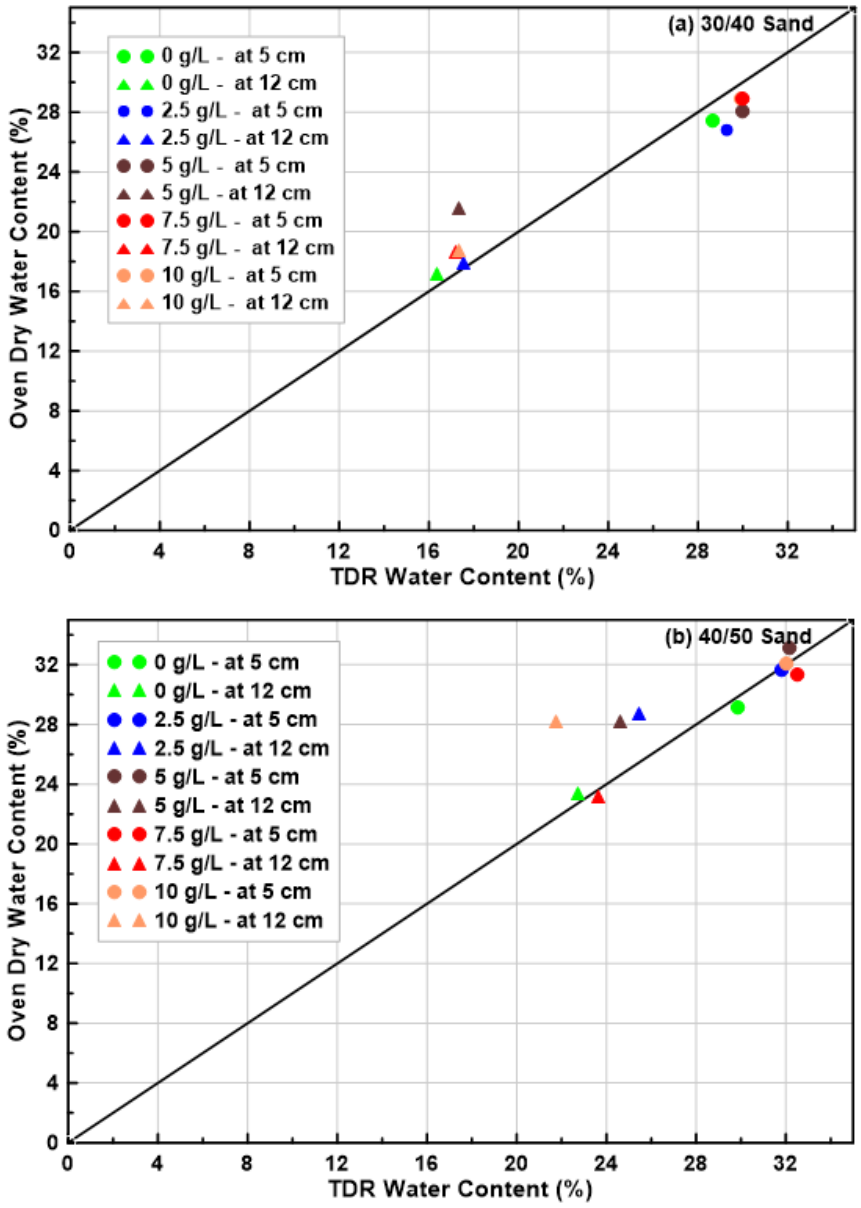

Figure 3.10: Oven dry water content (%) vs. TDR water content (%) for the (a) 30/40 sand, and (b) 40/50 sand

3.4.2 Results for Solution and Bulk Electrical Conductivity

Prior to imbibing the solution in the column, the solution electrical conductivity of each salt concentration solution was measured using TDR as well as a lab *EC* meter for validation. The solution electrical conductivity ranged from 5 dS/m to 19 dS/m for salt concentrated solutions

whereas for deionized water, electrical conductivity was measured as 0 dS/m. Figure 3.11 below shows a comparison between the solution electrical conductivity measured by the lab *EC* meter and TDR for both sand grades tested. Generally, the data points plot closely to the direct variation line showing that TDR can accurately measure solution electrical conductivity.

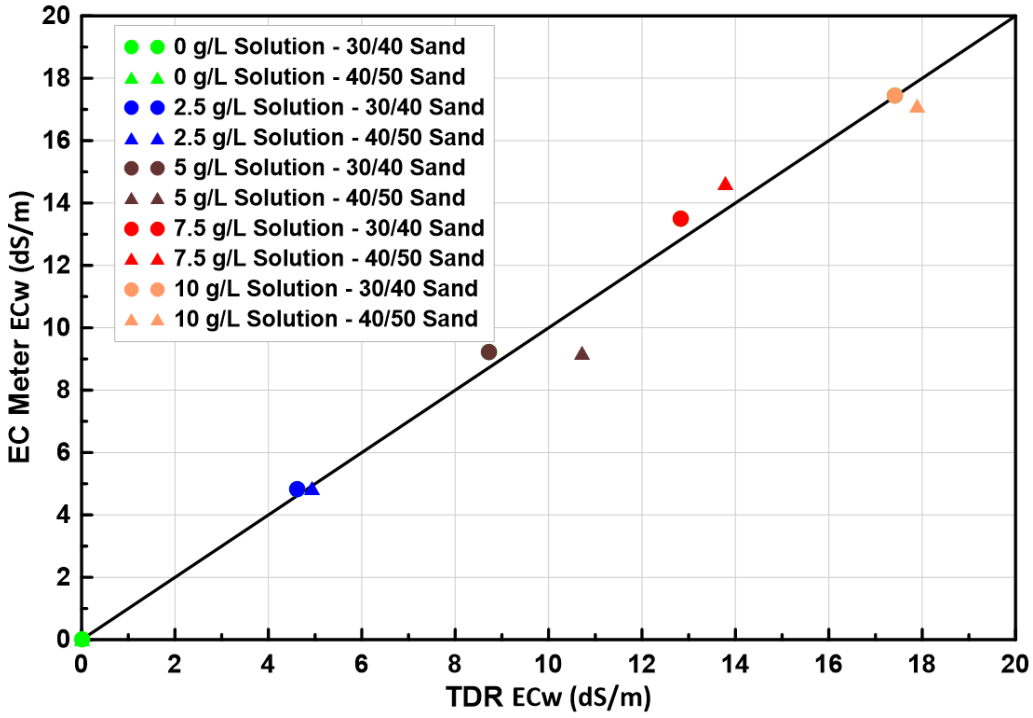

Figure 3.11: EC meter solution ECw (dS/m) vs. TDR solution ECw (dS/m)

In Figure 3.12, the bulk electrical conductivity (EC_b) measured by TDR is plotted with time for the 30/40 sand. The EC_b is shown to increase from 0 dS/m to a maximum of 2.4 dS/m as the salt concentration increased from 0 g/L to 10 g/L. The TDR located at 5 cm shows EC_b increased from 0 dS/m to 2.4 dS/m whereas the TDR located at 12 cm shows EC_b increased from 0 dS/m to 0.7 dS/m. Generally, the observed trend is that as the salt concentrated solution increased from 0 g/L to 10 g/L, the EC_b also increases. Since the bottom of the column is more saturated, the EC_b is also higher at that location as more salt concentrated water is near the bottom.

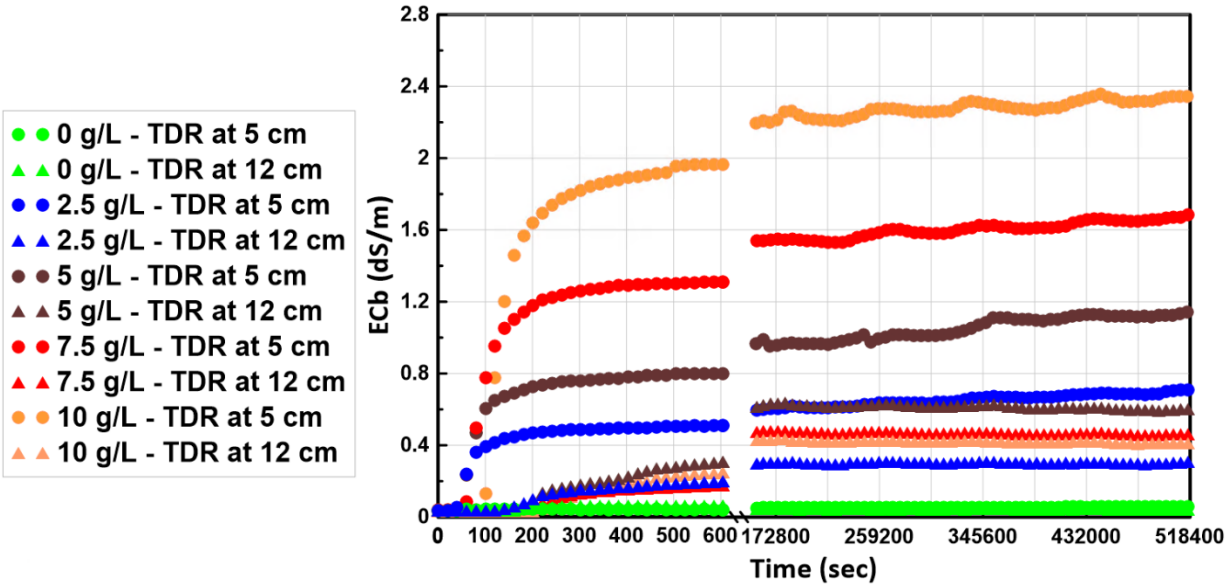

Figure 3.12: Bulk electrical conductivity (dS/m) vs. Time (sec) for 30/40 sand

In Figure 3.13, the 40/50 sand TDR results for bulk electrical conductivity and time are shown. The EC_b is shown to increase from 0 dS/m to 2.8 dS/m as the salt concentration is increased. The TDR located at 5 cm shows that at a column height of 5 cm, the EC_b increases from 0 dS/m to 2.8 dS/m as salt concentration is increased whereas the TDR located at 12 cm shows EC_b increases from 0 dS/m to 2 dS/m. There is a spike in EC_b for the TDR located at 12 cm for the 10 g/L experiment which could be because the 40/50 sand is finer and more salt concentrated water went into the column thus showing an increase in the EC_b. However, this could also be an overestimation made by TDR as Wyseure et al. (1997) reported that as the EC_b approaches 3 dS/m, the data may show more fluctuations in water content and EC_b.

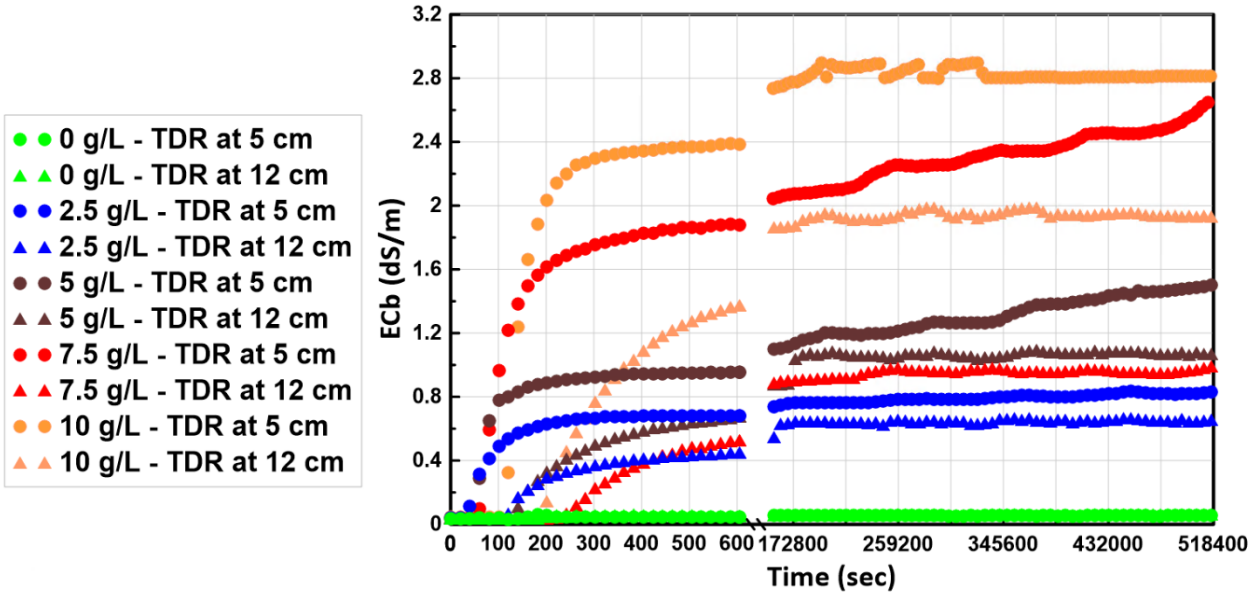

Figure 3.13: Bulk electrical conductivity (dS/m) vs. Time (sec) for 40/50 sand

The bulk electrical conductivity of the samples was measured using a lab *EC* meter upon completion of the experiments. The EC_b of the samples located at 5 cm were graphed along a direct variation line along with the EC_b measured by the TDR located at 5 cm as shown in Figure 3.14 below for both sands. The same was done for the TDR located at 12 cm.

From the above experimental results, it can be concluded that TDR can be used to estimate volumetric water content in a column experiment as well as bulk electrical conductivity. However, the bulk electrical conductivity may fluctuate as the concentrated solutions reach the limitation of the TDR. The result for the 40/50 experiment 5 (10 g/L) at 12 cm shows the greatest deviation between *EC* meter and TDR results which can be due to the fact that TDR results fluctuate as the limiting EC_b of TDR is reached as well as the fact that the *EC* meter does not get an accurate reading if the sample is not very saturated. The *EC* meter may not have been able to get a representative reading as it reads only the *EC* of the sample it is immersed in whereas the TDR outputs the average EC_b along the length of the probe. The Pearson correlation coefficient was obtained to compare the bulk electrical conductivities measured using the two methods which showed that at the 5 cm location, the correlation coefficient was 1.0 for both sands, suggesting a

high correlation. At the 12 cm location, the correlation coefficient was 1.0 for the 30/40 sand and 0.6 for the 40/50 sand. Generally, TDR is observed to have higher measurements of the EC_b in comparison to the *EC* meter results, but overall, the EC_b results correlate between the *EC* meter and TDR.

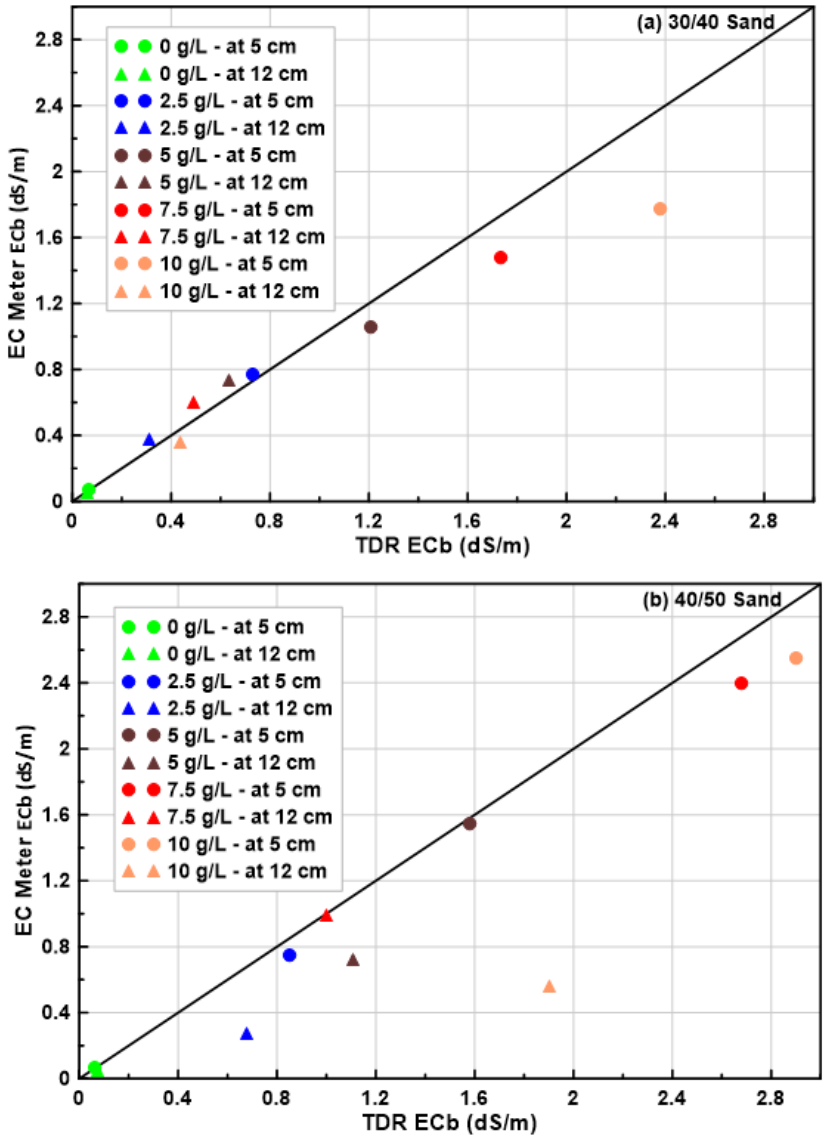

Figure 3.14: EC meter ECb (dS/m) vs. TDR ECb (dS/m) for (a) 30/40 sand, and (b) 40/50 sand

3.4.3 Determining Height and Rate of Capillary Rise Using Experimental Results and Analytical Solutions

The TDR locations were chosen such that the expected capillary rise for both sand grades could be estimated. Experimental results and observations for the height of capillary rise were compared with empirical relationships that can be used to estimate the theoretical maximum capillary rise.

Table 3.3 summarizes the soil properties that were used to determine the theoretical maximum capillary height that was found for both sands used for the experiments, using relationships reported in literature. Note that the salt concentrations used in the capillary rise experiments were small and therefore the density effects of the salt concentrated solutions in comparison to the control test with deionized water were minimal (0.25% - 1% difference). Therefore, the density reported below only considers the control test.

Table 3.3: Properties used to determine height of capillary rise

Properties	**30/40 Sand**	**40/50 Sand**
Surface Tension, σ (mN/m)	72.8	72.8
Contact Angle, γ	0	0
Density of Liquid, ρ (g/cm^3)	1	1
Gravitational Acceleration, g (cm/s^2)	981	981
Radius of Column, r_c (cm)	4.75	4.75
Effective Grain Diameter, d_{10} (mm)	0.43	0.30
Porosity, n (obtained using dry density from column experiments)	0.365	0.363
Air Entry Head, h_a (cm) (from HYPROP measured SWCC)	14	18

Effective Pore Radius, r_e (cm) *Retrieved from McGinnis (2001)	0.011	0.009
Void Ratio, *e*	0.575	0.570

The theoretical maximum capillary height is summarized in Table 3.4 below. Details on these relationships can be found in Chapter 2. The theoretical maximum capillary height ranges from 4.1 cm to 94.7 cm for the 30/40 sand and 5.8 cm to 103.9 cm for the 40/50 sand.

Table 3.4: Maximum theoretical capillary height

Maximum Theoretical Capillary Height (cm)					
Sand Grade	**Polubarinova - Kochina (1962)**	**Jurin's Law**	**Jurin's Law (using $r = 0.2d_{10}$)**	**Peck et al. (1974)**	**Kumar and Malik (1990)**
30/40	18.4	13.4	17.3	4.1 - 20.5	94.7
40/50	26.3	16.3	24.5	5.8 - 29.2	103.9

The values reported in Table 3.4 were compared to the maximum capillary rise observed during the experiments through visual inspection of a scale attached to the column. The capillary rise observed is summarized in Table 3.5 below. The theoretical capillary height estimated using empirical relationships was generally higher than those observed in the experiments. Jurin's Law and Polubarinova-Kochina (1962) provide the closest estimates of capillary height to those height values observed visually and those obtained from gravimetric results (16 cm for 30/40 and 20 cm for 40/50 sand). Kumar & Malik (1990) relationship shows the highest deviation from experimentally obtained capillary heights. This relationship uses the air-entry head to obtain the capillary height, and the air-entry head was obtained using the measured SWCC from HYPROP, which may not be able to accurately represent the air-entry head from the capillary rise experiments. The use of such empirical relationships can only be used to provide a general estimation. However, they do not capture the true height as shown in visual observations. The observed capillary heights showed that as the salt concentration increased, the capillary height

decreased by 1 - 2 cm. Capillary rise estimates from the measured SWCC was estimated as 14 cm and 18 cm for the 30/40 and 40/50 sand, respectively which is close to visual observations. Furthermore, the capillary height values obtained through gravimetric results correlate closely with those heights obtained visually. McGinnis (2001) conducted capillary rise column experiments using 30/40 and 40/50 sand grades. The capillary height reported was 12 cm and 16 cm for the 30/40 and 40/50 sand grades, respectively (McGinnis, 2001). These results show agreement with the observed capillary heights from this research (within ± 2 cm).

Table 3.5: Observed experimental capillary height

Sand Grade	**Observed Capillary Height (cm) for each Solution Concentration**				
	0 g/L	**2.5 g/L**	**5 g/L**	**7.5 g/L**	**10 g/L**
30/40	14	14	14	14	13
40/50	17	17	15	15	15

The capillary height with time can be verified using analytical solutions. McGinnis (2001) uses the mass with time data to estimate the capillary height over time. The following equation can be used to obtain the capillary height (h_c):

$$h_c = \frac{m_i}{\pi r_c^2 \rho \phi} \quad [3.3]$$

where, m_i is the mass of water, r_c is the radius of the column, ρ is the density of the liquid and ϕ is the porosity. The mass balance results were used to estimate the changing capillary height with time along with the TDR locations. The time at which the TDR detects a change in the water content can be taken as the time at which the water first arrives at that particular TDR location.

The experimental results for the height of capillary rise with time (using TDR locations and mass balance results) can be used to obtain the rate of rise which can then be compared to the analytical solution for the rate of capillary rise by Terzaghi (1943) and Lu & Likos (2004). The Terzaghi (1943) equation for the rate of capillary rise assumes that Darcy's Law is valid for

unsaturated flow and that hydraulic gradient can be calculated using the difference between the capillary rise and wetting front divided by the wetting front. Terzaghi (1943) and Lu & Likos (2004) relationships can be found in Chapter 2 as equations 2.8 and 2.11, respectively.

The Lu & Likos (2004) equation was solved using the Lerch transcendent function in Wolfram Mathematica (Weisstein, 2024). The Lerch transcendent, also known as Lerch Phi function, is as follows:

$$\Phi(w,s,a) = \sum_{j=0}^{\infty} \frac{w^j}{(j+a)^s} \quad [3.4]$$

where, *w*, *s*, and *a* are complex numbers. This function is a general form of the Hurwitz zeta function and polylogarithm function (Erdélyi, et al. 1953, Weisstein, 2024).

The Lu & Likos (2004) equation can be inputted into Wolfram Mathematica, where the Lerch Phi function can be used to solve the equation. The Lu & Likos (2004) equation can be written in series form in Mathematica as follows:

$$\{t[\phi,\alpha,h_c,k_s,z], Sum[\frac{\phi\alpha^j({h_c}^{1+j}Log[\frac{h_c}{h_c-z}]+(\frac{h_c}{z})^{-1+j}z^{1+j}((\frac{z}{h_c})^j LerchPhi[\frac{z}{h_c},1,2+j]+\frac{{h_c}^2 Log[\frac{h_c-z}{h_c}]}{z^2}))}{k_s j!}, \{j,0,\infty\}]\} \quad [3.5]$$

where, the parameter *t* is the arrival time of the wetting front, ϕ is porosity, α is the inverse of the air-entry head, h_c is the height of capillary rise, k_s is the saturated hydraulic conductivity, and *z* is the wetting front.

The porosity calculated based on the soil dry density (for capillary rise experiments) was 0.365 and 0.363, for the 30/40 and 40/50 sand, respectively. This is equivalent to the saturated water content (at 100% saturation, volumetric water content is about 36%). However, this is not the saturated water content that was achieved post-experiment, as shown in the results for volumetric water content measured using TDR as well as gravimetric measurements. The average water content achieved post-experiment for the 30/40 and 40/50 sand was 29% and 32%, respectively.

This translates to a porosity of 0.29 for the 30/40 sand and 0.32 for the 40/50 sand. These porosities were used as inputs in the analytical solutions for rate of capillary rise as well as in Equation 3.3 reported by McGinnis (2001) for obtaining the capillary height using mass data.

Figure 3.15 and Figure 3.16 summarize the analytical solution results in comparison to the experimental results for the rate of capillary rise for both 30/40 and 40/50 sands, respectively. The experimental results utilize the mass balance results in conjunction with Equation 3.3 to obtain the height of capillary rise with time as well as the two TDR locations and their respective water content with time data. The two locations of the TDR probes (5 cm and 12 cm) were used to obtain the capillary height resulting in only two data points for each experiment.

Figure 3.15 shows that the experimental results for the 30/40 sand lie around both the Terzaghi (1943) and Lu & Likos (2004) predictions for rate of rise. The rate of rise predicted from the analytical solutions initially show agreement with the mass balance experimental results until about 0.01 days after which the experimental results show the rate of rise to slow down and no significant change in the capillary rise is observed. The rate of rise obtained using TDR locations shows that a height of 12 cm is achieved at around 0.003 days, consistent with Terzaghi (1943). Figure 3.15 also shows that generally the rate of rise between the different experiments is consistent. However, for the 10 g/L experiment, the rate of rise decreased in comparison to the other experiments. It should be noted that mass balance experimental results are known to fluctuate as additional saltwater solution is added into the glass tray, which explains why there is a drop in the height at around 0.008 days for the 5 g/L experiment (using mass results).

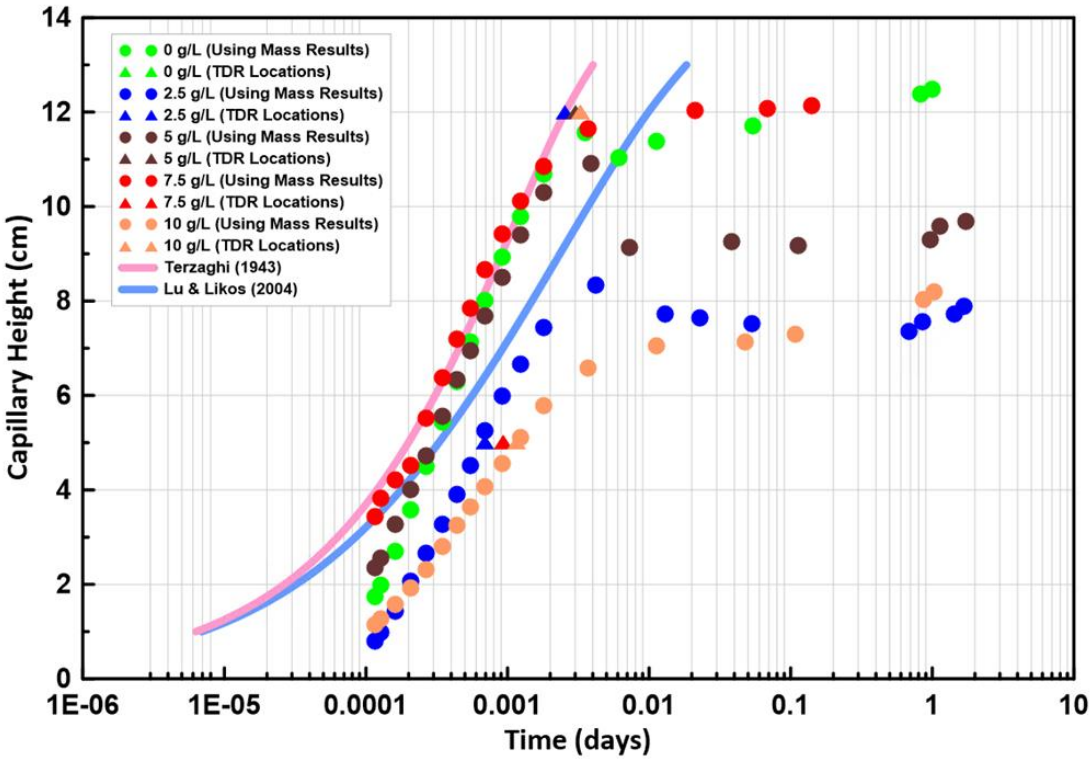

Figure 3.15: Rate of capillary rise for 30/40 sand

Figure 3.16 shows that the 40/50 experimental results depict a closer correlation with the Terzaghi (1943) prediction than the Lu & Likos (2004) prediction, however the control experiment (0 g/L) shows agreement with Lu & Likos (2004). The analytical solutions show agreement with experimental mass balance results until about 0.01 days after which the experimental results observe a slower rate of rise, and the predicted results show the maximum height of capillary rise to have been achieved around 0.01 days (for Terzaghi 1943) to 0.04 days (for Lu & Likos 2004). In comparison to the 30/40 sand, the 40/50 sand shows a slower rate of rise predicted due to its lower hydraulic conductivity. However, the maximum capillary rise observed for the 40/50 sand is slightly higher than that of the 30/40 sand, due to its smaller pore sizes. The 40/50 sand does not show a consistent trend between increasing salt concentration and its effect on the rate of rise as the 0 g/L is observed to have a slower rate of rise than those experiments with salt concentrations ranging from 2.5 g/L to 10 g/L, however the 10 g/L experiment is shown to have a rise less than

that of the 2.5 g/L to 7.5 g/L experiments which is consistent with that observed for the 30/40 sand. The rate of rise results obtained using TDR locations show agreement with Terzaghi (1943), similar to that observed for the 30/40 sand.

The salt concentrations used for these experiments were low (0 g/L to 10 g/L), therefore a significant effect of the salt concentration on the rate of rise as well as height of rise was not observed. However, from literature it is known that high salt concentrations (at least 33 g/L) can decrease the rise and affect the hydraulic conductivity of the soil (Truc et al. 2022). Additional testing at higher concentrations is required to understand and quantify the impact of the salt concentration on the rise. It should also be noted that the analytical solutions are highly dependent upon hydraulic conductivity measurements and porosity. Accurate measurements (or interpretation) of soil properties will yield better results when relying on the use of analytical solutions to determine the rate of capillary rise.

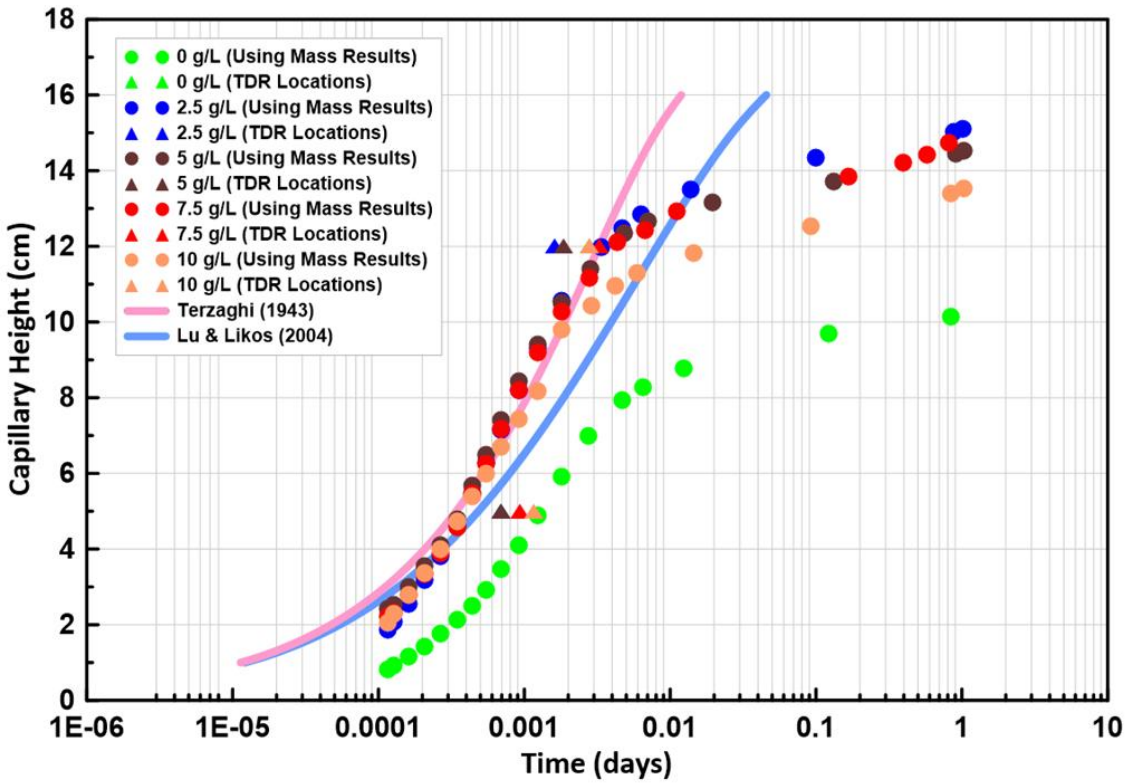

Figure 3.16: Rate of capillary rise for 40/50 sand

3.5 Use of HYDRUS-1D to Determine Soil Hydraulic Properties

HYDRUS-1D was used to simulate one-dimensional water flow and determine soil hydraulic properties for the two sand grades used in the experiments. Soil hydraulic properties estimated using HYDRUS-1D were compared to soil hydraulic properties determined from HYPROP measurements as well as the SWCC estimated using gravimetric water content. A modelling procedure along with modelling results is presented.

3.5.1 Soil Hydraulic Modelling Procedure

The flow chart in Figure 3.17 summarizes the methodology used to inversely model the soil hydraulic properties. The first step in inverse modelling requires collecting all available experimental data such as volumetric water content results from TDR. The boundary conditions and geometry were set to replicate the experiments. Figure 3.18 depicts the graphical editor extracted from HYDRUS-1D to show the profile discretization, along with the observation nodes and boundary conditions. The geometry consisted of specifying the column height (30 cm), the number of layers (1), and the number of materials (1). The time information consists of specifying initial and final times as well as time steps. Experimental data for 600 seconds was considered therefore the final time was input as 600 seconds with a minimum and maximum time step of 20 and 60 seconds, respectively. The boundary conditions assigned include a constant upper boundary of zero flux and a constant pressure head lower boundary. An initial pressure head of 0 cm was used as the bottom boundary (assumed to represent groundwater table). The average volumetric water content data for each TDR location with time was inputted into the inverse model to estimate soil hydraulic properties. Observation nodes were assigned to represent the location of the TDR in the column. Initial estimates for soil hydraulic properties are required in the inverse model. HYDRUS-1D has a built-in soil catalog in which properties for various soil types are available which can be used as initial estimates and optimized. The soil hydraulic parameters are summarized in Table 3.6. It should be noted that in each inverse model simulation, only one set

of observation data can be entered at a single observation node (or sub-region for water content simulations only). This means that each set of data from a single location was modelled independently. Therefore, having data from additional probes will not improve the accuracy of the model output as the model can only simulate results at one location at a time. Sub-regions as well as observation nodes were used in the model and compared to experimental TDR results for water content and time. The optimized soil hydraulic properties for each location were statistically analyzed to find the best estimated model parameters that fit all the experimental data for each respective sand grade tested. The soil hydraulic properties obtained from the inverse model were then compared to experimentally measured soil hydraulic properties.

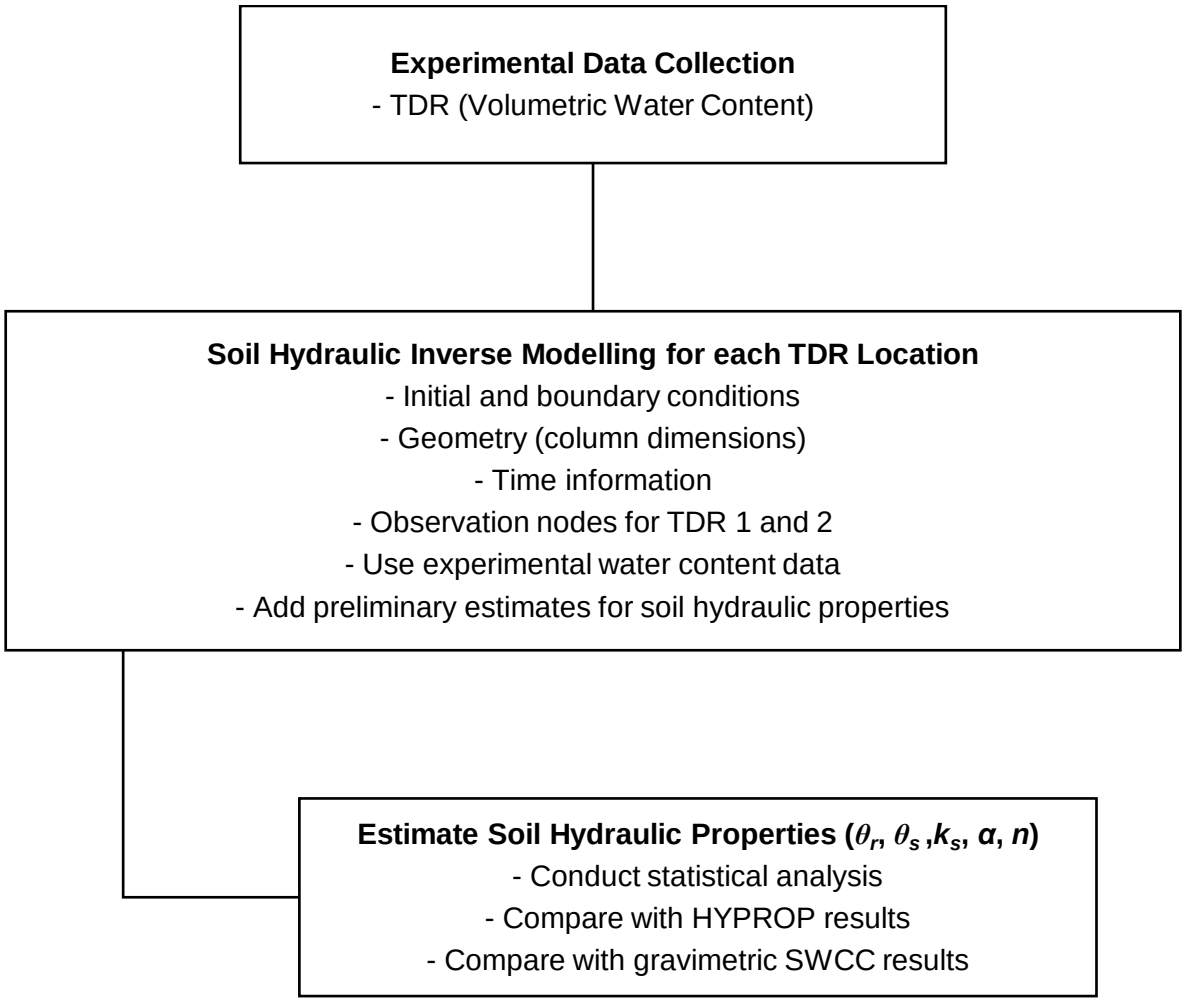

Figure 3.17: Modelling flow chart for estimating soil hydraulic properties

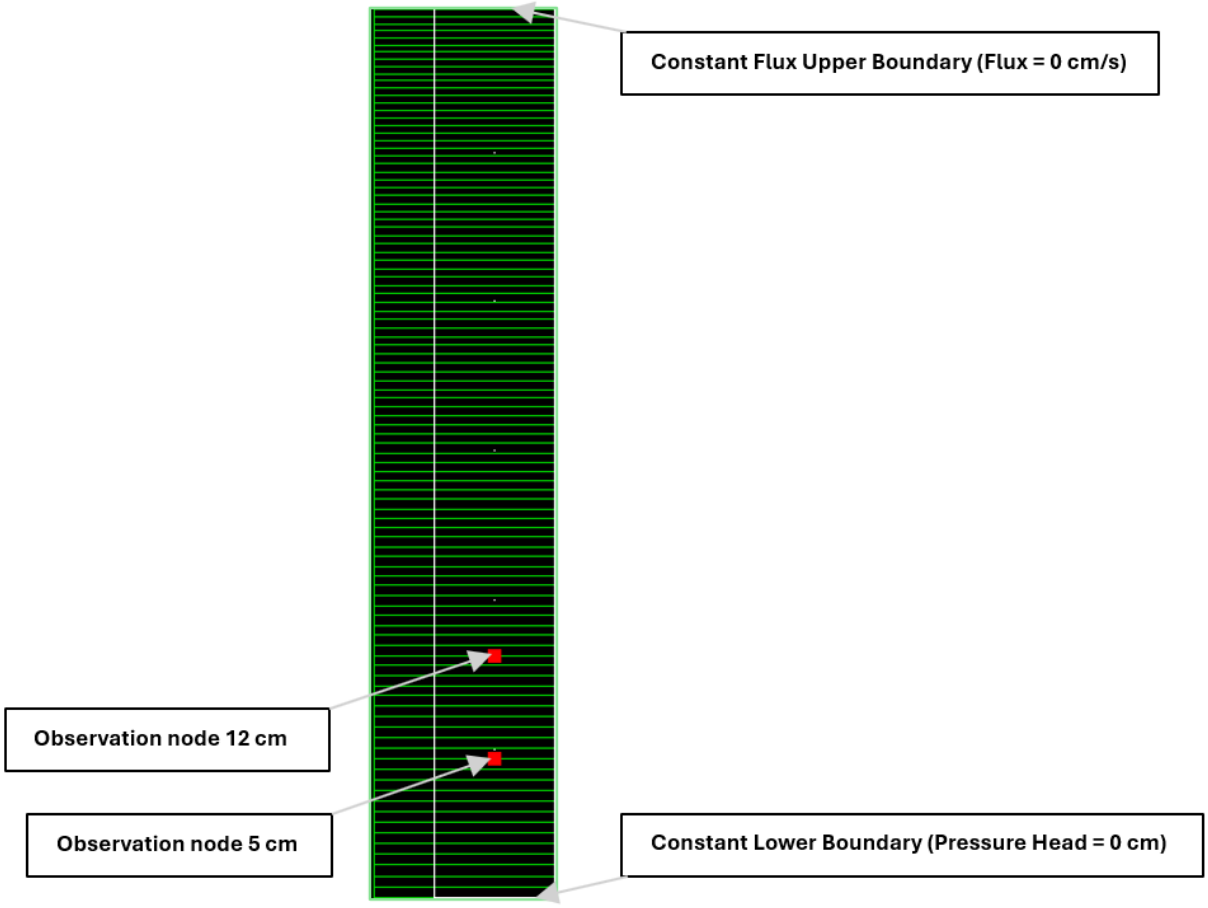

Figure 3.18: HYDRUS-1D profile discretization for water flow model

Table 3.6: Summary of initial soil hydraulic properties used in HYDRUS-1D (input parameters)

Material	Residual Water Content, θ_r (%)	Saturated Water Content, θ_s (%)	Saturated Hydraulic Conductivity, k_s (cm/s)	Fitting Parameter, α	Fitting Parameter, n
30/40	2.50	35.0	0.008	0.145	2.68
40/50	2.50	35.0	0.001	0.145	2.68

3.5.2 Modelling Results and Discussion

Descriptive statistics were conducted for each soil hydraulic property using the data obtained from each inverse model simulation at each TDR location. Table 3.7 provides a summary of the soil hydraulic properties obtained using observation nodes as well as sub-regions (mean values are

presented from descriptive statistics). The soil hydraulic properties obtained using sub-regions (average water content specified for a region contrasting with TDR sensing range) were comparable to those obtained using observation nodes, with some differences in the fitting parameter '*n*'. The average fitting parameter '*n*' obtained using sub-regions was found to be higher than that obtained using observation nodes. However, the median of the fitting parameter '*n*' using sub-regions was found to be 2.41 for the 30/40 sand and 2.30 for the 40/50 sand which is comparable to the fitting parameter '*n*' obtained using observation nodes. The results predicted using observation nodes showed better correlation with the experimental results, therefore soil hydraulic properties obtained using observation nodes were used to obtain the predicted water content and time results as well as the SWCC.

Table 3.7: Summary of soil hydraulic properties obtained from HYDRUS-1D using nodes and sub-regions (output parameters)

Simulation	Residual Water Content, θ_r (%)	Saturated Water Content, θ_s (%)	Saturated Hydraulic Conductivity, k_s (cm/s)	Fitting Parameter, α	Fitting Parameter, n
30/40 – Using observation nodes	1.82	28.0	0.02	0.14	2.81
30/40 – Using sub-region	1.87	29.3	0.04	0.14	3.53
40/50 – Using observation nodes	2.56	28.0	0.01	0.10	2.60
40/50 – Using sub-region	1.25	29.3	0.02	0.11	4.56

Figure 3.19 shows the experimental results of the volumetric water content for 30/40 sand as well as the HYDRUS-1D inverse modelling results. The legend in Figure 3.19 shows the volumetric water content predicted from the model at a soil profile height of 5 cm from the groundwater table. This correlates with the location of the TDR at 5 cm in the soil column from the bottom up.

Likewise, the volumetric water content prediction from the model at 12 cm correlates with the TDR that was located at 12 cm from the bottom of the column. The experimental data for the first 600 seconds was used in the model as the most significant change in water content with time occurs within this time frame. The experimental results show a good correlation with the curves obtained from the HYDRUS-1D model for both locations (using observation nodes). The arrival of the wetting front in the soil profile is at 80 seconds for the TDR located at 5 cm and 200 seconds for the TDR located at 12 cm.

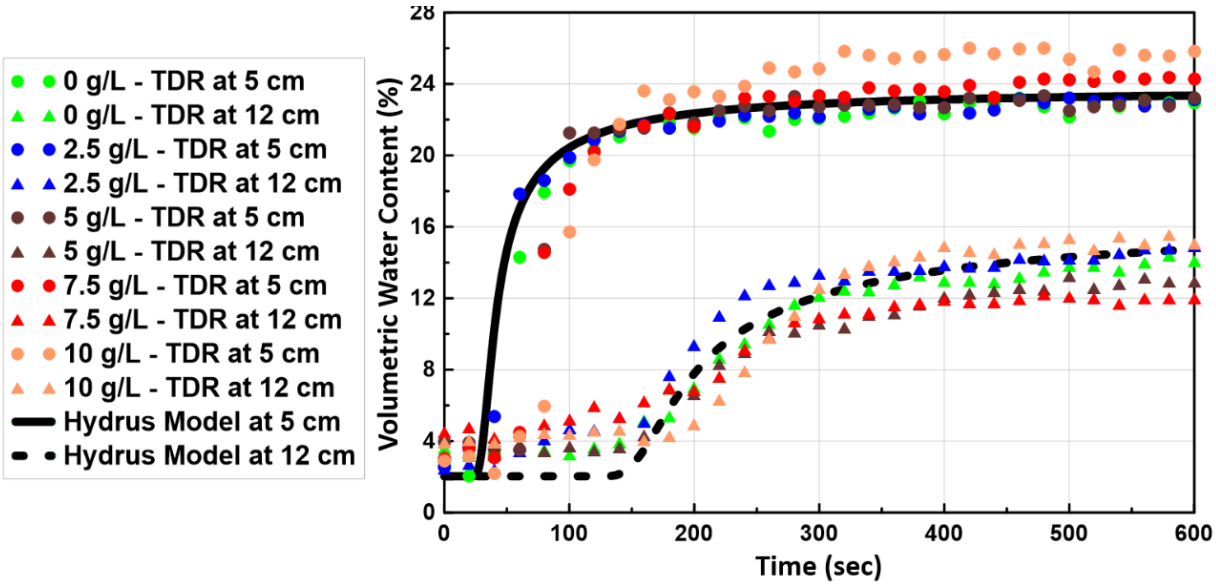

Figure 3.19: HYDRUS-1D predicted volumetric water content for 30/40 sand

Figure 3.20 shows the experimental results for the volumetric water content for the 40/50 sand experiments for the first 600 seconds along with the HYDRUS-1D inverse model results (obtained using observation nodes). Generally, the experimental results show agreement with the HYDRUS-1D predictions. The arrival of the wetting front in the soil profile is at 80 seconds for the TDR located at 5 cm and 150 seconds to 200 seconds for the TDR located at 12 cm.

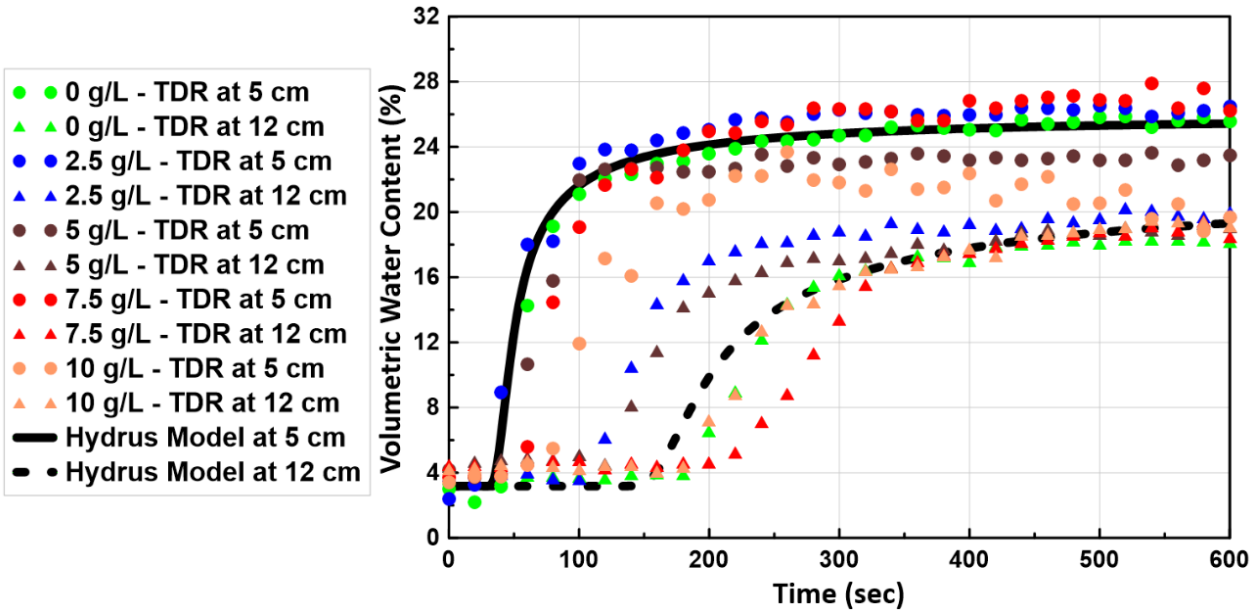

Figure 3.20: HYDRUS-1D predicted volumetric water content for 40/50 sand

HYDRUS-1D can also be used to estimate the capillary rise as it shows the distribution of the water content within the soil profile. Figure 3.21 shows the variation of volumetric water content with depth for both sands after a period of 6 days (same as the duration of the capillary rise experiments). The distribution of water content within the soil profile can be printed at various time steps. From Figure 3.21, it is observed that the water reaches a column height or capillary rise of at least 15 cm and 22 cm for the 30/40 and 40/50 sand, respectively (at water content of 8%). This is comparable to the capillary rise observed from gravimetric measurements (16 cm for 30/40 sand and 20 cm for 40/50 sand).

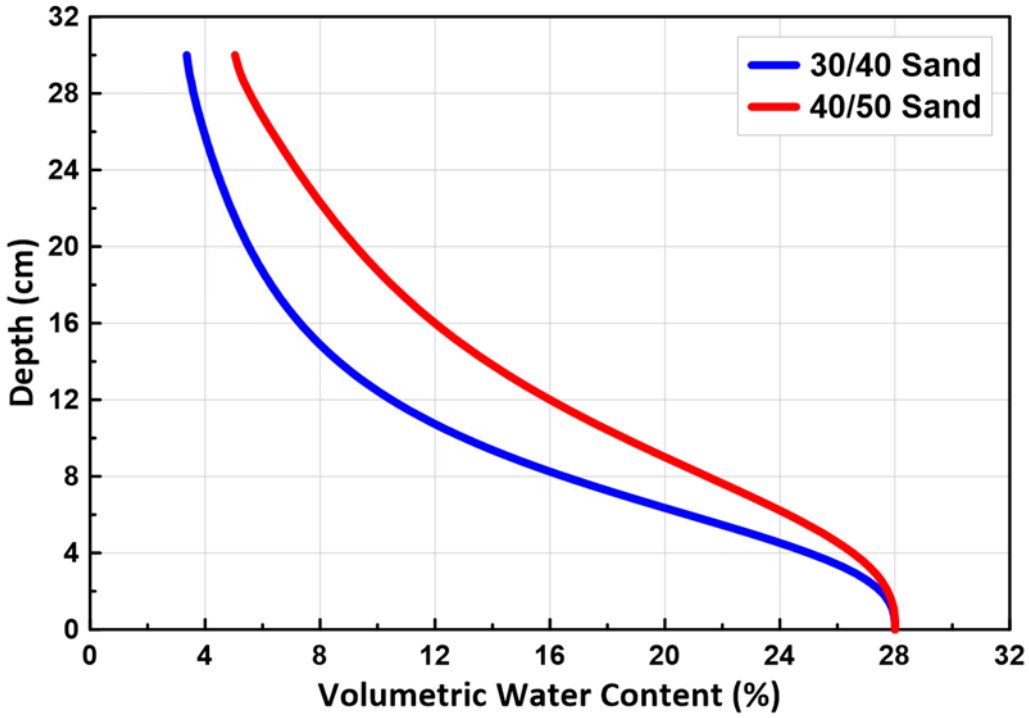

Figure 3.21: HYDRUS-1D volumetric water content (%) variation with depth (cm)

Table 3.8 and Table 3.9 summarize the soil hydraulic properties estimated from the HYDRUS-1D model, measured with HYPROP, and the estimates from gravimetric water content measurements for the 30/40 and 40/50 sands, respectively. The HYPROP device uses the evaporation method to determine the soil water retention properties and hydraulic conductivity, thus representing the drying curve whereas the HYDRUS-1D results predicts a wetting curve as the simulation essentially simulates a wetting process for soil at a residual water content. Due to hysteresis, the soil can have different water contents at the same matric suction, resulting in different drying and wetting branches of the SWCC.

Generally, the parameters obtained from HYPROP are higher than those obtained from HYDRUS-1D. The saturated water content is higher in HYPROP because the sample was carefully prepared and saturated with deaired water whereas the HYDRUS-1D and gravimetric results are from the column experiments in which there are more chances for air entrapment to occur and fill the voids which can hinder the path of water. The measured saturated hydraulic

conductivity (ASTM D5084) was 0.008 cm/s and 0.001 cm/s for the 30/40 and 40/50 sand, respectively, which is lower than the estimated hydraulic conductivity from both HYPROP and HYDRUS-1D.

The fitting parameter 'α' (inverse of the air-entry head) for the wetting curve is 2 times the fitting parameter 'α' for the drying curve (Kool and Parker 1987). This aligns with the fitting parameter 'α' obtained for both sand grades. For the 30/40 sand, the inverse of the air-entry head reported from the HYDRUS-1D results was 0.14 which is approximately 2 times the inverse of the air-entry head obtained from HYPROP and gravimetric SWCC (0.06). For the 40/50 sand, HYDRUS-1D results show 0.10 as 'α' which is 2 times the 'α' obtained from HYPROP and gravimetric SWCC (0.05). The soil can be on the drying or wetting curve as well as in between the two curves (scanning curves) due to hysteresis (Fredlund et.al. 2011). The differences between the soil hydraulic properties obtained experimentally and from the model can be attributed towards hysteresis.

Table 3.8: Summary of soil hydraulic properties for 30/40 sand (estimated and measured)

Soil Hydraulic Parameters, 30/40 Sand	**HYDRUS-1D**	**HYPROP**	**Gravimetric**
Residual Water Content, θ_r (%)	1.82	2.62	1.77
Saturated Water Content, θ_s (%)	28.0	37.7	28.2
Saturated Hydraulic Conductivity, k_s (cm/s)	0.02	0.03	-
Fitting Parameter, α	0.14	0.06	0.06
Fitting Parameter, n	2.81	18.83	7.13

Table 3.9: Summary of soil hydraulic properties for 40/50 sand (estimated and measured)

Soil Hydraulic Parameters, 40/50 Sand	**HYDRUS-1D**	**HYPROP**	**Gravimetric**
Residual Water Content, θ_r (%)	2.56	2.04	0.94
Saturated Water Content, θ_s (%)	28.0	38.4	31.4

Saturated Hydraulic Conductivity, k_s (cm/s)	0.01	0.003	-
Fitting Parameter, α	0.10	0.05	0.052
Fitting Parameter, n	2.60	14.67	7.15

Figure 3.22 shows all 3 SWCCs (HYPROP, Gravimetric, and HYDRUS-1D). The graphed results account for the fact that the fitting parameter 'α' for the wetting curve is 2 times the fitting parameter 'α' for the drying curve. Generally, the SWCC obtained from HYDRUS-1D and HYPROP correlate, with the major difference being in the saturated water content. The saturated water content from HYPROP is 37.7% and 38.4% for the 30/40 and 40/50 sand, respectively. HYDRUS-1D shows a saturated water content of 28% for both sands which is realistic as it relates closely to that observed in the capillary rise experiments. Furthermore, air entrapment effects hinder water movement, making it difficult to achieve the saturated water content measured using HYPROP. As mentioned previously, HYPROP measurement system requires carefully saturated samples using degassed water which is not realistic in real-world applications. These findings suggest that HYDRUS-1D inverse modelling coupled with capillary rise experiments can be used to estimate soil hydraulic properties.

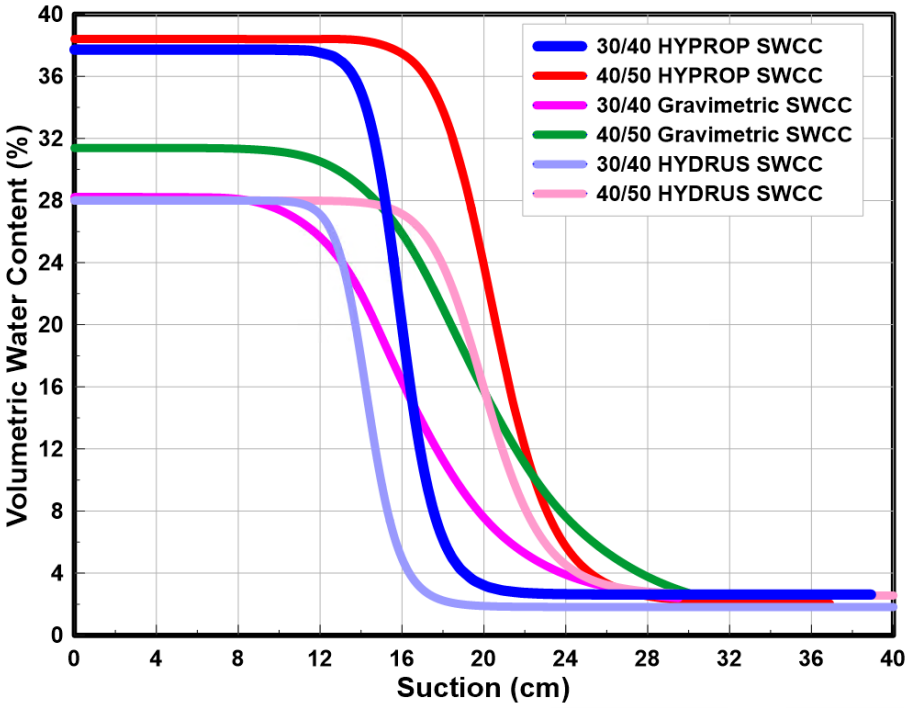

Figure 3.22: Comparison of SWCC

3.6 Summary and Conclusions

Capillary rise experiments were instrumented with TDR and used to estimate soil hydraulic properties as well as the height of capillary rise. Capillary rise experiments were conducted on two sand grades using saltwater concentrations ranging from 0 g/L to 10 g/L. The TDR results for water content and electrical conductivity for the two sand grades were compared to other means of measurement such as gravimetric method for determining water content and using an *EC* meter to measure electrical conductivity. The results suggest that TDR can be used to accurately measure the water content and electrical conductivity. Furthermore, gravimetrically obtained SWCC was comparable with the SWCC measured by HYPROP with the only major difference being in saturated water content which can be due to air entrapment effects in the soil pores.

The height of capillary rise was quantified through visual observations, TDR results for water content, as well as gravimetric water content measurements post experiment. Visual observations showed the height of capillary rise to range from 13 cm to 14 cm for the 30/40 sand and 15 cm to

17 cm for the 40/50 sand. This correlates well with the heights obtained gravimetrically (16 cm for 30/40 sand and 20 cm for 40/50 sand). The TDR locations and their sensing range within the soil column was also used to estimate the height of capillary rise which showed that the height of capillary rise was at least 15 cm for the two sands. Through visual observations, a slight decrease in the height of capillary rise can be observed as the salt concentration was increased. However, the salt concentrations considered in this study are small (2.5 g/L to 10 g/L) in comparison to the solubility limit of NaCl (360 g/L). Therefore, additional testing at higher concentrations is needed to capture the effect of salt concentration on capillary rise.

Analytical solutions developed by Terzaghi (1943) and Lu & Likos (2004) were used to verify the experimental results for the rate of capillary rise. It was observed that as salt concentration increased there was no significant change in the rate of capillary rise, however the highest tested concentration (10 g/L) showed a slightly lower rate of rise in comparison to the other concentrations tested. Furthermore, analytical solutions were found to be highly dependent upon accurate estimations or measurements of soil properties, namely hydraulic conductivity and porosity. Generally, the analytical solutions show agreement with the experimental results for rate of rise.

TDR results for the volumetric water content with time were used to estimate soil hydraulic properties through inverse modelling. The soil hydraulic properties estimated using the model in comparison with measured soil hydraulic properties show that capillary rise experiments in conjunction with TDR can be insightful for quantifying water movement. The SWCC predicted from the inverse model was compared to that measured using HYPROP as well as the SWCC obtained from gravimetric results. Generally, all 3 SWCCs correlate with each other with some differences that can be attributed to the fact that the results predicted by the HYDRUS-1D model show the wetting branch of the SWCC whereas HYPROP results show the drying branch. Instrumented TDR columns are beneficial in quantifying water dynamics and providing insight on

the movement of saltwater through a sand column. Furthermore, obtaining soil hydraulic properties can be used in areas where soil retention properties may be required such as model inputs for conducting seepage analysis.

Chapter 4: Use of TDR to Determine Soil Water Concentration and Solute Transport Parameters

4.1 Introduction

Rising saltwater due to capillary rise in soils can significantly degrade soil structure and affect soil hydraulic properties. To effectively monitor these changes, real-time observation of soil salinity is crucial. Time-Domain Reflectometry (TDR) offers a valuable tool for measuring both volumetric water content and bulk electrical conductivity over time. This study employed capillary rise experiments equipped with TDR probes to investigate the impact on two distinct sand fractions (30/40 and 40/50). To establish a relationship between bulk and pore water electrical conductivity, additional tests were conducted. An appropriate method was used for extracting pore water from the soil. The extracted pore water's electrical conductivity was then compared to the bulk electrical conductivity measurements to develop an empirical relationship, potentially following the method outlined by Rhoades et al. (1976). Furthermore, the time-series data collected during the capillary rise experiments, including the salt concentration, was utilized for inverse modelling. By fitting breakthrough curves of salt using an unsaturated flow and transport model, valuable solute transport parameters that are difficult to measure directly, were obtained.

4.2 Relating Bulk Electrical Conductivity to Pore Water Electrical Conductivity

Electrical conductivity measurements play a crucial role in analyzing soil properties. Bulk electrical conductivity (EC_b) reflects the combined conductivity of soil, water, and air within a given volume. Pore water electrical conductivity (EC_w), on the other hand, specifically refers to the conductivity of the water phase in the soil pores. While directly measuring EC_w can be challenging, researchers have established relationships to estimate it from EC_b. Chen et al. (2010) proposed a method to bridge between bulk and pore water electrical conductivity, acknowledging that bulk electrical conductivity is influenced by various factors including porosity, soil structure, water composition, conductivity forces, and temperature. Empirical models, such as Archie's law (Archie, 1942),

Rhoades et al. (1976), Rhoades et al. (1989), Vogeler et al. (1996), and Hilhorst (2000), offer insights into these relationships.

Archie's law (1942) expresses the relationship as:

$$EC_w = \phi^{-x} EC_b \quad [4.1]$$

where, EC_w is the pore water electrical conductivity, ϕ is the porosity, x is an empirical constant, and EC_b is the bulk electrical conductivity.

Rhoades et al. (1976) introduced a comprehensive model, connecting bulk electrical conductivity (EC_b) to pore water electrical conductivity (EC_w), considering soil solid component electrical conductivity (EC_s), volumetric water content (θ), and calibration constants (a and b) as follows:

$$EC_b = (a\theta^2 + b\theta)EC_w + EC_s \quad [4.2]$$

Other models by Rhoades et al. (1989) and Vogeler et al. (1996) further refine this relationship with additional calibration constants.

Hilhorst (2000) proposed a method utilizing dielectric permittivity, which can be derived from Time-Domain Reflectometry (TDR) output. The relationship incorporates bulk electrical conductivity (EC_b), permittivity of bulk soil (ϵ_b), and dielectric permittivity of pore water (ϵ_w) as follows:

$$EC_w = \frac{\epsilon_w EC_b}{\epsilon_b - \epsilon \ at \ EC_{b=0}} \quad [4.3]$$

Practical application of these models necessitates measurements of bulk electrical conductivity and pore water electrical conductivity, along with water content, for estimating the calibration constants. These measurements can be obtained using techniques such as TDR and laboratory *EC* meter for bulk electrical conductivity, and laboratory methods for pore water electrical conductivity, as detailed in subsequent sections.

4.2.1 Laboratory Methods to Determine Pore Water Electrical Conductivity

Numerous laboratory techniques are available to assess pore water electrical conductivity, each offering distinct advantages and considerations. These methods include soil-to-water ratio approaches, centrifugation, and various other soil solution extraction methodologies.

One widely utilized method for determining soil salinity is the *EC* (Electrical Conductivity) 1:5 method, recommended by authorities such as the Government of Western Australia (2022) and others (Kargas et al. 2020; Ismayilov et al. 2021;). This method involves combining 5 parts distilled or deionized water with 1-part dry soil to ascertain the soil's electrical conductivity or salt content. After thorough mixing and settling, the electrical conductivity is measured using an *EC* meter. It's noted that variations in agitation duration and methods may yield differing electrical conductivity estimates (Kargas et al. 2020).

Alternatively, Muñoz-Carpena et al. (2005) proposed a calibration method utilizing a soil suction extractor. This method involves testing soil columns with varied electrical conductivities and saturation levels. After mixing with a concentrated solution, TDR and lab *EC* meter measurements are taken to determine bulk electrical conductivity. Subsequently, a soil suction extractor extracts the soil solution for pore water electrical conductivity assessment. Additionally, saturation extract analysis aids in further characterization.

MacDonald et al. (2008) has reviewed various field and laboratory methods that can be used to extract soil solutions. This includes zero-tension and tension lysimeters, micro lysimeters, centrifugation, miscible displacement, and pressure syringe. Lysimeters are recommended for extracting soil solution in the field whereas centrifuge or syringe pressure methods may be used in a laboratory setting (MacDonald et al. 2008). Tension lysimeters employ the use of a porous cup that is placed into the soil and a suction or vacuum force is used to take the soil solution out of the soil. Microlysimeters also make use of a vacuum to extract the soil solution however they are smaller and can be employed in areas where spatial variability is a concern. Zero-tension

lysimeters do not use a vacuum source but instead rely on the force of gravity to allow the water from the soil to move downward for collection. Additionally, they can only extract the soil solution if the water content within the soil is more than its field capacity. Centrifugation is a quick method of extraction that can be used within a laboratory setting. Centrifuges rotate at selected speeds to separate components within a sample. The method proposed by MacDonald et al. (2008) refers to Davies and Davies (1963). It is recommended to centrifuge at a relative centrifugal force of 1500 g for 30 minutes. A filter paper can be used after centrifuging to further filter out the soil solution. Another laboratory method includes the syringe pressure in which soil is packed into a syringe and then pressure is applied using a compression system after which the solution can be collected (Ross and Bartlett, 1990). It is important to note that both laboratory methods result in small solution quantities extracted therefore several repetitions may be required to retrieve an appropriate quantity of solution for the measurement of the electrical conductivity. Table 4.1 is a summary of pros and cons of the various methods mentioned.

Table 4.1: The pro and cons of various methods to obtain the soil solution, reproduced from MacDonald et al. (2008)

Method	**Pros**	**Cons**
Zero-tension lysimeter	• Samples can be obtained overtime from the same soil set up • Low maintenance	• Only collects solutions from saturated mixtures • Long period of stabilization is needed before measurements for *EC* can be obtained

Tension lysimeter	• Samples can be obtained overtime from the same soil set up • Low maintenance	• Long period of stabilization is needed before measurements for *EC* can be obtained • Results vary with soil moisture
Microlysimeter	• Small scale sample collections • Spatial variability considered • Can collect samples recurrently from same area	• Requires a lot of maintenance • Stabilization time needed • Small quantity of solution extracted
Centrifugation	• Fast method of extraction	• Results are not always reproducible • Small quantity of solution extracted
Syringe pressure	• Fast method of extraction • Minimum soil disturbance during sampling	• Results are not reproducible • Small quantity of solution extracted if the soil is on the drier side

4.3 Experimental Methodology

To determine the pore water electrical conductivity, several methods were considered to select the most appropriate method for the sand grades being used. Experimental methods include the $EC_{1:5}$ method and soil water extraction methods (using centrifuge, tempe cell, and a Büchner funnel).

The $EC_{1:5}$ method requires that the material from the capillary rise experiments be dried out first (Kargas et al. 2020; Ismayilov et al. 2021;). This method requires mixing 1 part of soil with 5 parts deionized water. The mixture is agitated for 30 seconds every 30 minutes and repeated 4 times. After the final mixing, the soil is allowed to sit in the water. The electrical conductivity of the water is then measured using the TetraCon® 925 lab *EC* meter. The limitation of this method is that it can only provide the pore water electrical conductivity at the final saturation level and bulk electrical conductivity, as the measurements are taken after the completion of the capillary rise experiment. Another limitation is that the force and duration of agitation to the soil-water mixture can impact the results. Furthermore, this method is destructive in nature and was not able to quantify the salt concentration changes within the soil profile with time, as it could only provide one pore water electrical conductivity value at the final saturation of the soil. Table 4.2 summarizes the results obtained using the $EC_{1:5}$ method along with the electrical conductivity of the tested solutions. As the salt concentration is increased, the pore water electrical conductivity increases from 0.04 dS/m to 1.81 dS/m for the 30/40 sand and 0.04 dS/m to 2.61 dS/m for the 40/50 sand. These values were lower than expected in comparison to the electrical conductivity of the solutions used (0 dS/m to 18 dS/m), therefore they were discarded.

Table 4.2: Summary of pore water electrical conductivity results using $EC_{1:5}$ method

Salt Concentration	Solution Electrical Conductivity (dS/m)		Pore Water Electrical Conductivity (dS/m)	
	30/40 Sand	40/50 Sand	30/40 Sand	40/50 Sand
0 g/L	0.005	0.006	0.04	0.04
2.5 g/L	4.62	4.93	0.60	0.82
5 g/L	8.73	10.72	0.99	1.22
7.5 g/L	12.83	13.79	1.36	1.82
10 g/L	17.42	17.89	1.81	2.61

Another approach to develop a relationship between EC_b and EC_w was similar to the approach proposed and used by Muñoz-Carpena et al. (2005). Soil samples were packed into columns with a height of 14 cm and diameter of 10 cm as shown in Figure 4.1. In total, 50 column samples were prepared (25 for each sand grade). Five saturation levels (40%, 50%, 60%, 80%, and 90%) were tested at the different salt concentrated solutions as well as the control test (0, 2.5, 5, 7/5, and 10 g/L) which totalled to 25 tests per sand grade. The bulk electrical conductivity of each soil column was checked using a CS640 TDR probe as well as a lab *EC* meter (TetraCon® 925), after which a soil suction extraction method was used to extract pore water.

The complete details of all samples are summarized in Table 4.3. Note that average dry density values are also reported for each set of concentration tested (i.e. results for 40%, 50%, 60%, 80%, and 90% saturation for each concentration are averaged). The standard deviation for each 5 set of experiment replicates is also presented.

Figure 4.1: Columns used for ECw experiments

Table 4.3: Summary of tested column samples for pore water electrical conductivity experiments

Experiment	Salt Concentration (g/L)	Solution Electrical Conductivity (dS/m)	Saturation (%)	Average Dry Density (g/cm^3)	Standard Deviation in Dry Density
30/40 - 1 to 5	0	0.007	40	1.71	0.02
30/40 - 6 to 10	2.5	4.92	50	1.70	0.02
30/40 - 11 to 15	5	9.91	60	1.70	0.02
30/40 - 16 to 20	7.5	14.39	70	1.68	0.02
30/40 - 21 to 25	10	17.61	90	1.68	0.02
40/50 - 1 to 5	0	0.007	40	1.70	0.02
40/50 - 6 to 10	2.5	4.79	50	1.70	0.02
40/50 - 11 to 15	5	9.54	60	1.69	0.03
40/50 - 16 to 20	7.5	14.18	70	1.69	0.02
40/50 - 21 to 25	10	17.75	90	1.70	0.03

Three methods were tried to extract the pore water from the soil samples at various saturation levels. This included the use of a centrifuge, tempe cells, and a Büchner funnel.

For the centrifuge extraction, the Allegra X-30 centrifuge was used with a conical tube rotor, C0650, which holds the sample tubes in place and spins to separate the material within the tubes. The maximum revolutions per minute (RPM) for the C0650 is 9000. It has a maximum capacity of 6 vials with capacity of 50 mL each. For this set up, the samples were placed into the vials and various relative centrifugal forces were tried for different durations to see if the water can be extracted from the soil however it was found this technique did not work as the water would not separate from the soil-water mixture.

After this, Tempe cells were tried for water extraction. The Tempe cell setup is shown in Figure 4.2. The soil was packed into Tempe cells with a 100 kPa (1 bar) porous disc at the bottom. The set up was connected to an air pressure valve. The top plate of the Tempe cell has a pipe attached to which the pressure is applied. The bottom plate has a pipe attached to a small vial that can collect the water for measurements. The Tempe cell set up only worked for saturation levels above 70%. The water was not extracted from the saturation levels below 60% even after having the set up run overnight. Therefore, this method was abandoned.

Finally, a Büchner funnel setup was employed as shown in Figure 4.3. This setup requires a small bottle that is placed within the flask to collect the water sample, a funnel to hold the soil sample, a filter paper placed underneath the soil sample, a clamp to secure the funnel in place, and a vacuum source.

Figure 4.2: Tempe Cell experimental set up

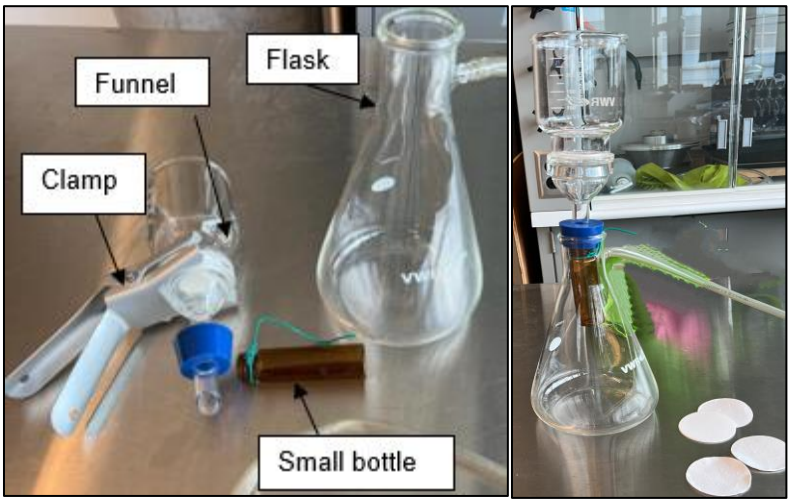

Figure 4.3: Büchner funnel materials

The soil (about 30 g at a time) that was previously used in the columns for TDR bulk electrical conductivity measurements, was placed into the funnel with a filter paper at the bottom. Vacuum pressure was applied to the flask through the pipe, which allowed water to be extracted from the soil and into the small bottle within the flask. For higher levels of saturation (above 60%) the water extraction process was very quick and porewater was extracted within seconds, however in order

to retrieve enough water for testing, it is recommended to repeat this process and continue testing 30 g of soil at a time until enough pore water has been extracted for testing. This process can be repeated to obtain more water if needed.

The pore water electrical conductivity was measured by using the TetraCon® 925, lab conductivity meter. The lab *EC* meter requires at least 5 mL of solution to provide a reading. This set up allowed adequate water to be extracted for saturation in 40%-90% range. The results were used to form a relationship between the bulk electrical conductivity and pore water electrical conductivity.

4.4 Experimental Results and Discussion

This section summarizes the results from the batch experiments, including measurements of pore water electrical conductivity and the development of an empirical relationship between bulk and pore water electrical conductivity. Additionally, it discusses how this empirical relationship was used to determine salt concentration using TDR EC_b data from the capillary rise experiments.

4.4.1 Empirical Relationship Between Bulk Electrical Conductivity and Pore Water Electrical Conductivity

The measurements as described above were used to develop an empirical relationship between bulk electrical conductivity (EC_b) and pore water electrical conductivity (EC_w). The pore water electrical conductivity can then be used to determine the salt concentration. Figure 4.4 presents the results for EC_b and EC_w for the 30/40 sand. In Figure 4.4 (a) the results are labeled according to solution concentration while in Figure 4.4 (b) according to the soil saturation. Several observations can be made from this figure. The results indicate that there is a near linear relationship between EC_b and EC_w for each saturation level considered in this research. The EC_w appears to remain relatively constant for each of the concentrations considered. Furthermore, the EC_w shows a strong correlation with the *EC* of the solution. Similar observations can be made for 40/50 sand as shown in Figure 4.5. For both sands the EC_w is shown to range from 0 dS/m to 20

dS/m whereas the EC_b ranges from 0 dS/m to 2.5 dS/m for the 30/40 sand, and 0 dS/m to 2.9 dS/m for the 40/50 sand.

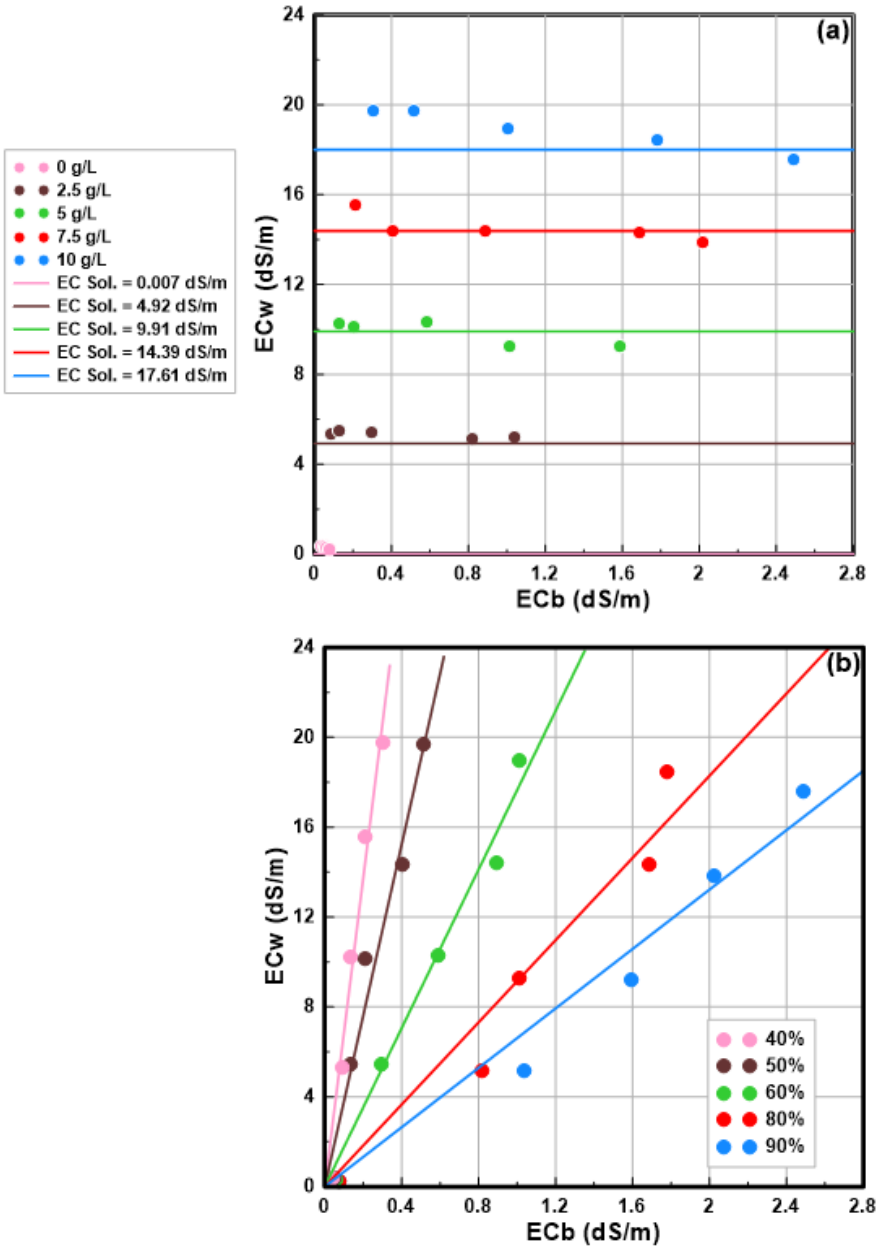

Figure 4.4: Bulk electrical conductivity (ECb) vs. Pore water electrical conductivity (ECw) for the 30/40 sand grouped by (a) solution concentration, and (b) soil saturation

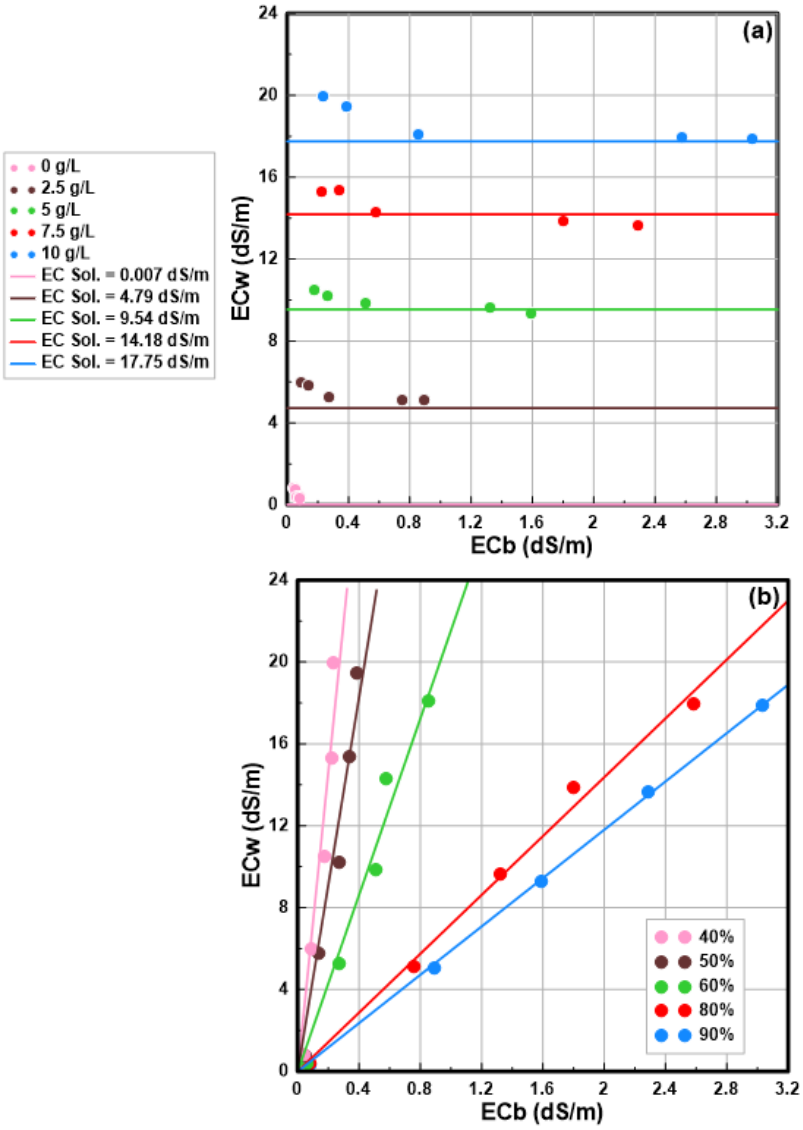

Figure 4.5: Bulk electrical conductivity (ECb) vs. Pore water electrical conductivity (ECw) for the 40/50 sand grouped by (a) solution concentration, and (b) soil saturation

The empirical relationship for the pore water electrical conductivity was established using the procedure outlined by Rhoades et al. (1976). First, the ratio of EC_b/EC_w for both sands is plotted versus the volumetric water content as shown in Figure 4.6 and Figure 4.7. The EC_w values plotted in these figures are those that were measured for the extracted pore water. The results are plotted according to the *EC* of the solution. The initial soil solution of 0.007 dS/m has a very low EC_w, therefore, the ratio of EC_b/EC_w is high in comparison to the other solutions tested.

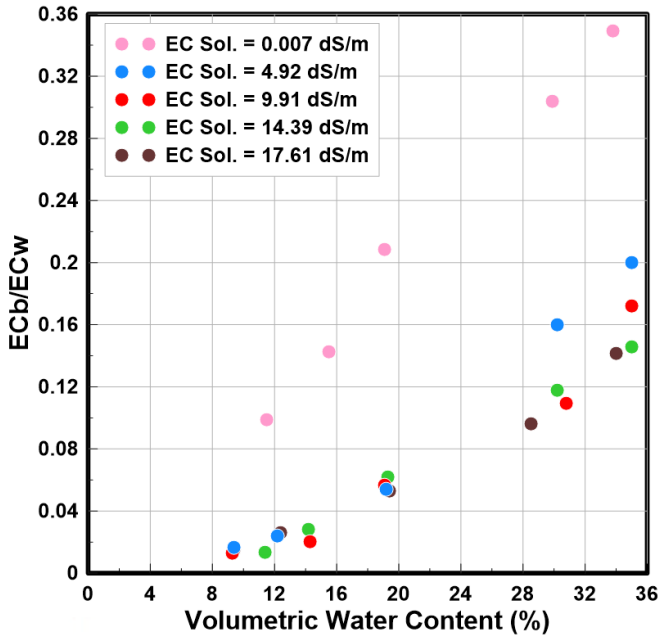

Figure 4.6: Bulk electrical conductivity/Pore water electrical conductivity (EC_b/EC_w) vs. Volumetric water content for the 30/40 sand

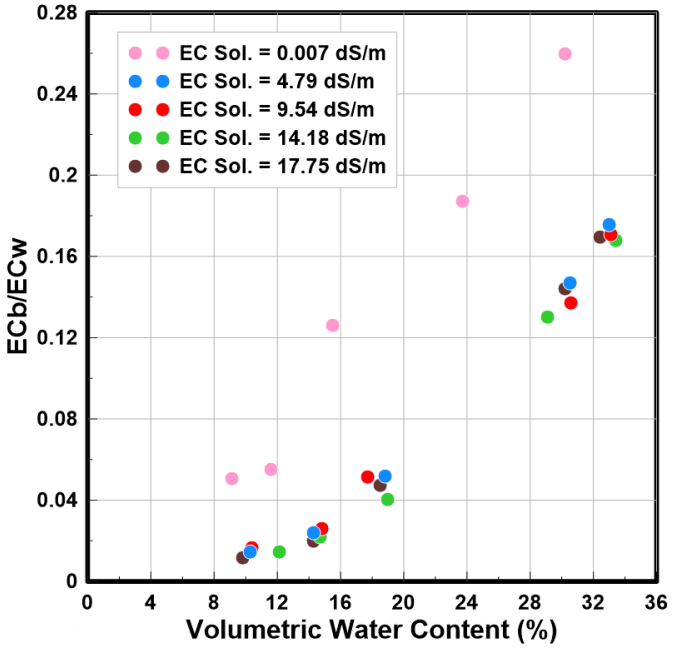

Figure 4.7: Bulk electrical conductivity/Pore water electrical conductivity (EC_b/EC_w) vs. Volumetric water content for the 40/50 sand

Next, the surface electrical conductivity (EC_s) is subtracted from the bulk electrical conductivity and divided by the pore water electrical conductivity. This is plotted against the water content as shown below in Figure 4.8 and Figure 4.9 for each sand. The surface conductivity is the bulk electrical conductivity when the pore water electrical conductivity is 0 dS/m and was measured as 0.038 dS/m and 0.042 dS/m for the 30/40 and 40/50 sands, respectively.

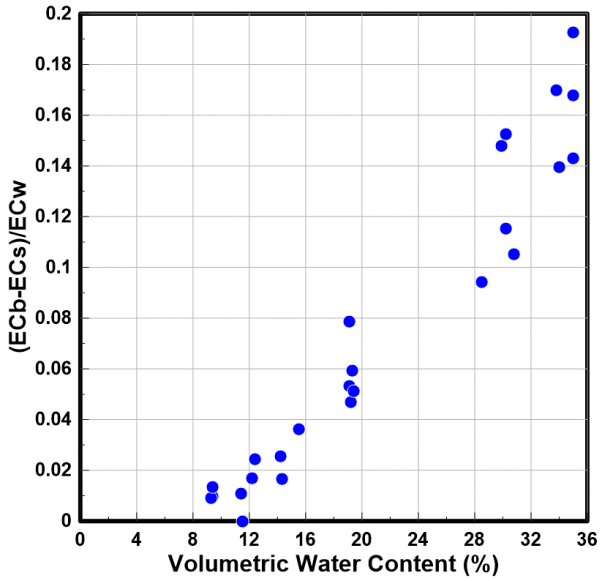

Figure 4.8: $(EC_b\text{-}EC_s)/EC_w$ vs. Volumetric water content for the 30/40 sand

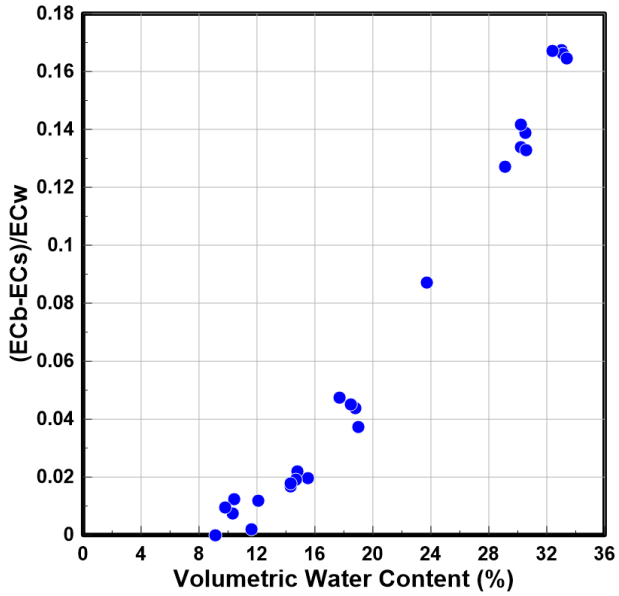

Figure 4.9: $(EC_b\text{-}EC_s)/EC_w$ vs. Volumetric water content for the 40/50 sand

Figure 4.8 and Figure 4.9 can be used to obtain a linear relationship between water content and (EC_b – EC_s / EC_w). This can be done using Equation 4.2 proposed by Rhoades et al. (1976). Equation 4.2 be rearranged as:

$$\frac{ECb-ECs}{ECw} = (\mathrm{a}\theta^2 + \mathrm{b}\theta) \quad [4.4]$$

$$\frac{ECb-ECs}{ECw} = \theta(\mathrm{a}\theta + \mathrm{b}) \quad [4.5]$$

$$(\frac{ECb-ECs}{\theta ECw}) = (\mathrm{a}\theta + \mathrm{b}) \quad [4.6]$$

Here, the right side of Equation 4.6 can be taken as the slope of a line, where $T = a\theta + b$. T denotes a transmission coefficient that considers the tortuous paths of current lines, and a and b are calibration constants (Rhoades et al. 1976). The left side of Equation 4.6 is simply the y-axis in Figure 4.8 and Figure 4.9 divided by the volumetric water content (x-axis).

Finally, Figure 4.10 and Figure 4.11 below show T versus the water content with a linear fit. The linear fit can be used to obtain parameters, a and b defined above. R^2 is also shown on the plots along with the equation obtained from the line of best fit. The R^2 is 0.83 and 0.97 for the 30/40 and 40/50 sands, respectively.

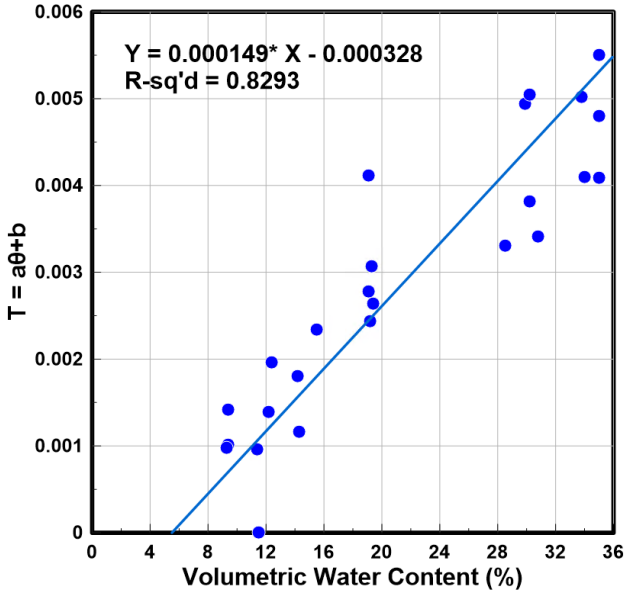

Figure 4.10: T vs. Volumetric water content for the 30/40 sand

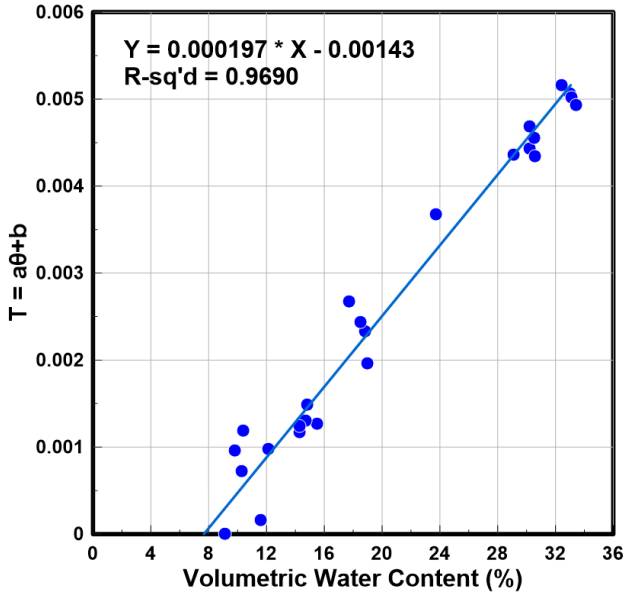

Figure 4.11: T vs. Volumetric water content for the 40/50 sand

Rhoades et al. (1976) relationship for EC_w from Equation 4.6 can be rearranged for EC_w as follows:

$$EC_w = \frac{EC_b - EC_s}{a\theta^2 - b\theta} \quad [4.7]$$

Using the graphs above, the following relationships can be defined for the 30/40 sand and 40/50 sands, respectively:

$$EC_w = \frac{EC_b - EC_s}{0.000149\theta^2 - 0.000328\theta} \quad [4.8]$$

$$EC_w = \frac{EC_b - EC_s}{0.000197\theta^2 - 0.00143\theta} \quad [4.9]$$

These relationships can be used to convert the bulk electrical conductivity obtained from the capillary rise experiments to the pore water electrical conductivity.

The pore water electrical conductivity can then be converted to NaCl concentration using the molar mass of NaCl and the following correlations between *EC* and molarity (Government of Western Australia 2022).

$$1\frac{dS}{m} = 10\ mM\ NaCl \quad [4.10]$$

Here, 1 dS/m is equivalent to 10 millimolar (mM) NaCl. Considering that 1 mM is equivalent to 1 millimoles per liter (mmol/L) and that the molar mass of NaCl is 58.4 g/mol (or 0.058 g/mmol):

$$\frac{1dS}{m} = 10\frac{mmol}{L} * \frac{0.0584g}{mmol} \quad [4.11]$$

NaCl concentration (*C*) can be found using the above correlation and pore water electrical conductivity (EC_w):

$$C = 0.584\ g/L \times EC_w \quad [4.12]$$

Figure 4.12 and Figure 4.13 show the concentration with time for each sand from the capillary rise experiments. The concentration ranges from 0 g/L to 11 g/L for the 30/40 sand and 0 g/L to 16 g/L for the 40/50 sand. The 40/50 sand results show some discrepancy and overestimated concentration values which may be due to the complexity of establishing the empirical relationship

between EC_b and EC_w. Nonetheless, this data can be used to obtain breakthrough curves and estimate solute transport properties using inverse models.

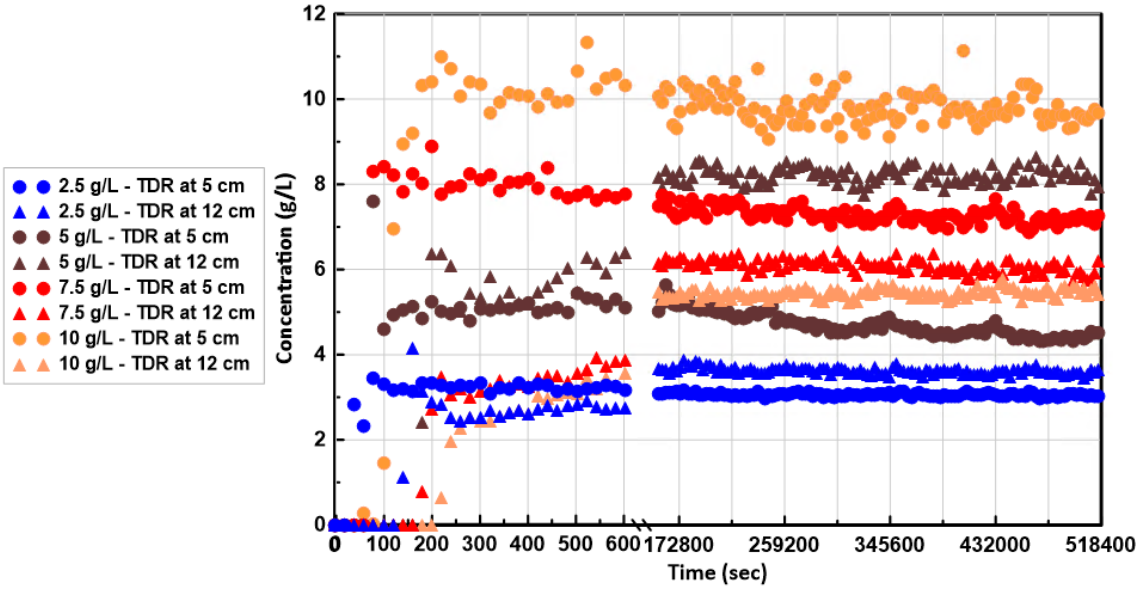

Figure 4.12: Concentration vs. Time for 30/40 sand

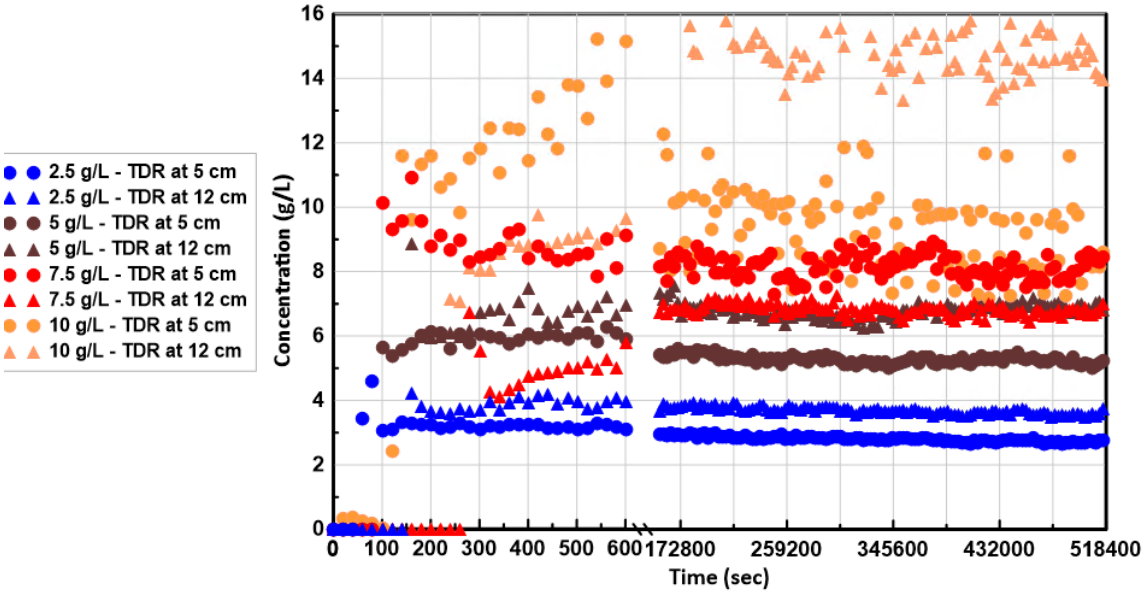

Figure 4.13: Concentration vs. Time for 40/50 sand

4.5 Use of HYDRUS-1D to Determine Solute Transport Properties

An unsaturated flow and transport model using HYDRUS-1D was used to determine solute transport properties for the two sand grades used in the capillary rise experiments. A modelling procedure along with modelling results is presented within this section.

4.5.1 Solute Modelling Procedure

The modelling procedure for inverse solute transport modelling is summarized in the flow chart below in Figure 4.14. First, the experimental data for concentration is retrieved. Initial model inputs require entering water flow and solute boundary conditions, the concentration with time data, and observation nodes to replicate the measured concentration data at two locations. Only one set of observed concentration data at one location may be entered into each inverse model simulation. Modelling solute transport requires the use of the water flow model as well. Figure 4.15 shows the profile discretization which includes the observation nodes, and water flow and solute transport boundary conditions. The water flow geometry and initial and boundary conditions are same as that discussed in Chapter 3 (section 3.5.1). The soil hydraulic properties that were established using the HYDRUS-1D inverse model as discussed in Chapter 3 (section 3.5.2), were used as model inputs for the solute transport model and are summarized in Table 4.4. Solute boundary conditions require the user to input the upper and lower boundary concentration. The upper boundary condition is 0 g/L concentration flux whereas the lower boundary condition is the salt concentration used in the solution for the capillary rise experiment (ranges from 2.5 g/L to 10 g/L). Initial conditions for concentration include assigning a concentration to the soil which was found to be 0.02 g/L for both sands. Initial estimates for solute transport properties including dispersivity and diffusion coefficient are also required.

Dispersivity is the spreading of solutes as they move through the soil. Diffusion is the movement of molecules from higher concentrations to lower concentrations. The effective diffusion coefficient is the rate of the molecular diffusion in porous media and can be determined using the

concentration profiles with time or position (Leij et al. 1999). The following equation can be used to solve for the effective diffusion coeffcient:

$$D_e = D_d \times \tau \quad [4.11]$$

where, D_e is the effective diffusion coefficient, D_d is the molecular diffusion coefficient, and τ is the tortuosity factor.

The dispersion coefficient can then be defined as:

$$D = \lambda v \quad [4.12]$$

where, λ is longitudinal dispersivity and v is the average pore water velocity (Šimůnek et al. 2008): Initial estimates for dispersivity and diffusion coefficient are summarized in Table 4.5. This model was used to back predict solute transport. The estimated solute transport parameters were statistically analyzed to assess the parameters that showed the best correlation with the experimental data. For this research, the equilbrium solute model was used which assumes uniform flow.

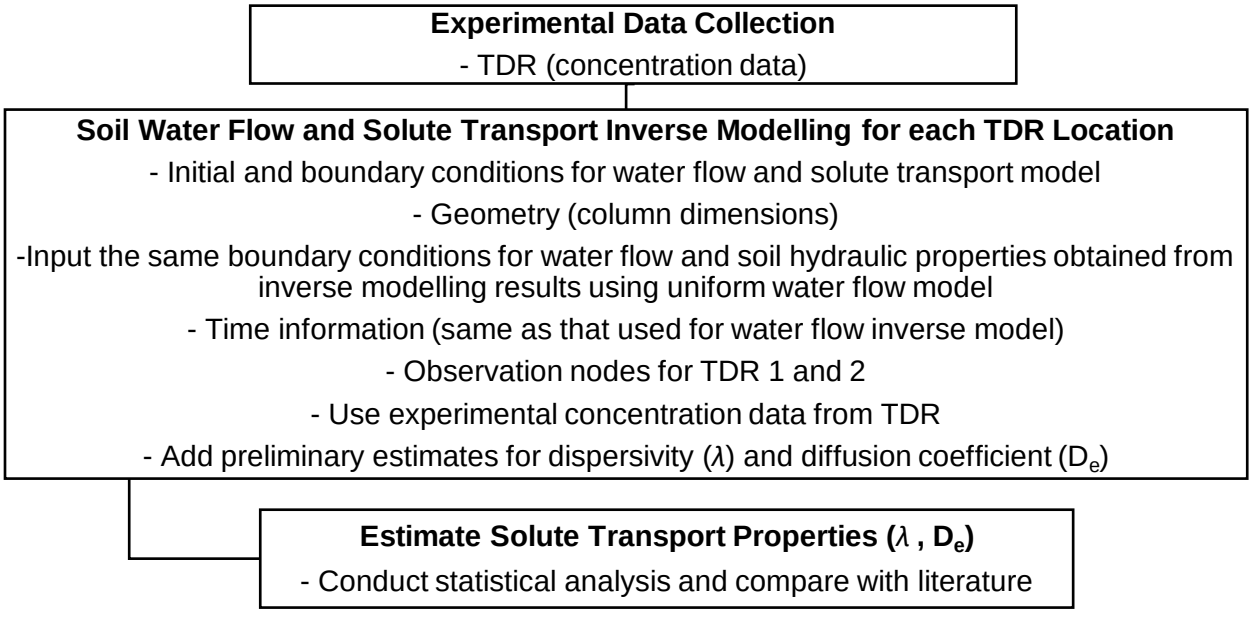

Figure 4.14: Modelling flow chart for estimating solute transport properties

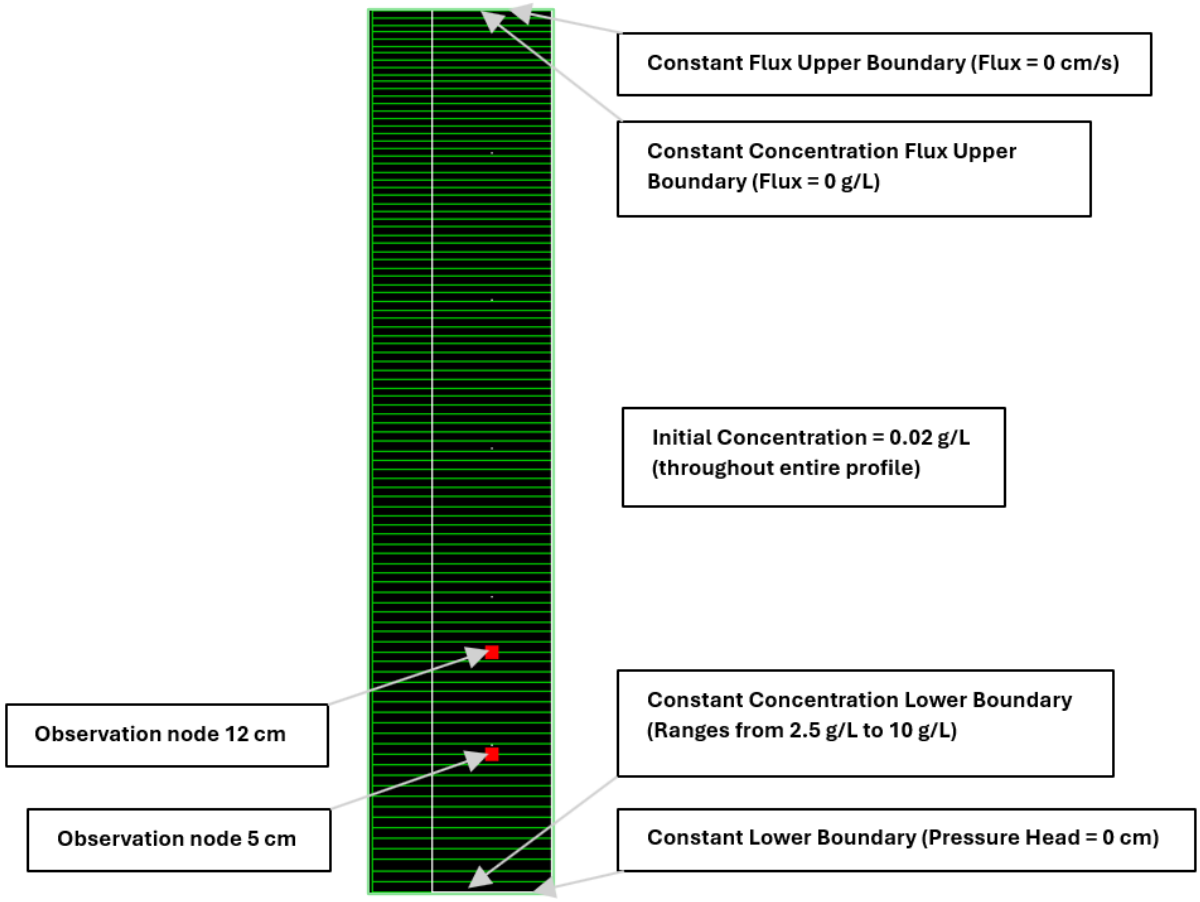

Figure 4.15: HYDRUS-1D profile discretization for solute transport model

Table 4.4: Summary of initial soil hydraulic properties used in HYDRUS-1D (input parameters)

Material	Residual Water Content, θ_r (%)	Saturated Water Content, θ_s (%)	Saturated Hydraulic Conductivity, K_s (cm/s)	Fitting Parameter, α	Fitting Parameter, n
30/40	1.82	28.0	0.02	0.14	2.81
40/50	2.56	28.0	0.01	0.10	2.60

Table 4.5: Summary of initial estimates for dispersivity and diffusion coefficient used in HYDRUS-1D (input parameters)

Experiment	Dispersivity (cm)	Diffusion Coefficient (cm/s)
30/40	3	0.000011
40/50	3	0.000011

4.5.2 Modelling Results and Discussion

The inverse solute modelling results for each set of experiments are summarized in this section along with the estimated solute transport properties. Figure 4.16 shows the results for experiments 2 to 5 (2.5 g/L, 5 g/L, 7.5 g/L and 10 g/L) for the 30/40 sand. The arrival time for the concentration at 5 cm on average is 80 seconds whereas the arrival time at 12 cm increases with salt concentration, ranging from 150 seconds to 180 seconds. The sharp increase in concentration can be denoted as the breakthrough point, where the solute is first detected in the soil pores, in which initally there is neglible concentration (0.02 g/L). The estimated concentrations for the experiments were higher than those estimated from the modelling (at the 5 cm location). The concentrations for the 30/40 experiments ranged from 2.5 g/L to 11 g/L. In the solute model, lower and upper boundary conditions are inputted. The lower boundary condition was taken as a concentration boundary condition equal to the concentration measured of the solution in the tray. Therefore, the modelling predictions are from 2.5 g/L to 10 g/L to match the boundary condition. The initial concentration of the soil itself was found to be small (0.02 g/L for both sands) and did not have a significant impact on the breakthrough curves. The experimental concentrations are higher which can be due to experimental errors in deriving the empirical relationship relating bulk and pore water electrical conductivity and evaporation of water causing higher solute concentration in the soil pores. Furthermore, the uncertainty associated with the empirical relationship developed can be contributing to the higher concentrations estimated.

In addition, HYDRUS-1D inverse modelling has some limitiations as the observation data that is input into the inverse model can only be specified at a certain observation node (or one location). TDR probes have a high sensing range as mentioned previously. TDR output results are an average along the sensing range. Due to the model limitations, it was not possible to specifiy concentration data along the entire sensing range of each TDR, which may cause discrepancies in arrival time and peak concentrations, specifically at the 12 cm location. Furthermore, HYDRUS-

1D does not allow the user to enter multiple observation data for different locations in a single simulation, therefore each TDR probe data from one location must be modelled independently, which may cause errors in the predicted concentration profile.

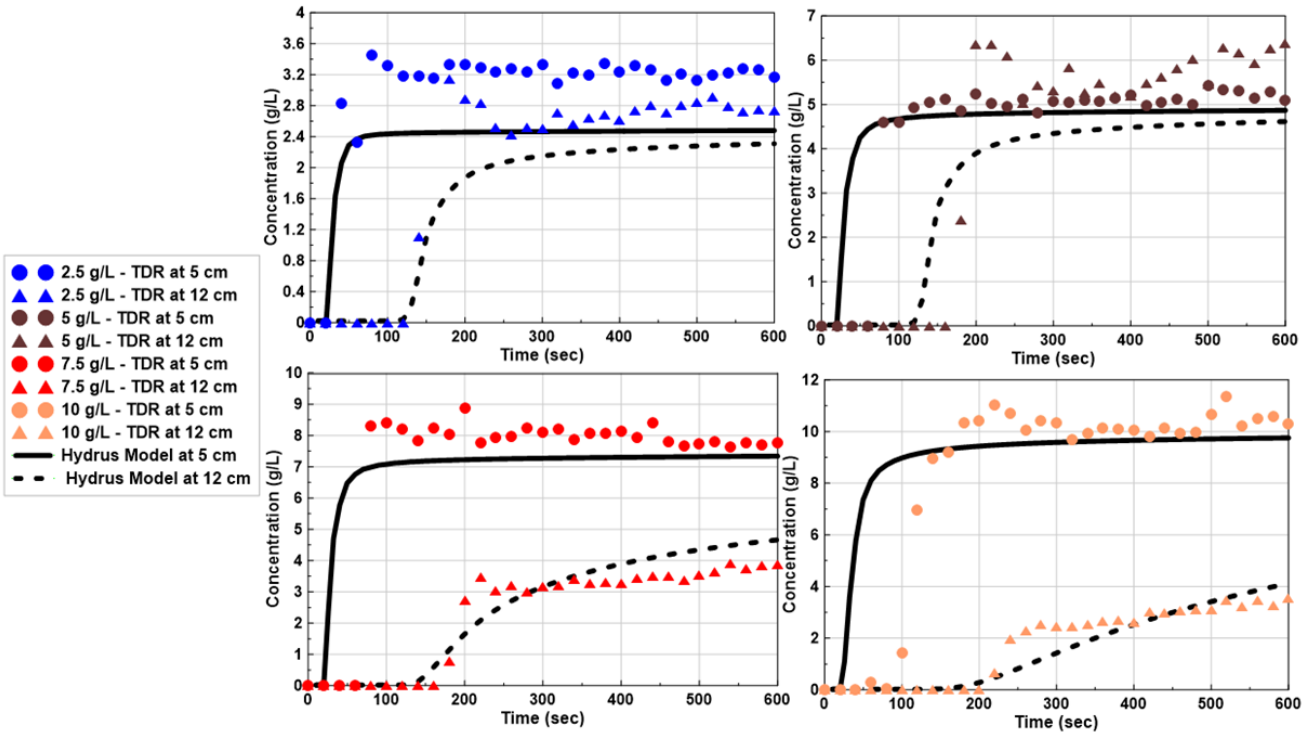

Figure 4.16: Concentration vs. Time HYDRUS-1D modelling results for 30/40 sand

Figure 4.17 shows the solute model results for the 40/50 sand for experiments 2 through 5. For the 40/50 sand, the experimental concentrations are observed to be 2.5 g/L to 15 g/L whereas the model concentrations range from 2.5 g/L to 10 g/L. This is similar to that observed for the 30/40 sand. The arrival times for the concentration to reach 5 cm height in the soil profile is on average at 100 seconds whereas at 12 cm, the average arrival time is 200 seconds to 250 seconds.

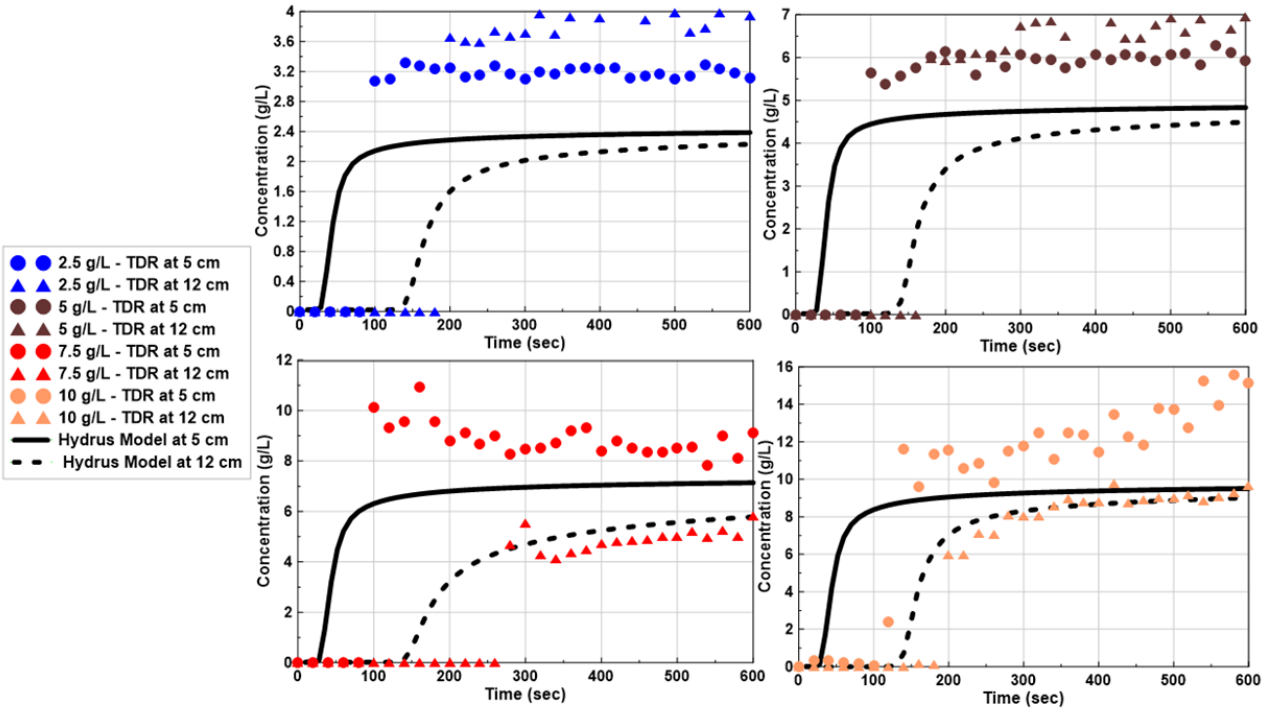

Figure 4.17: Concentration vs. Time HYDRUS-1D modelling results for 40/50 sand

The solute transport parameters estimated for both sands are summarized below in Table 4.6 for each experiment and TDR location. Table 4.7 summarizes the results from the descriptive statistical analysis for each solute transport property (for each sand). Due to wide range in solute transport parameters (minimum and maximum values), it was not possible to use the average dispersivity or diffusion coefficient in the model and obtain a good correlation with the experimental results. The standard deviation for dispersivity and diffusion coefficient for the 30/40 sand was found to be 0.73 and 0.09. The standard deviation for dispersivity is high due to the wide range in dispersivity values as salt concentration was increased (particularly for the 10 g/L experiment). The standard deviation for dispersivity and diffusion coefficient for the 40/50 sand was found to be 0.14 and 0.04. The model predicted results in Figure 4.16 and Figure 4.17 use independently simulated model parameters that are summarized in Table 4.6. The average dispersivity was 1.3 cm and 0.9 cm for the 30/40 and 40/50 sand, respectively. This falls within

the range provided by Huang et al. (1995) for homogenous soil columns (0.1 to 2.0 cm). The average effective diffusion coefficient was obtained as 0.094 cm^2/s and 0.091 cm^2/s, for the 30/40 and 40/50 sand, respectively. The expected diffusion coefficient for sands ranges from 0.07 cm^2/s to 0.09 cm^2/s (Li et al. 2011).

Table 4.6: Summary of estimated solute transport parameters for 30/40 and 40/50 sands (output parameters)

	Solute Transport Parameters	
Experiment	**Dispersivity (cm)**	**Diffusion Coefficient (cm^2/s)**
30/40 Sand – 2.5 g/L (5 cm Location)	1.50	0.30
30/40 Sand – 2.5 g/L (12 cm Location)	1.30	0.10
30/40 Sand – 5 g/L (5 cm Location)	2.03	0.07
30/40 Sand – 5 g/L (12 cm Location)	1.80	0.08
30/40 Sand – 7.5 g/L (5 cm Location)	2.01	0.10
30/40 Sand – 7.5 g/L (12 cm Location)	0.38	0.00001
30/40 Sand – 10 g/L (5 cm Location)	0.95	0.10
30/40 Sand – 10 g/L (12 cm Location)	0.08	0.001
40/50 Sand – 2.5 g/L (5 cm Location)	0.92	0.09
40/50 Sand – 2.5 g/L (12 cm Location)	0.90	0.09
40/50 Sand – 5 g/L (5 cm Location)	0.91	0.17
40/50 Sand – 5 g/L (12 cm Location)	1.23	0.093
40/50 Sand – 7.5 g/L (5 cm Location)	0.80	0.09
40/50 Sand – 7.5 g/L (12 cm Location)	0.90	0.01
40/50 Sand – 10 g/L (5 cm Location)	0.79	0.09

40/50 Sand – 10 g/L (12 cm Location)	0.99	0.09

Table 4.7: Summary of descriptive statistics of the solute transport parameters for 30/40 and 40/50 sands

Descriptive Statistics of Solute Transport Parameters				
	30/40 – Dispersivity (cm)	**30/40 – Diffusion Coefficient (cm^2/s)**	**40/50 – Dispersivity (cm)**	**40/50 – Diffusion Coefficient (cm^2/s)**
Mean	1.26	0.094	0.93	0.091
Median	1.40	0.089	0.90	0.091
Standard Deviation	0.73	0.09	0.14	0.04
Standard Variance	0.54	0.009	0.02	0.002
Minimum	0.08	0.00001	0.79	0.01
Maximum	2.03	0.30	1.23	0.17

4.6 Summary and Conclusions

Instrumented TDR columns were used to perform capillary rise column experiments along with a set of batch experiments to estimate the pore water electrical conductivity. The bulk electrical conductivity results from TDR were successfully converted to pore water electrical conductivity using an empirical relationship developed through batch experiments. The empirical relationship followed an approach outlined by Rhoades et al. (1976).

The results from this relationship were used to inversely model solute transport using a variably saturated flow model in HYDRUS-1D. The solute transport model in HYDRUS-1D also makes use of the water flow model, thus necessitating model inputs for soil hydraulic parameters. These parameters were obtained using the inverse model and TDR water content results from the capillary rise experiments. Breakthrough curves were fitted to experimental results for concentration at two locations of the soil profile (5 cm and 12 cm) and solute transport parameters,

dispersivity and the diffusion coefficient, were estimated. Both dispersivity and diffusion coefficient are important parameters in the advection-dispersion equation and can be used to better understand the movement of solutes in applications such as groundwater contamination. The model predictions show some discrepancy in comparison to the experimental breakthrough curves, which may be attributed to the uncertainty of the empirical relationship that was used to obtain salt concentration for the capillary rise experimental results as well as model limitations. HYDRUS-1D does not allow the user to inversely model concentration within a sub-region, but instead it uses a single observation node which is not representative of the results from TDR (due to the high sensing range of TDR). However, the HYDRUS-1D inverse model can still be used to gain an insight on solute transport parameters. Furthermore, the values obtained for dispersivity (1.3 cm for 30/40 sand and 0.9 cm for 40/50 sand) and diffusion coefficient (0.094 cm^2/s for 30/40 sand and 0.091 cm^2/s for 40/50 sand) fall within the range reported in literature. Therefore, the inverse modelling results suggest that HYDRUS-1D coupled with TDR column capillary rise experiments can be used to successfully estimate solute transport parameters for sands.

Chapter 5: Summary, Conclusions, and Recommendations for Future Research

Salt brought up by the capillary rise phenomenon is concerning as it can impact soil strength and hydraulic properties (Tang et al. 2021). This research aims to evaluate the accuracy of instrumented capillary rise columns and how the rise of water and salt concentration can be quantified in real-time. A summary of the research along with conclusions, contributions and recommendations are presented within this chapter.

5.1 Summary and Conclusions

The upward movement of saltwater in soils through capillary rise poses a concern, given its potential to adversely affect both the soil structure and hydraulic properties. This underscores the vital importance of implementing real-time monitoring systems to precisely gauge and evaluate the salt concentration in the soil. The purpose of this research was to use instrumentation in capillary rise sand column experiments to quantify the capillary rise and solute concentration in real-time.

Time-Domain Reflectometry (TDR) can be used to simultaneously measure the volumetric water content and bulk electrical conductivity of soil over time. Bulk electrical conductivity can be used to estimate the pore water electrical conductivity, which provides a basis for establishing a correlation with the salt concentration in the soil. TDR can provide valuable insights into the dynamics of water movement and the behavior of saltwater in soil. Non-instrumented columns are simpler and more accessible for basic observations of capillary rise, but they offer limited quantitative data. Instrumented columns, on the other hand, provide accurate and continuous measurements, enabling a more comprehensive understanding of capillary rise dynamics.

Capillary rise experiments, instrumented with TDR probes, were conducted to measure the volumetric water content and bulk electrical conductivity of two distinct sand grades (30/40 and 40/50). These experiments encompassed a series of trials involving varying concentrations of salt solutions, juxtaposed with a control test utilizing deionized water.

Five sets of experiments with salt solutions including 0 g/L, 2.5 g/L, 5 g/L, 7.5 g/L, and 10 g/L were conducted for each sand. Two TDR probes at 5 cm and 12 cm of the column height were placed into the column to account for the capillary rise height. The experimental water content results from TDR showed agreement with those obtained gravimetrically, suggesting the accuracy of TDR in measuring the water content. Furthermore, the bulk electrical conductivity results from TDR were compared to those obtained using a lab *EC* meter, indicating that TDR can be used to obtain electrical conductivity during capillary rise experiments for varying salt concentrations (within the TDR limits). The results showed that using TDR in column capillary rise experiments can provide accurate real-time data.

Further batch testing was conducted using the same sands to establish empirical relationships between bulk electrical conductivity and soil pore water concentration. These tests involved using a Büchner funnel and suction to extract the pore water from the sands so that the electrical conductivity of that pore water can be measured and then can be used to develop empirical relationships. The empirical relationship developed was successful in estimating the changing salt concentration.

The time series data, containing experimental volumetric water content and concentration from the capillary rise experiment, was used for inverse modelling. HYDRUS-1D was used to model the water flow and solute transport in a one-dimensional variably saturated column. The water content data from the two TDR locations was used to obtain soil hydraulic properties to define the soil water characteristic curve (SWCC) and unsaturated hydraulic conductivity. The water content predictions from HYDRUS-1D showed agreement with the TDR obtained water content results. The HYDRUS-1D estimates for the soil water retention properties differed from those measured using HYPROP due to hysteresis in drying and wetting processes. In addition, breakthrough curves of salt were fitted to observed concentration data to obtain solute transport parameters that are difficult to measure directly.

The height of capillary rise was estimated for each experiment through visual observations as well as using the TDR water content results. The results showed that the capillary height obtained from gravimetric results (16 cm for 30/40 sand and 20 cm for 40/50 sand) correlated closely with those heights obtained visually as well as using TDR locations. The effect of the NaCl solutions on the capillary rise was minimal which may be attributed to the fact that the density of the NaCl solutions ranged from 1002.5 g/L to 1010 g/L with increasing salt concentration (2.5 g/L to 10 g/L), which is a 0.25% to 1% difference in comparison to the density of deionized water. Furthermore, the addition of NaCl in water is expected to increase the cohesion forces of the saltwater mixture, which would impact the capillary rise. However, based on the low salt concentrations investigated in this research in comparison to the solubility limit of NaCl (360 g/L), increasing salinity did not show any significant effects on the capillary rise. The mass of the water going into the column experiments as well as TDR water content data was used to obtain the capillary height over time. The experimental results were compared to analytical relationships proposed by Terzaghi (1943) and Lu and Likos (2004). Generally, the analytical relationships were shown to correlate with the experimental results, but with increasing time the experimental results depicted a slower rate of rise whereas the analytical solutions showed the rate of rise to reach a maximum capillary height (around 0.01 days to 0.04 days). Analytical solutions can be useful in quantifying the changes in capillary rise with time and are highly influenced by hydraulic conductivity and porosity. The results from this research show that instrumented TDR columns can be used to measure the height of capillary rise, water content, and soil salinity in real-time.

5.2 Contribution of Research

This proposed approach can provide valuable quantitative data and enhance the understanding of saltwater dynamics in soil systems. This research can be applied in areas where capillary rise is of concern, such as agriculture or environmental areas or in geotechnical engineering. Knowledge of the salt concentration within the soil at various depths and locations can allow the

development of salt concentration maps which will make it easier to implement targeted remediation strategies or irrigation practices in agriculture. Furthermore, understanding of salt dynamics within an area will allow for better planning in terms of material selection in engineering. In areas where salt is of concern, one may want to use corrosion resistant materials (to avoid corrosion from chloride ions) or implement additional safety measures. TDR may also be used to monitor the performance of subgrade soils used in pavement design. Baldovino et al. (2022) reported that the subgrade soils under pavements may undergo changes in their stress-strain response under applied loads due to the increase in saturation attributed towards capillary rise effects. Using TDR to monitor the capillary rise in soils may allow for targeted mitigation efforts, where needed (i.e. placement of drainage systems).

The observed data obtained from instrumented columns can be utilized for inverse modelling purposes. With an instrumented column, the collected data can be quantitatively analyzed to determine the rate of capillary rise, the height of capillary rise, and temporal and spatial changes in soil moisture and salinity profiles. The detailed data obtained from instrumented columns allows for a deeper understanding of the behavior of saltwater capillary rise in soils. Furthermore, the findings from this research show that the use of TDR in column experiments can be used in HYDRUS-1D variably saturated models to inversely determine the soil hydraulic and solute transport properties which are difficult to measure experimentally. Inverse modelling can aid in decision-making processes, such as designing infrastructure, optimizing resource management strategies, and assessing the potential impacts of saltwater intrusion.

One of the key contributions of this research is the potential to obtain the SWCC from gravimetric water content measurements. One can set up a traditional capillary rise column experiment and post-experiment, obtain the SWCC using gravimetric water content measurements along the soil column. The soil column can be divided into several slices and the water content can be obtained gravimetrically, post-experiment. The results can be used to plot the soil moisture distribution with

depth and obtain the SWCC. Using other means to measure the SWCC (such as HYPROP) can be tedious and complex, however this research suggests that the SWCC obtained gravimetrically shows correlation with the measured SWCC from HYPROP.

5.3 Recommendations for Future Research

The current research considered the use of TDR in sand column experiments of two grades (30/40 and 40/50). Therefore, this research is limited to sand and how solute concentrations can impact sand in capillary rise column experiments. Current research provides a basis for future research possibilities. In light of this, the following recommendations may be considered for future research:

- The use of TDR in clay soils or highly conductive soils is not well researched due to the maximum bulk electrical conductivity limit for TDR being 5 dS/m. Insulated probes can be used to overcome this limitation. This research can be further extended to include highly conductive soils along with insulated probes to evaluate the performance of TDR in limiting conditions.
- The current research used homogenous material columns; however, the use of TDR should be evaluated in columns that vary in material (heterogenous column experiments).
- This research can also be further extended to encompass the use of different salt compositions and how they impact capillary rise and whether TDR can accurately determine the effect of other salts on capillary rise.
- Other TDR probe models such as CS605, CS610, CS630, etc. can also be tested in capillary rise column experiments to determine whether a certain model works better than another or whether experimental results are reproducible using different TDR probe models.

References

Archie, G.E. (1942). The electrical resistivity log as an aid in determining some reservoir characteristics. *Trans.* 146(01): 54–62.

ASTM International. (2014). ASTM D854-14 Standard Test Methods for Specific Gravity of Soil Solids by Water Pycnometer. *ASTM International*.

ASTM International. (2016). ASTM D5084-16a Standard Test Methods for Measurement of Hydraulic Conductivity of Saturated Materials Using a Flexible Wall Permeameter. *ASTM International*.

Baldovino, J., Izzo, R., & Millan-Paramo, C. (2022). Analysis of the capillary rise of a sedimentary soil in a subtropical region. *IAENG International Journal of Applied Mathematics*. *52*(4).

Barghi, M. H. (2018). Use of capillary action to control soil moisture. PhD Theses. University of Birmingham.

Brooks, R.H., & Corey, A.T. (1964). Hydraulic properties of porous medium. Colorado State University (Fort Collins), Hydrology Paper, Nr. 3.

Campbell Scientific, Inc. (2015). TDR100 Instruction Manual. *Campbell Scientific, Inc*.

Chen, R. P., Chen, Y. M., Xu, W., & Yu, X. (2010). Measurement of electrical conductivity of pore water in saturated sandy soils using time domain reflectometry (TDR) measurements. *Canadian Geotechnical Journal*. 47: 197-206.

Chung, C. C., & Lin, C. P. (2011). High concentration suspended sediment measurements using time domain reflectometry. *Journal of Hydrology*. 401(1-2): 134-144.

Chung, C. C., & Lin, C. P. (2019). A comprehensive framework of TDR landslide monitoring and early warning substantiated by field examples. *Engineering Geology*. 262,105330.

Corwin, D., & Yemoto, K. (2017). Salinity: Electrical conductivity and total dissolved solids. In *Methods of Soil Analysis* (Vol. 2).

Cwiakala, M., Kolodziejczyk, U., & Rafalski, L. (2012). The influence of selected chemical compounds used in winter road maintenance on the active capillarity of soils. *Springer J Soil Sediments*. 13: 63-71.

Dalton, F. N., & van Genuchten, M. T. (1986). The time-domain reflectometry method for measuring soil water content and salinity. *Geoderma*, Elsevier Science Publishers. *38*: 237–250.

Davies, B.E. & Davies, R.I. (1963). A simple centrifugation method for obtaining small samples of soil solution. *Nature*. 198(4876): 216–217.

Dragonetti, G., Farzamian, M., Basile, A., & Coppola, A. (2022). In situ estimation of soil hydraulic and hydrodispersive properties by inversion of electromagnetic induction measurements and soil hydrological modeling. *Hydrology and Earth System Sciences*. 5119-5136.

Erdélyi, A., Magnus, W., Oberhettinger, F., & Tricomi, F.G. (1953). Higher Transcendental Functions. Vol 1. *McGraw-Hill Book Company, Inc*. New York. (1): 27-31.

Fetter, C.W. (1994). *Applied Hydrogeology*. 3rd Edition. Macmillan College Publishing Company, New York.

Fraters, D., Boom, G. J., Boumans, L. J., de Weerd, H., & Wolters, M. (2017). Extraction of soil solution by drainage centrifugation-effects of centrifugal force and time of centrifugation on soil moisture recovery and solute concentration in soil moisture of loess subsoils. *Environmental monitoring and assessment*, *189*(2), 83.

Fredlund, D.G., Sheng, D., & Zhao, J. (2011). Estimation of soil suction from the soil-water characteristic curve. *Canadian Geotechnical Journal*. 48: 186-198.

Fredlund, D.G. & Xing, A. (1994). Equations for the soil-water characteristic curve. *Canadian Geotechnical Journal*. 31(3): 521-532.

Gardner, W.R. (1958). Some steady-state solutions of the unsaturated moisture flow equation with application to evaporation from a water table. *Soil Science*. 85(4): 228-232.

Giese, K., & Tiemann, R. (1975). Determination of the complex permittivity from thin-sample time domain reflectometry improved analysis of the step response waveform. *Advances in Molecular Relaxation Processes*. 7(1): 45-59.

Government of Western Australia (WA). (2022). Measuring soil salinity. *Department of Primary Industries and Regional Development. Agriculture and Food*. https://www.agric.wa.gov.au/soil-salinity/measuring-soil-salinity#:~:text=EC%20using%20the%201%3A5,%3A5w%2Fv)%20method&text=agitate%20the%20soil%20mix%20to,hours%20for%20high%20EC%20soils

He, X., Zeng, X., Dong, R., & Yang, J. (2023). Analysis of the effect of capillary water absorption on the resistivity of cementitious materials. *Applied Sciences*. 13: 3562.

Hilhorst, M. A. (2000). A Pore Water Conductivity Sensor. *Soil Science Society of America Journal*, 64(6): 1922–1925.

Hird, R., & Bolton, M. D. (2017). Clarification of capillary rise in dry sand. *Engineering Geology Journal*. 230: 77-83. Elsevier Science Publishers.

Hu, Y., Vu, H., & Hubble, D. W. (2006). Water content measurement in highly plastic clay using dielectric based probes. *Canadian Geotechnical Conference*. 59: 1-10. NRC Publications.

Hu, Y., Vu, H. Q., & Hubble, D. W. (2010). Evaluation of dielectric-based probes for expansive soils: application to Regina clay. *Canadian Geotechnical Journal.* 47: 346-358. NRC Research.

Huang, K., Toride, N., & van Genuchten, M.T. (1995). Experimental investigation of solute transport in large, homogeneous and heterogeneous, saturated soil columns. *Transport in Porous Med*ia. 18: 283–302.

Huo, W., Zhu, Z., Peng, Y., Pu, S., Wan, Y., & Zhang, C. (2021). Experimental study on capillary water rise and influencing factors in silty soil. *Arabian Journal of Geosciences*. 14: 2706.

IAEA. (2008). Field estimation of soil water content. *Soil and Water Management & Crop Nutrition Section International Atomic Energy Agency.*

Inoue, M., Šimůnek, J., Shiozawa, S., & Hopmans, J.W. *(2000).* Simultaneous estimation of soil hydraulic and solute transport parameters from transient infiltration experiments. *Advances in Water Resources.* 23: 677-688*.* Elsevier Science Publishers*.*

Ismayilov, A.I., Mamedov, A.I., Fujimaki, H., Tsunekawa, A., & Levy, G.J. (2021). Soil salinity type effects on the relationship between the electrical conductivity and salt content for 1:5 soil-to-water extract. *Sustainability*. MDPI.

Jitrapinate, N. (2016). Capillary rise simulation of saline waters of different concentrations in sandy soils*. KKU Engineering Journal.* 43(2): 78-84.

Jones, S.B., Wraith, J.M., & Or, D. (2002). Time domain reflectometer measurement principles and applications. *Hydrological Processes*. John Wiley & Sons. 16: 141-153.

Jorenush, M. H., & Sepaskhah, A. R. (2022). Modelling capillary rise and soil salinity for shallow saline water table under irrigated and non-irrigated conditions. *Agricultural Water Management*. 125-141. Elsevier Science Publishers.

Jurin, J. (1918). An account of some experiments shown before the Royal Society; with an enquiry into the cause of the ascent and suspension of water in capillary tubes. *Philosophical Transactions of the Royal Society of London*. 30: 739-747

Kargas G, Londra P, & Sgoubopoulou A. (2020). Comparison of soil EC values from methods based on 1:1 and 1:5 soil to water ratios and EC_e from saturated paste extract based method. *Water*. 12(4):1010.

Kerkhoff, B. (2007). Effects of substances on concrete and guide to protective treatments. *Portland Cement Association.*

Kirkham, J., Smith, C., Doyle, R., & Brown, P. (2019). Inverse modelling for predicting both water and nitrate movement in a structured-clay soil (Red Ferrosol). *PeerJ*.

Kool, J. B., & Parker, J. C. (1987). Development and evaluation of closed-form expressions for hysteretic soil hydraulic properties. *Water Resources Research*. 23(1): 105–114.

Kumar, S. & Malik, R.S. (1990). Verification of quick capillary rise approach for determining pore geometrical characteristics in soils of varying texture. *Soil Science Society of America Journal.* 150(6): 883–888.

Ledieu, J., De Ridder, P., De Clerck, P., & Dautrebande, S. (1986). A method measuring soil water moisture by time-domain reflectometry. *Journal of Hydrology*. 88: 319–328.

Leij, F.J. & van Genuchten, M.T. (1999). Principles of solute transport. *American Society of Agronomy*.

Li, H., Zand, A. R., Sikorski, Y., Markicevic, B., Meyers, J., Rincon, C., Bowden, E., Bethel, T., Sanders, M. S., Navaz, H. K., & Smith, M. R. (2011). Simple and effective method to measure the diffusion coefficient of organic vapors in porous media. *Analytical Methods*, *3*(12), 2809–2814.

Limsuwat, A., Sakaki, T., & Illangasekare, T.T. (2009). Experimental quantification of bulk sampling volume of ECH2O soil moisture sensors. *29th Annual American Geophysical Union Hydrology Days*.

Liu, D., Lu, C., Minjie, L., Gu, Q., & Jing, Y. (2022). Experimental study on capillary water migration characteristics of tailings with different particle sizes. *Hindwai Geofluids*.

Liu, Q., Yasufuku, N., Miao, J., & Ren, J. (2014). An approach for quick estimation of maximum height of capillary rise. *Soils and Foundation*. Elsevier Science Publishers. 54(6): 1241–1245.

Lu, N., & Likos, W. J. (2004). Rate of capillary rise in soil. *ASCE Journal of Geotechnical and Geoenvironmental Engineering*.

Lu, N., & Likos, W. J. (2004). Unsaturated Soil Mechanics. *John Wiley & Sons*. New Jersey.

Lubelli, B. (2006). Sodium chloride damage to porous building materials. PhD dissertation. Delft University of Technology.

Lubelli, B., Cnudde, V., Diaz-Goncalves, T., Franzoni, E., Van Hees, R. P. J., Ioannou, I., Menendez, B., Nunes, C., Siedel, H., Stefanidou, M., Verges-Belmin, V., and Viles, H. (2018). Towards a more effective and reliable salt crystallization test for porous building materials: state of the art. *Materials and Structures.* 51(2): 55.

MacDonald, J. D., Belanger, N., Sauve, S., Courchesne, F., & Hendershot, W. H. (2008). Soil sampling and methods of analysis. *Taylor & Francis Group*, LLC. 2: 179-196.

McGinnis, T. (2001). Determining contact angle of solutions with varying surface tension of dry and pre-wetted silica sands. Master's Theses. Oregon State University.

Meter Group. (2018). Operation Manual Hyprop 2. Meter Group AG.

Meter Group. (2023). LABROS Soilview-Analysis for Hyprop. Meter Group AG.

Mojid, M. A., Wyseure, G. C. L., & Rose, D. A. (1998). The use of insulated time-domain reflectometry sensors to measure water content in highly saline soils. *Springer Irrigation Science.* 18: 55-61.

Muñoz-Carpena, R., Regalado, C. M., Ritter, A., Alvarez-Benedí, J., & Socorro, A. R. (2005). TDR estimation of electrical conductivity and saline solute concentration in a volcanic soil. *Geoderma*, *124*(3), 399–413.

Or, D., & Tuller, M. (2005). Capillarity. *Encyclopedia of Soils in the Environment*. Elsevier Science. 155-164.

Or, D., & Wraith, J. M. (1999). Temperature effects on soil bulk dielectric permittivity measured by time domain reflectometry: A physical model. *Water Resources Research.* 35(2): 371– 383..

Pansu, M., & Gautheyrou, J. (2003). Handbook of Soil Analysis: Mineralogical, Organic, and Inorganic Methods. Springer.

Peck, R.B., Hanson, W.E., & Thornburn, T.H. (1974). Foundation Engineering. *John Wiley & Sons*. New York.

Polubarinova-Kochina, P. Ya. (1951). Theory of filtration of liquids in porous media. *Advances in Applied Mechanics Advances in Applied Mechanics*. Volume 2: 153-225. Web.

Polubarinova-Kochina, P. (1959). Ground water movements at water level fluctuations in a reservoir with a vertical boundary. *Journal of Applied Mathematics and Mechanics*, 23(3), 762-769.

Polubarinova-Kochina, P. (1962). Theory of ground water movement. Princeton University Press. Princeton, N.J.

Ramli, H., Lee, Z. X., Azmi, M., & Ahmad, F. (2020). Capillary rise determination using simplified image analysis method. *E3S Web of Conferences.* 195,03017. *EDP Sciences.*

Rhoades, J. D., Manteghi, N. A., Shouse, P.J., Alves, W.K. (1989). Soil electrical conductivity and soil salinity: new formulations and calibrations. *Soil Science Society of America Journal*. 53: 433-439.

Rhoades, J. D., Raats, P. A. C., & Prather, R. J. (1976). Effects of liquid-phase electrical conductivity, water content, and surface conductivity on bulk soil electrical conductivity. *Soil Science Society of America Journal*. 40.

Rinaldi, V. A., & Cuestas, G. A. (2002). Ohmic conductivity of a compacted silty clay. *Journal of Geotechnical and Geoenvironmental Engineering*. *128*(10): 824–835.

Ross, D., & Bartlett, R. (1990). Effects of extraction methods and sample storage on properties of solutions obtained from forested spodosols. *Journal of Environmental Quality.* 19(1): 108-113.

Salahou, M., Chen, X., Zhang, Y., Jiao, X., & Lü, H. (2022). Inverse modelling to estimate soil hydraulic properties at the field scale. *Mathematical Problems in Engineering*. 2022: 1-11.

Salehi, M. M., Omidvar, P., & Naeimi, F. (2017). Salinity of injection water and its impact on oil recovery absolute permeability, residual oil saturation, interfacial tension and capillary pressure. *Egyptian Journal of Petroleum*. 26(2): 301-312.

Salim, R. L. (2016). Extent of capillary rise in sands and silts. Master's Theses. Western Michigan University.

Seki, K. (2007). SWRC fit – A nonlinear fitting program with a water retention curve for soils having unimodal and bimodal pore structure. *Hydrology and Earth System Sciences*. 4: 407-437.

Sghaier, N., Prat, M., & Ben Nasrallah, S. (2006). On the influence of sodium chloride concentration on equilibrium contact angle. *Chemical Engineering Journal*. 122: 47-53. Elsevier Science Publishers.

Šimůnek, J., Šejna, M., Saito, H., Sakai, M., & & van Genuchten, M.T. (2018). The HYDRUS-1D software package for simulating the one-dimensional movement of water, heat, and multiple solutes in variably-saturated media. *Department of Environmental Sciences. University of California Riverside.*

Šimůnek, J., & van Genuchten, M.T. (2008). Modeling nonequilibrium flow and transport processes using HYDRUS. *Vadose Zone Journal*. 7: 782-797.

Tang, S., She, D., & Wang, H. (2021). Effect of salinity on soil structure and soil hydraulic characteristics. *Canadian Journal of Soil Science*. 101(1): 62–73.

Topp, G. C., Davis, J. L., & Annan, A. P. (1980). Electromagnetic determination of soil water content: measurements in coaxial transmission lines. *Water Resources Research*. 6(3): 574-582.

Truc, N. N., & Hoang, N. V. (2022). Comparative study of capillary rise characteristics of saltwater in loose materials. *Marine Georesources and Geotechnology*. 40(11): 1341-1358

Truc, N. N., Hoang, N. V., & Tu, T. N. (2022). Capillary rise characteristics and saltwater propagation in fine aggregate: toward developing the anti-salinity shallow foundation. *Springer.*

Truc, N. N., Mihova, L., Mukunoki, T., & Do, D. M. (2019). Effect of saline intrusion on the properties of cohesive soils in the Red River Delta, Vietnam. *Marine Georesources & Geotechnology.* 38(1): 23–39.

Terzaghi, K. (1943). Theoretical Soil Mechanics. *John Wiley and Sons*. New York.

van Genuchten, M. T. (1980). A closed-form equation for predicting the hydraulic conductivity of unsaturated soils. S*oil Science Society of America Journal*. 44: 892–898.

Vieira Concrete Supplies (n.d.) Bell & Mackenzie 50 lb Silica Sand #4751. TDS.

Ward's Science. (2013). Safety Data Sheet No. SS0430. Sodium Chloride. https://ca.vwr.com/assetsvc/asset/en_CA/id/13962832/contents

Weisstein, E.W. (2024). Lerch Transcendent. MathWorld - A Wolfram Web Resource. https://mathworld.wolfram.com/LerchTranscendent.html

Vogeler, I., Clothier, B.E., Green, S.R., Scotter, D.R. and Tillman, R.W. (1996), Characterizing water and solute movement by time domain reflectometry and disk permeametry. *Soil Science Society of America Journal. 60: 5-12.*

Wraith, J. M., Robinson, D. A., Jones, S. B., & Long, D. S. (2005). Spatially characterizing apparent electrical conductivity and water content of surface soils with time domain reflectometry. *Computers and Electronics in Agriculture*. 46(1–3): 239-261.

Wyseure, G. C. L., Mojid, M. A., & Malik, M. A. (1997). Measurement of volumetric water content by TDR in saline soils. European Journal of Soil Science. 48: 347-354.

Xing, X., Li, X., & Ma, X. (2019). Capillary rise and saliferous groundwater evaporation: Effects of various solutes and concentrations. *IWA Publishing Hydrology Research*. 50(20).